# Multi-Component Mass Transfer and Chemical Oxidation

by

Saeid Shafieiyoun

A thesis
presented to the University of Waterloo
in fulfillment of the
thesis requirement for the degree of
Doctor of Philosophy
in
Civil Engineering

Waterloo, Ontario, Canada, 2017

# Examining Committee Membership

The following served on the Examining Committee for this thesis. The decision of the Examining Committee is by majority vote.

| | |
|---|---|
| External Examiner | NAME: Subhasis Ghoshal<br>Title: Associate Professor – McGill University |
| Supervisor | NAME: Neil R. Thomson<br>Title: Professor - University of Waterloo |
| Internal Member | NAME: James Craig<br>Title: Associate Professor - University of Waterloo |
| Internal-external Member | NAME: Marios Ioannidis<br>Title: Professor - University of Waterloo |
| Internal-external Member | NAME: James Barker<br>Title: Professor Emeritus - University of Waterloo |

# Author’s Declaration

I hereby declare that I am the sole author of this thesis. This is a true copy of the thesis, including any required final revisions, as accepted by my examiners.

I understand that my thesis may be made electronically available to the public.

# Abstract

The remediation of soil and groundwater contaminated with multi-component non-aqueous phase liquids (NAPLs) such as coal tars from former manufactured gas plants (MGPs) is associated with a number of challenges. Due to thermodynamic considerations, the presence of more than one compound within multi-component NAPLs (especially when they are structurally dissimilar) can restrict intra-NAPL diffusion. Since diffusion is the dominant process in the dissolution of organic compounds, any diffusion limitations can restrict mass transfer between the NAPL and the aqueous phase. Consequently, the efficiency of conventional water-based remediation methods can be restricted. *In situ* chemical oxidation (ISCO) has been a possible remediation technology touted for the treatment of multi-component NAPLs. However, chemical oxidation occurs only in the aqueous phase and consequently the mass transfer between NAPLs and the aqueous phase indirectly controls the overall treatment efficiency. The primary objective of this research effort was to theoretically and experimentally investigate mass transfer processes from complex multi-component NAPLs subjected to water and chemical oxidants.

For the purpose of this evaluation, the feasibility of chemical oxidants to degrade MGP residuals needs to be quantified. A series of physical model trials supported by a host of aqueous and slurry batch experiments were conducted to assess the performance of two chemical oxidants (persulfate and permanganate) using impacted sediments collected from a former MGP site. The results indicated that dissolved components were readily degraded with persulfate or permanganate (except for benzene) in the aqueous batch systems. In addition, in the well-mixed slurry systems when contact with the oxidant was achieved, permanganate, unactivated persulfate, and alkaline activated persulfate were able to degrade >95%, 45% and 30% of the initial mass quantified, respectively. However, insignificant quantifiable mass was lost in all physical models under dynamic conditions which are more representative of *in situ* conditions.

A simple single-cell numerical model was constrained by the experimental results and used to investigate treatment expectations and the potential long-term behaviour of dissolved phase concentrations as a result of treatment using 6 pore volumes of oxidant. A specified inlet oxidant concentration and NAPL composition (22 compounds (34 %), and bulk mass (66 %) composed of unidentified material) were prescribed, and the effluent concentrations of the known soluble constituents were estimated from mass balance considerations. A variety of long-term simulation scenarios were performed. In general, for a NAPL saturation of 6 %, the results indicated that the effluent profiles over a 10-year period were reduced temporality as a result of the oxidant injection

and then rebounded to a profile that was coincident with a no-treatment scenario. Based on a sensitivity analyses, neither water velocity or oxidant concentration affected the long-term behavior of dissolved phase concentrations; however, increasing the mass transfer rate coefficient had a dramatic impact, and chemical oxidant injections were only effective for low NAPL saturations (<1 %).

Intra-NAPL diffusion is one of the most critical processes which can influence NAPL-water mass transfer processes. A comprehensive experimental and computational study was performed to investigate the role of intra-NAPL diffusion on the mass transfer between multi-component NAPLs and water, and to identify some of the controlling situations where this process should be considered. A diffusion-based numerical model was developed, and two different physical systems were simulated; a spherical single NAPL blob with total surface area available for mass transfer, and an isolated rectangular NAPL with only one side available for mass transfer. A series of batch and physical model experiments were conducted using coal tars collected from a former MGP site to capture multi-component diffusion-limited mass transfer behavior under static and dynamic conditions, respectively. This series of experiments was intended to focus on the direct interaction of multi-component NAPLs with water and a persulfate solution without the presence of sediment.

The results from the static experiments indicated that under the diffusion-controlled mass transfer conditions, the estimated mass transfer rate coefficients were lower than typical mass transfer rate coefficients determined under continuous mixed conditions. Although, no overall trend was observed between the mass transfer rate coefficients for the various organic compounds identified, an inverse dependency between the mass transfer rate coefficient and molecular weight was clear but different for BTEX and some PAHs compounds suggesting that the intra-NAPL diffusion behavior of these two organic compound classes are different.

The results indicated that molecular weight and concentration of each component are the most important parameters affecting intra-NAPL diffusion coefficients. A combination of NAPL composition, NAPL geometry, and interphase mass transfer rate may result in the depletion of more soluble compounds at the interface which can restrict NAPL-water mass transfer. When the main intra-NAPL diffusion coefficients are in the range of the self-diffusion coefficients, dissolution is not limited by internal diffusion except for high interphase mass transfer rates or long diffusional distances. In the case of complex and highly viscous NAPLs, smaller intra-NAPL diffusion coefficients are expected and even the low range of mass transfer rates can result in the depletion

of more soluble compounds at the NAPL-water interface and diffusion-limited dissolution. Depending on the NAPL properties (i.e., constituent components, viscosity, temperature), interfacial depletion of the more soluble compounds can vary and influence mass transfer and dissolved phase concentrations. The comparison of experimental and simulated results indicated that rate-limited intra-NAPL diffusion within complex multi-component NAPLs as well as persulfate-NAPL interactions can restrict mass loss and chemical oxidation efficiency compared to the no-treatment scenario. It was determined that during 64 days of persulfate injection the multi-component mass transfer rate coefficients were ~70 % smaller than those estimated during an equivalent water injection period.

The experimental and computational effort described in this study is the first effort to provide comprehensive information about the role of intra-NAPL diffusion on dissolution of multi-component NAPLs and the direct interaction of persulfate with MGP residuals. The diffusion-based model developed in this study provides a realistic platform to capture the temporal and spatial mass fluxes and compositional changes within complex NAPLs. While chemical oxidants (persulfate or permanganate) are able to degrade MGP residuals in well-mixed conditions, rate-limited NAPL-water mass transfer restricts treatment in systems more representative of *in situ* conditions. Therefore, methods to overcome the mass transfer limitations and intra-NAPL resistances are required for the remediation of complex multi-component NAPLs.

# Acknowledgement

I would like to express my sincere gratitude to my advisor Professor Neil R. Thomson for the continuous support of my PhD study, for his patience, motivation, desire to make me think deeply, and for giving me the opportunity to join his research team. His guidance helped me in all the time of research and writing of this thesis. Thank you Neil, for all your help and support. I would also like to thank my thesis committee: Dr. Subhasis Ghoshal, Dr. James Craig, Professor James Barker, and Professor Marios Ioannidis for their insightful comments and encouragement.

My sincere thanks also goes to amazing super experienced lab technicians without their precious support it would not be possible to conduct this research: Shirley Chatten, Wayne Nobel, Mark Sobon, Mark Merlau, Terry Ridgway, and Rachel Karimi. I would also like to thank my friends and fellow grad students at University of Waterloo for their kind support during my study; Dr. Vahid Sohrabi, Felipe Solano, Dr. Mehrdad Mastali Majdabadi, Dr. Mahsa Shayan, Dr. Mohammed AL-Shamsi, Michelle Cho, Yunxiao Wei, Summer Jin, Zahra Sadeghi Ardestani, Sonia Jaberi, Lorenzo Simonetti.

Financial support for this investigation was provided by a Natural Sciences and Engineering Research Council (NSERC) of Canada Collaborative Research and Development Grant (N.R. Thomson) for which I am very grateful.

I am truly indebted to Sadat Educational Complex, Isfahan, Iran, where I completed my elementary and high school. I had a wonderful opportunity to learn from amazing teachers and I am always thankful to them: late Ali Fathi, Mohsen Fathi, Mostafa Fathi, Alireza Doostani, Mehdi Sadri, and Meisam Sharif.

Foremost, I would like to thank my parents, Parvin and Aboulghasem, who supported me unconditionally and gave up many things for me throughout my life, and to my brother, Shahram, my sister, Elham, my brother in law, Majid, and my sister in law, Samira, for supporting me spiritually all these years. I am also truly grateful to my cousins, Firoozeh, Farzaneh, and Farahnaz, for their kindness and hospitality during my PhD study in Canada.

# Dedication

To my parents, Parvin and Aboulghasem, although nothing can be comparable to all their dedications.

# Table of Contents

# List of Figures

# List of Tables

# Chapter 1

# Introduction

## 1.1 GENERAL BACKGROUND

Soil and groundwater contamination resulting from organic compounds such as coal tar, creosote, diesel fuel, and other petroleum-derived compounds is an important environmental issue (Peters et al. 1999). Accidental releases and leakage from waste disposal, storage sites, and industrial facilities are the most widespread causes of subsurface contamination by these compounds (Soga et al. 2004). Due to their low solubility, these contaminants often persist in subsurface systems as a separate non-aqueous phase liquid (or NAPL). When groundwater flows through the contaminated area containing a NAPL (the NAPL source zone), a small amount of the NAPL will dissolve in the aqueous phase which leads to a dissolved plume downgradient of the source zone (Soga et al. 2004). The maximum solubility of some organic compounds in a NAPL can be more than two-orders of magnitude higher than the regulatory limit resulting in potential risk of harmful effects to the surrounding environment and human health (Miller et al. 1990).

NAPL dissolution is often modeled based on either a local equilibrium assumption or a rate-limited mass transfer (Powers et al., 1991). Traditionally it was assumed that the concentration of an organic compound in the aqueous phase is equal to the equilibrium concentration of that compound in water (Abriola & Pinder, 1985; Sleep & Sykes, 1993). However, field and laboratory data (e.g., Powers et al. 1992) indicate that the concentration of organic compounds in groundwater is usually less than their corresponding equilibrium concentration which implies that some physical and chemical processes impose a resistance to dissolution.

One of the possible reasons for rate limited mass transfer is the presence of more than one compound (especially when they are structurally dissimilar) within the NAPL which can restrict intra-NAPL diffusion and hence, influence interfacial NAPL properties and the effective solubility of constituent compounds. For example, coal tar from a former manufactured gas plant (MGP) is composed of hundreds to thousands of organic compounds with no single predominant compound. It is usually possible to identify only a portion of a MGP residual and even analysis of the identified portion is extremely complicated (Brown et al. 1999). As MGP residuals are exposed

to groundwater, the more soluble compounds will gradually deplete and higher molecular weight compounds will remain in the NAPL (a phenomenon called aging or weathering) which can change the NAPL composition. Due to these changes a high viscous layer can be formed on the NAPL surface which affects diffusion across the NAPL-water interface and consequently, the dissolution of organic compounds will be reduced (Ghoshal et al. 2004; Luthy et al. 1993).

Various physical, chemical and biological methods have been developed for the remediation of NAPL contaminated sites. In situ chemical oxidation (ISCO) has been demonstrated as an effective technique which is capable of degrading a variety of common organic contaminants and relies on the delivery of a chemical oxidant to the contaminated media to degrade the organic contaminant into less harmful compounds (Soga et al., 2004; Huling & Pivetz, 2006; Tsitonaki et al., 2010). Krembs et al. (2010) reviewed data from 242 ISCO projects and reported that ISCO has been used in different subsurface conditions and for a variety of contaminants with chlorinated solvents being the most frequent. They also indicated that except at some sites where dense NAPLs (DNAPLs) were present, ISCO has typically been able to achieve concentrations below the maximum concentration limit (MCL) in the aqueous phase.

Since ISCO is able to oxidize most of the common organic compounds (Krembs et al., 2010), it should be possible to use chemical oxidation for the treatment of MGP residuals. However, chemical oxidation occurs only in the aqueous phase and consequently the mass transfer between multi-component NAPLs and the aqueous phase indirectly controls the overall treatment efficiency. Thus, a comprehensive mass transfer study which incorporates internal and interfacial NAPL limitations is required to estimate ISCO treatment efficiency. While intra-NAPL diffusion and compositional changes within multi-component NAPLs are critical for mass transfer, they have not been considered extensively in simulation studies (Brahma & Harmon, 2003; Holman & Javandel, 1996). In addition, studies dealing with the chemical oxidation of multi-component NAPLs have been limited in scope with widely varied results (Hauswirth & Miller, 2014). To the best of our knowledge, no study has investigated intra-NAPL diffusion and compositional changes in complex multi-component NAPLs, and the direct interaction of MGP NAPLs with chemical oxidants.

## 1.2 RESEARCH OBJECTIVES

The major objectives of this research are:

1) To investigate the feasibility of different chemical oxidants to degrade MGP residuals in well-mixed systems.
2) To explore the interaction of different chemical oxidants with MGP residuals in systems representative of *in situ* conditions.
3) To mathematically demonstrate NAPL/water mass transfer and spatial/temporal mass fluxes within complex multi-component NAPLs.
4) To theoretically and experimentally quantify intra-NAPL diffusion and compositional changes of organic compounds within MGP NAPLs subjected to water and a chemical oxidant.

## 1.3 THESIS SCOPE

The thesis is organized into five chapters. Chapters 2, 3, and 4 are the core chapters that address the research objectives. Chapter 1 provides the framework, and Chapter 5 summarizes the major conclusions and contributions, and discusses areas for future work.

To assess the performance of two chemical oxidants (persulfate and permanganate) to degrade MGP residuals in a dynamic flow system representative of *in situ* conditions, a series of physical model trials supported by a host of aqueous and slurry batch experiments were conducted. Mass loss estimates as well as aqueous concentrations of organic components were used to investigate chemical oxidation efficiency. In addition, temporal treatment expectations were explored using a single-cell mathematical representation constrained by the treatability test data collected. Chapter 2 is devoted to a discussion of the experimental and simulation methods and results that address Objectives 1 and 2 of this research.

To investigate the role of intra-NAPL diffusion on mass transfer from multi-component NAPLs and interfacial depletion of the more soluble compounds, a diffusion-based numerical model was developed. Chapter 3 focuses on the development and application of this numerical model. A series of static experiments were conducted using coal tar collected from a former MGP site to capture multi-component diffusion-limited mass transfer behavior. These experiments were designed to generate relevant model parameters for simulation purposes. The developed model was calibrated and then used to simulate temporal discharge, intra-NAPL concentration gradients,

and to identify some conditions where these processes need to be considered. Chapter 3 addresses Objective 3 of this research.

To determine the role of intra-NAPL diffusion on the dissolution of multi-component NAPLs subjected to persulfate, a series of physical model experiments were performed. This series of experiments was intended to investigate the direct interaction of NAPLs with persulfate or water under controlled conditions in flow through systems without sediments. The experimental results were employed to constrain the developed diffusion-based numerical model under dynamic conditions. Chapter 4 elucidates the methodology used and results, and addresses Objective 4 of this research.

Chapters 2, 3, and 4 were edited by N.R. Thomson and prepared with the intent to submit them to the Journal of Contaminant Hydrology, Advances in Water Resources, and Environmental Science and Technology, respectively, and hence are written as stand-alone chapters and some repetition is unavoidable.

# Chapter 2

# Realistic Expectations for the Treatment of FMGP Residuals by Chemical Oxidants

## OUTLINE

Methods to remediate soil and groundwater contamination at former manufactured gas plant (FMGP) sites are scarce. The objective of this study was to investigate the ability of two chemical oxidants (persulfate and permanganate) to degrade FMGP residuals in a dynamic flow system representative of *in situ* conditions. A series of physical model trials supported by aqueous and slurry batch experiments using impacted sediments collected from a FMGP site were conducted. To explore temporal expectations, a single cell numerical model constrained by the experimental data was used. The results from the aqueous experiments showed that dissolved components (except for benzene) were readily treatable with persulfate or permanganate. In the well-mixed slurry systems, when contact with the oxidant was achieved, 95%, 45% and 30% of the initial mass quantified was degraded by permanganate, unactivated persulfate, and alkaline activated persulfate, respectively. In stark contrast, the total mass removed in the physical model trials was low for both permanganate (~30%) and persulfate (not significant) irrespective of the bleb or lense architecture utilized. Hence the net benefit of flushing 6 pore volumes of permanganate or persulfate at a concentration of 30 g/L under the physical model operating conditions was minimal. The long-term simulation results indicated that the concentration of organic compounds in the effluent were reduced temporality as a result of oxidant presence and then rebounded to a profile that was coincident with a no-treatment scenario. Neither changes in velocity or oxidant concentration affected the long-term behavior of the dissolved phase concentrations; however, increasing the mass transfer rate coefficient had a dramatic impact. The results of this investigation indicate that permanganate or persulfate treatment efficiency for FMGP residuals is mass transfer limited.

Key Words: Coal tar, MGP, Persulfate, Permanganate, End-point treatment, Long-term

# 2.1 INTRODUCTION

Prior to 1950, thousands of manufacturing plants produced a combustible gas from coke, coal or oil that was used in urban environments for lighting, heating, and cooking (Hatheway, 2012). Due to poor process operations and residual management practices, there currently exists serious soil and groundwater contamination problems at many of these former manufactured gas plant (FMGP) sites (Cassidy et al., 2015; Wang et al., 2015; Hauswirth et al., 2012). FMGP residuals are usually found in the subsurface as non-aqueous phase liquids (NAPLs) that are typically denser and more viscous relative to water, and composed of hundreds to thousands of organic compounds (Mueller et al., 1989). Based on observations from various site characterization efforts, the *in situ* architecture of these coal tar NAPLs range from sheens, stains, tar blebs and tar coatings to saturated lenses or pools. Despite vast advancements in analytical methods, it is currently only possible to quantify a portion of the organic compounds present in FMGP coal tars, and even the analysis of this identified portion is extremely complicated (Birak & Miller, 2009). Moreover, the composition of FMGP tars varies between sites due to differences in source material and processing operations (Birak & Miller, 2009). When FMGP tars are initially exposed to groundwater, the more soluble compounds will gradually be depleted over time (a phenomenon called aging or weathering) and the higher molecular weight compounds, which are generally the less soluble compounds, will remain in the NAPL. The presence of these FMGP tars in subsurface environments may pose a long-term threat to groundwater quality and potentially human health if left untreated.

Remediation initiatives at many FMGP sites have been limited to isolation or removal of the source materials (USEPA, 2013; Birak & Miller, 2009; Luthy et al., 1994). Over the last 15 years, *in situ* chemical oxidation (ISCO) has been growing steadily as a remediation technology used to treat a range of environmentally relevant contaminants (Siegrist et al., 2011). Although different types of chemical oxidants have been employed, persulfate and permanganate are the two most frequently used as they are typically more persistent in subsurface systems (Petri et al., 2011a,b; USEPA, 2006). Since chemical oxidation has been shown to successfully degrade a number of the organic compounds typically present at FMGP sites (polyaromantic hydrocarbons (PAHs); benzene, toluene, ethylbenzene, and xylenes (BTEX)) (Krembs et al., 2010), it is speculated that it could be a beneficial technology to treat FMGP tars *in situ*.

Published studies dealing with the chemical oxidation of FMGP residuals have been diverse in scope with varied and often conflicting results (Hauswirth & Miller 2014; Gan et al. 2009). Table

2.1 provides a comprehensive summary of published bench-scale studies which have used either persulfate or permanganate to degrade FMGP residuals in batch (i.e., well-mixed slurry) or column systems.

Some of the investigations detailed in Table 2.1 have used impacted aquifer or river sediments collected from FMGP sites, while others have used soils "spiked" with a MGP NAPL (Peng et al., 2016; Usman et al., 2012; Brown et al., 2003). Although spiked-soil studies provide valuable insight into the chemical reactivity of different oxidants to attack MGP residuals, the use of impacted materials collected from FMGP sites better represents the *in situ* chemical composition. Employing a series of batch experiments, Usman et al. (2012) observed that magnetite-activated persulfate was able to degrade 70 to 80% of the total PAHs ($PAH_T$) in spiked sand, but no PAH mass was removed when a FMGP soil was used. In contrast, Cassidy et al. (2015) reported mass removal of 55 to 65% using alkaline-activated persulfate (~37 g/L) in a batch system for soil material with an initial BTEX concentration of 0.58 g/kg, and a $PAH_T$ concentration of 3.06 g/kg (sum of 18 compounds). Nadim et al. (2005) observed between 75 to 100% $PAH_T$ removal (7 compounds) using iron-activated persulfate (5 g/L) for a less impacted soil (0.01 g/kg $PAH_T$). Only a few studies have directly compared the effectiveness of different chemical oxidants to degrade organic mixtures (Lemaire et al., 2013; Ferrarese et al., 2008; Rivas 2006; Gates-Anderson et al., 2001). For example, Ferrarese et al. (2008) identified that a 158 g/L permanganate solution and a 120 g/L persulfate solution were able to degrade 96 and 88% of the $PAH_T$ present in impacted soil with an initial $PAH_T$ concentration of 2.8 g/kg, respectively.

Batch systems normally provide the most ideal environment to maximize treatment due to high oxidant dosing (mass of oxidant/mass of contaminant), maximum contact between the oxidant and the NAPL (well-mixed), and long reaction times. In contrast, column systems are often considered more representative of a dynamic subsurface situation where preferential pathways exist, there is less direct oxidant contact with the NAPL, and the reaction time is controlled by the flow system. For example, despite a $PAH_T$ removal of 47% (14 compounds) in a series of batch experiments, Richardson et al. (2011) observed no reduction in PAH mass from column experiments using a heat-activated persulfate system in spite of a relatively low $PAH_T$ concentration of ~0.3 g/kg. In comparison, Hauswirth and Miller (2014) performed column experiments using FMGP impacted soils (initial $PAH_T$ concentration of 1.99 g/kg of tar; 25 compounds) and reported a 53% removal of $PAH_T$ after injecting 52 pore volumes (PVs) of a 50 g/L alkaline-activated persulfate solution. Since a typical field injection event is < 1 PV (Crimi et

al., 2011), this high number of PVs is impractical at most field sites and hence the results from this experiment should be viewed as highly optimistic.

In addition to the ability of chemical oxidants to degrade multi-component NAPLs such as FMGP residuals, aquifer material and NAPL architecture, in part, dictate contaminant availability and consequently treatment effectiveness (Zhang et al. 2007). The NAPL surface area to volume ratio is much less for a lense or pool architecture compared to bleb architecture, and hence the relative surface or contact area is lower (Powers et al., 1994). Moreover, the aqueous hydraulic conductivity is reduced within regions with a lense architecture, and thus the ability to flush remedial fluids into these areas is limited (Zhang et al., 2008). This can restrict the efficiency of a chemical oxidation system and in such conditions multiple injection episodes to effectively degrade the NAPL are required (Petri et al., 2011a).

Due to complex entrapment and multicomponent aspects of FMGP residuals it is generally not possible to remove all of the NAPL mass during treatment with a chemical oxidant (Soga et al., 2004). For example, Thomson et al. (2008) monitored the short-term (months) and long-term (years) behaviour of a plume originated from a multi-component NAPL source zone after treatment with permanganate. They concluded that, while the short-term organic compound concentrations were reduced significantly, there was a rebound of all of the monitored compounds after four years post-treatment. Hence, predicting the long-term behaviour of dissolved phase concentrations following chemical oxidation treatment is necessary for the evaluation of post-treatment behaviour and risk assessment. The few studies that have investigated the long-term behavior of dissolved phase concentrations from FMGP residuals have indicated that dissolution kinetics depends on NAPL composition, and the time scale for complete removal can vary between weeks to more than thousands of years for different NAPL architectures (Eberhardt & Grathwohl, 2002).

Based on the current literature (Table 2.1), it is unclear what the dissolved phase concentration behaviour is following treatment of FMGP tars with different NAPL architectures by various chemical oxidants. The objective of this study was to investigate the performance of two chemical oxidants (sodium persulfate ($Na_2S_2O_8$) and potassium permanganate ($KMnO_4$)) to degrade FMGP residuals in a dynamic flow system representative of *in situ* conditions. Supported by aqueous and slurry batch experiments, a series of physical model trials were conducted using impacted sediments collected from a FMGP site. Each physical model was subjected to three oxidant flushing episodes (6 PVs in total) and the effluent was sampled between each episode. At the

termination of each trial, sediment samples were collected from the physical model and analyzed for a suite of organic compounds to determine mass removed. A simple single-cell numerical model was constrained by the experimental results and used to investigate treatment expectations and the potential long-term behaviour of dissolved phase concentrations as a result of treatment using these chemical oxidants.

# 2.2 MATERIALS AND METHODS

## 2.2.1 Aquifer materials and NAPL

Impacted groundwater and FMGP residuals used in this study were obtained from the former West Florida Natural Gas Company Site located in Ocala, Florida. From the late 1890s until about 1953, water gas or carbureted water gas was manufactured at this location by the "Lowe" carbonization process or destructive distillation of bituminous coal and coke. According to Brown's directory of North American gas companies (1964), gas production was ~48 x $10^3$ $m^3$/yr in 1900 and steadily increased to 900 x $10^3$ $m^3$/yr by 1950. In 1952, manufacturing stopped at the plant and the facility converted to the sale of butane-propane-air. Residues from the MGP process, including tars and oily wastewaters, were deposited in the area of the former gas plant facilities during operations. There was an historic coal tar pit or area where residual tars were stored prior to sale for off-site use as roofing materials.

Groundwater samples were collected in 1000 mL amber glass containers from two monitoring wells screened from 19.8-21.3 and 36.-39.6 m below ground surface (bgs) utilizing a low flow (< 0.2 L/min) purge sampling technique. The samples were placed in coolers maintained at ~4 °C and transported to the University of Waterloo where they were stored in a walk-in refrigerator at 4 °C.

During extensive drilling activities at the site, both impacted and non-impacted aquifer materials were collected from a weathered limestone unit using rotosonic drilling methods. Cores were recovered in 1.5 m runs using a 10.2 cm diameter core barrel with a button-carbide drill bit. Core materials assigned as "impacted weathered limestone unit material" and "non-impacted weathered limestone unit material" collected from inside the delineated source zone were used in this investigation. The weathered limestone unit is part of an erosional surface of the Miocene Age, and its composition includes clayey limestone, sandy limestone and limey clay. Impacted aquifer material was immediately transferred into 500 mL glass jars, sealed with a self-sealing lid held in place with a metal screw-top ring, and stored on-site in a freezer at -20 °C (see Figure

A.1(a) in Appendix A). Non-impacted aquifer material was stored in polyethylene bags (Figure A.1(b) in Appendix A). Samples of impacted aquifer material were collected from two boreholes and are representative of depths ranging from 10 to 30 m bgs, while non-impacted aquifer materials were collected from five boreholes and are representative of depths ranging from 15 to 20 m bgs. Sufficient core materials were express shipped to the University of Waterloo on ice. Samples of the impacted aquifer materials were stored at -40 °C, while samples of the non-impacted aquifer materials were stored at 4 °C. The inventory of impacted aquifer materials received was categorized into those useful for slurry treatability experiments and those more appropriate for the physical model experiments based on the quantity of NAPL present as determined visually (Figure A.2 in Appendix A).

A NAPL sample (density of 1.04 g/cm$^3$) collected from a well screened from 24 to 27 m bgs within the weathered limestone was submitted to Alpha Analytical Laboratories Westborough, MA for analyses of BTEX, total petroleum hydrocarbons (TPH), and PAHs. A summary of these results are listed in Table A-1 in Appendix A and indicate that ~34% of the NAPL mass was quantified (66% of the NAPL mass was unidentified). Consistent with the composition of others FMGP NAPLs (e.g., Brown et al. 2006) the most abundant compounds in the quantified portion of the NAPL are naphthalene (24.6 %), 2-methylnaphthalene (13.7 %), 1-methylnaphthalene (7.5 %), and acenaphthene (2.9 %).

### 2.2.2 Natural Oxidant Interaction

Naturally occurring reductants and catalysts can be reactive and thus influence oxidant persistence. Typically, the role of the dissolved groundwater species is overshadowed by the aquifer solids. Inorganic species containing iron (Fe), manganese (Mn), sulfur (S), and the natural organic matter (NOM) associated with the aquifer solids are of concern. The possibility of multiple inorganic species, as well as a range of NOM, creates an extremely heterogeneous environment in which reactions may occur. The result of the interaction between an oxidant and aquifer material leads to either an increase in the consumption of the oxidant by the aquifer solids, or an enhancement in the oxidant decomposition rate. Since the reactive species associated with the aquifer solids are finite, the oxidant consumption or natural oxidant demand (NOD) is also finite. Once the maximum NOD is satisfied there is minimal additional oxidant aquifer material interaction and, thus, any additional oxidant delivered is available to interact with the contaminant. Conversely, an enhancement in the oxidant decomposition rate implies that there is infinite interaction capacity available. To capture these behavioral differences and the associated

underlying processes for all oxidant behavior the term natural oxidant interaction (NOI) is used rather than NOD.

NOI tests were used to estimate the potential *in situ* interaction of persulfate and permanganate with non-impacted aquifer materials from three (3) representative locations. For these NOI tests the oxidant mass to solids ratio ranged from 5 to 40 g/kg (nominal). NOI tests were conducted for three persulfate systems: (1) unactivated persulfate, (2) chelated ferrous iron activated persulfate, and (3) alkaline activated persulfate. Details of the experimental procedures employed are provided in Appendix A (Tables A.2 and A.3).

### 2.2.3 Aqueous Treatability Experiments

Since the chemical oxidation of organic compounds occurs in the aqueous phase, experiments were conducted using impacted groundwater exposed to permanganate or persulfate (unactivated, ferrous iron activated (300 mg/L Fe(II) + 0.5 mol citric acid/mol Fe(II)), or alkaline activated) to determine aqueous degradation characteristics. A suite of five (5) tests was executed in well-mixed 20 mL batch reactors. Each test was performed in triplicate at a low (5 g/L) and a high (30 g/L) oxidant concentration in conjunction with appropriate experimental controls. Impacted groundwater was added to each reactor followed by the activator solution (if required) and then the oxidant. Initial reactor solution volumes were adjusted with Milli-Q water as required ensuring the same dilution of groundwater across all tests. Reactors were shaken gently by-hand daily and left in the dark at an ambient temperature of ~20 ˚C. Aliquots of the solution were taken after a reaction period of 1, 4, 8, 15 and 30 days, and analyzed for the concentrations of a suite of 28 organic compounds (Table A.4 in Appendix A) and the oxidant. The solution pH was also determined.

### 2.2.4 Slurry Treatability Experiments

A series of experiments were performed to capture the ability of the various oxidant systems (permanganate and persulfate) to degrade impacted aquifer sediments. The impacted weathered limestone unit material selected for these slurry treatability experiments were opened, emptied onto a sterilized tray and homogenized. Milli-Q water was added as required to improve mixing. Large size particles that were not suitable for this reactor design were removed by-hand during mixing. Random samples from the homogenized mixture were weighted and used without additional alteration. Prior to filling the reactors, five (5) sub-samples from the homogenized mixture were collected and used to establish the initial bulk soil concentrations. A 75 g random

sample of the impacted sediments was added to a 125 mL reactor. A 30 g/L oxidant solution (permanganate, unactivated persulfate, and alkaline activated persulfate) was added to achieve an oxidant mass to solids ratio of 30 g/kg (nominal). All reactors were constructed in replicates (4), and constantly mixed on a shaker table in the dark at an ambient temperature of ~20 ˚C. Every 7 days for a 35 day period the oxidant concentration and pH were determined, and a random sediment sub-sample from each reactor was collected and analysed to determine bulk soil concentrations. If the results from a sampling episode indicated that the oxidant concentration was depleted, additional oxidant mass was added to achieve a solution concentration of 30 g/L.

### 2.2.5 Physical Model Experiments

For the purpose of the evaluation conducted in this study we assumed that NAPL architecture that is characterized as sheens, staining, tar blebs, and tar coatings have a similar architecture with respect to the ability of a reagent solution to interact with the NAPL. When these NAPL forms are present in a permeable setting, there is a good likelihood of contact between the reagent solution and the NAPL. However, when the NAPL is present as a NAPL-saturated lense, the ratio of NAPL surface area to volume is significantly smaller and hence the reagent contact is at the surface of the NAPL and the ability to access NAPL constituents is more problematic. This ability decreases with increases in the thickness of the NAPL saturated lense or zone. The series of small-scale physical model experiments performed were designed with the intention to capture the two NAPL architecture end-points: blebs and tar coatings, and saturated lenses.

The physical model was a 7.7 cm long flow-through chamber with a cross-sectional area of 8.37 $cm^2$ (3.1 x 2.7 cm) (Figure 2.1). The influent and effluent ends of the chamber were packed with a 0.8 cm long zone of glass beads (diameter 1.6 mm) and a #20 stainless steel mesh to act as a flow distributor. The remaining 6.1 cm length was packed with impacted aquifer sediments. The chamber was sufficiently filled that when the lid was fastened it compressed the chamber contents, ensuring a seal between the top of the chamber contents and the bottom of the lid (i.e., minimized short-circuiting). For the "bleb" system, impacted materials were packed gradually in several 0.5 cm thick layers into the central portion of the physical model. For the "saturated lense" system, impacted samples were emptied directly into the bottom of the physical model to a depth of ~1.5 cm and the upper ~1.5 cm portion of the chamber was then packed with non-impacted material from the same borehole. During the filling process, five sub-samples were taken and used to establish the initial bulk soil concentrations. This system was then saturated with Milli-Q water and allowed to equilibrate for 7 days.

Following the 7-day equilibration period, flow was initiated at a nominal rate of 0.017 mL/min (approximate linear velocity of 10 cm/day). A peristaltic pump was connected to the influent end and a constant hydraulic head control was established at the outlet end. An in-line sampling system allowed aqueous samples to be collected from the effluent as required. A tracer test using NaBr was performed on each model system to ensure hydraulic consistency and packing. Following the tracer test, three oxidant injection episodes were performed. Between each episode, Milli-Q water was used to remove remnant oxidant from the system and facilitate the collection of aqueous effluent samples for analysis of organic compounds. Specifically, each physical model system was operated in the following sequence of steps:

(1) One PV of de-gassed Milli-Q water was injected to displace the pore water and allowed to equilibrate in the system for 7 days.
(2) Three to four PVs of 100 mg/L de-gassed NaBr solution were injected. During the tracer test, effluent samples were collected every 4 hours.
(3) At the end of the tracer test, an effluent sample was collected to establish a baseline effluent organic compound concentration signature.
(4) Two PVs of oxidant (permanganate or persulfate) at a concentration of 30 g/L were injected. During each oxidant injection episode, the effluent was sampled at least 4 times for EC, pH, and oxidant concentration.
(5) Three PVs of de-gassed Milli-Q water were injected. The system effluent was monitored for electrical conductivity (EC), pH and oxidant concentration during the initial 2 PVs to ensure remnant oxidant was removed from the system. During the third PV, an effluent sample was collected to determine the concentration of organic compounds in the effluent.
(6) Steps (4) and (5) were then repeated twice more.
(7) When the experimental test was concluded, the chamber lid was removed and three sub-samples equalled spaced along the length of the chamber were collected to establish post-treatment bulk soil concentrations. For the “saturated lense” system, the sub-samples were collected only from the lower ~1.5 cm portion of the chamber that contained impacted material.

Since the system PV and porosity was unknown at the start of each experiment, a nominal PV of 19.33 mL was used. This nominal PV was estimated from a porosity of 0.3 determined from a set of preliminary experiments, and the packed chamber volume of 64.45 mL (7.7 cm x 2.7 cm x 3.1 cm). Four physical systems were constructed for the "bleb" architecture, and four systems for the "saturated lense" architecture. Permanganate (30 g/L) was used for two "bleb" systems

(identified as PM-bleb-1 and PM-bleb-2), and two "saturated lense" systems (identified as PM-lense-1 and PM-lense-2). Persulfate (30 g/L) was used for the remaining two "bleb" systems (identified as PS-bleb-1 and PS-bleb-2), and two "saturated lense" systems (identified as PS-lense-1 and PS-lense-2). Based on the results from the aqueous and slurry batch experiments, persulfate activator systems were not investigated. In addition, two systems were constructed as experimental controls and identified as CO-bleb and CO-lense. The experimental controls received only de-gassed Milli-Q water.

## 2.2.6 Reagents and Analytical Methods

Potassium permanganate ($KMnO_4$, EM Science), sodium persulfate ($Na_2S_2O_8$, Sigma-Aldrich Inc.), sodium hydroxide (NaOH, Fisher Scientific), ferrous sulfate ($FeSO_4 \cdot 7H_2O$, Sigma-Aldrich), sodium bromide (NaBr, Sigma-Aldrich), citric acid ($C_6H_8O_7$, Sigma-Aldrich), and dichloromethane (DCM, EMD Millipore) were all reagent grade and used as received.

For analysis of the organic components in the aqueous phase, a 5 mL sample was mixed with 14 mL of water in a 20 mL vial. This was followed immediately by the addition of 1.0 mL of DCM (containing internal standards metafluoro-toluene (MFT) and fluoro-biphenyl (FBP) at 25 mg/L). The vial was quickly resealed and agitated on its side at 350 rpm on a platform shaker for 20 min. After shaking, the vial was inverted and the phases were allowed to separate for 30 min. Approximately 0.7 mL of the DCM was removed from the inverted vial with a gas tight glass syringe through the Teflon septum. The solvent was placed in a 2.0 mL Teflon sealed autosampler vial for injection into the gas chromatograph (GC). For the analysis of the organic components in the aquifer sediment, an ~8 g sub-sample was added directly to DCM and shaken for 18 hours. Samples were allowed to settle and 1 mL of the DCM was transferred to a 2.0 mL autosampler vial and crimp sealed with a Teflon cap. All aqueous and sediment samples were analyzed using a HP 5890 capillary GC, a HP7673A autosampler, and a flame ionization detector. Three (3) mL of methylene chloride was injected in splitless mode (purge on 0.5 min, purge off 10 min) onto a 0.25 mm x 30 m length, DB5 capillary column with a stationary phase film thickness of 0.25 µm. The helium column flow rate was 2.0 mL/min with a make-up gas flow rate of 30 mL/min. The injection temperature was 275 $^oC$, detector temperature was 325 $^oC$ and initial column oven temperature was 35 $^oC$ held for 0.5 min, then ramped up at 15 $^oC$/min to a final temperature of 250 $^oC$ and held for 2 min. A GC run time was 16 min. Data integration was completed with a SRI Model 302 Peak Simple chromatography data system. The method detection limits (MDLs) for each compound in the aqueous and sediment phases are presented in Table A.4 in Appendix A.

Using these analytical methods we are able to track ~27% of the compounds in the NAPL mass, and the behaviour of the compounds that comprise the other ~70% of the NAPL mass is unknown.

Permanganate concentration was determined by spectrophotometry (Thermo Scientific, GENESYS 10S UV-Vis) at 525 nm (MDL of 1.3 mg/L). The spectrophotometer was calibrated prior to each sampling episode with a calibration curve (1 to 100 mg/L) generated using standardized solutions. Persulfate analysis was performed following Liang et al. (2008). Bromide ($Br^-$) was analyzed using a Dionex ICS2000 Ion Chromatograph equipped with an ion eluent generator and conductivity detector. A 25-µL sample was injected using a Dionex AS-40 Autosampler onto a Dionex Ion Pac AS11-HC (4 × 250 mm) column. The mobile phase was 30 mM potassium hydroxide (KOH) at a flow rate of 1.0 mL/min. The chromatograph was obtained using Dionex Chromeleon software and the MDL was 0.5 mg/L. An Orion pH meter (model 290A) and EC meter (model A122) were used to measure pH and electrical conductivity.

### 2.2.7 Screening Model

To explore the temporal expectations for the treatment of FMGP residuals by chemical oxidants, a single-cell screening model was employed. In this system, a specified mass and composition of NAPL is assumed to be present within the sediment, and the aqueous phase is presumed completely mixed. The inlet oxidant concentration is prescribed and the effluent concentrations of the known soluble constituents are estimated from mass balance considerations. The objective of this *idealized* modeling effort was to provide insight into treatment expectations over longer time scales and under different operating conditions then those employed in the physical model experiments. It was not our intent to simulate *in situ* conditions, but rather to investigate what might be possible under ideal circumstances and hence yield the most optimistic predictor of field behavior. This screening model was deemed an appropriate tool to satisfy this requirement.

The mass balance of the individual soluble NAPL constituents is given by

$$\frac{dC_k}{dt} = -\frac{C_k}{t_r} - k_{ox,k}\, C_{ox} C_k + \lambda_k (C_k^{eff} - C_k) \tag{2.1}$$

with

$$\frac{dM_k}{dt} = -\lambda \theta (C_k^{eff} - C_k) V_s \tag{2.2}$$

$$C_k^{eff} = \frac{x_k \gamma_k S_k}{(f^S / f^L)_k} \tag{2.3}$$

and

$$t_r = \frac{L_s}{v} = \frac{\theta L_s}{q} \tag{2.4}$$

where $C_k$ is concentration of the $k^{th}$ constituent, $t_r$ is the system hydraulic residence time, $k_{ox,k}$ is the second-order reaction rate coefficient with respect to the oxidant for the $k^{th}$ constituent, $C_{ox}$ is the oxidant concentration, $\lambda_k$ is the lumped mass transfer rate coefficient for the $k^{th}$ constituent, $C_k^{eff}$ is the effective saturation of the $k^{th}$ constituent, $M_k$ is the NAPL mass associated with the $k^{th}$ constituent, $\theta$ is the system porosity, $V_s$ is the volume of the system, $x_k$ is the mole fraction of the $k^{th}$ constituent, $\gamma_k$ is the activity coefficient of the $k^{th}$ constituent, $S_k$ is the solubility of the $k^{th}$ constituent, $f^S$ and $f^L$ are the fugacity of the solid and liquid of the $k^{th}$ constituent, $L_s$ is the system length, $v$ is velocity, and $q$ is Darcy flux. Lee et al. (1992) investigated the aqueous equilibrium concentration of PAHs within coal tars and found that a modified form of Raoult's law (Eq. 2.3) is an reasonable estimation of effective concentration. The associated mass balance for the oxidant is given by

$$\frac{dC_{ox}}{dt} = -\frac{(C_{ox} - C_{ox}^{in})}{t_r} + \sum \beta_k k_{ox,k} C_{ox} C_k - \Gamma_{NOI} \tag{2.5}$$

where $C_{ox}^{in}$ is the inlet oxidant concentration, $\beta_k$ is the stoichiometric mass ratio defined as the mass of oxidant consumed per mass of constituent degraded, and $\Gamma_{NOI}$ is the rate of oxidant mass lost to the natural oxidant interaction sink reactions. Details of a representative $\Gamma_{NOI}$ expression for permanganate are provided by Xu and Thomson (2009) and for persulfate by Sra et al. (2010).

Eqs. 2.1 and 2.5 are coupled and must be solved in association with Eqs. 2.2 and 2.3 numerically. The following attributes are inherent is this screening model: (i) a completely mixed system (i.e., no preferential flow pathways and infinite dispersion); (ii) mineralization of organic compounds; (iii) the generation of by-products (e.g., manganese oxides, carbon dioxide) are ignored; and (iv) there are no diffusion limitations within the NAPL.

# 2.3 RESULTS AND DISCUSSION

## 2.3.1 Batch Experiments

The NOI profiles (average of replicates) for the selected un-impacted aquifer materials are presented in Figure A.3 in Appendix A. For the three aquifer materials tested, the maximum observed consumption of permanganate (expressed as NOD) after 30 days of exposure ranged from of 2 to 5 g/kg. The system pH remained stable between 8 and 9. The permanganate NOD manifested in these batch experiments as an initial rapid increase until Day 7 ($NOD_7$) followed by a minor increase until Day 30 as it asymptotically approached $NOD_{max}$ (Figure A.3(a) in Appendix A). The variations between the six series of experiments indicated that, consistent with Xu and Thomson (2009), a higher initial permanganate concentration as well as oxidant to solids mass ratio ($M_{ox/s}$) yielded a higher $NOD_{max}$ and a faster permanganate consumption rate.

For all three of the persulfate systems evaluated (Figures A.3(b-d) in Appendix A), there was very little loss of persulfate mass (< 10%) after the 30 day reaction period except for aquifer materials from one borehole location (identified as Sample 1) where the maximum change in persulfate concentration was ~7 g/L (17.5% decrease). The stability of persulfate in the presence of these aquifer materials implies that there is minimal NOI, and hence persulfate should be persistent *in situ*.

The data generated from the aqueous treatability experiments indicated that all of the 17 dissolved phase compounds detected in the impacted groundwater were readily degraded with persulfate or permanganate (except for benzene) to < MDL by Day 10 for the high (30 g/L) oxidant concentration systems (see Figure 2.2 for naphthalene and acenaphthene). As expected, the observed reaction rates for the dissolved phase compounds for the low (5 g/L) oxidant concentration systems were slower. While the oxidant concentration was in excess in all the high oxidant concentration systems, oxidant consumption followed the order: iron-activated persulfate > permanganate > persulfate ≅ alkaline-activated persulfate. Except for benzene, the order of reactivity of the remaining 16 quantified organic compounds was: iron-activated persulfate ≅ permanganate > persulfate ≅ alkaline-activated persulfate. Efforts were undertaken to determine a complete set of kinetic parameters (e.g., second-order reaction rate coefficients) for all 17 compounds from the data set assembled; however, due to limited temporal data only sporadic values could be estimated.

Temporal oxidant and the bulk soil concentration profiles for naphthalene and acenaphthene from the slurry experimental systems are shown in Figure 2.3. Although all attempts were made to homogenize the impacted materials prior to adding them to the reactors, there was some variability in the initial bulk soil concentrations of subsamples collected from the "stock" supply of impacted sediments and those emplaced in each reactor. The oxidant mass in the permanganate slurry reactors was replenished at Day 7 and Day 14, while the oxidant mass in the unactivated persulfate and alkaline activated persulfate slurry reactors was replenished only at Day 7. Following replenishment, permanganate continued to be depleted while the concentration of persulfate remained elevated. Compared to either of the persulfate systems explored, permanganate was more effective in treating all the target PAHs (e.g., naphthalene, 1-methylnaphthalene, 2-methylnaphthalene, and acenaphthene) over the 35-day reaction period. For the permanganate, unactivated persulfate, and alkaline activated persulfate systems it was estimated that 95%, 45% and 30% of the initial mass quantified was degraded, respectively. The overall bulk stoichiometry for these slurry experiments was estimated as the ratio of permanganate or persulfate consumed to the quantified mass degraded. This estimate varied from 100 g-$KMnO_4$/g for the permanganate system and 95 g-$NaS_2O_8$/g for the unactivated persulfate system to 150 g-$NaS_2O_8$/g for the alkaline activated persulfate system. These stoichiometric values are consistent in magnitude with those reported by Sra et al. (2013) for the total petroleum hydrocarbon (TPH) of dissolved gasoline degraded by various persulfate systems. This data set provides insight into the ability of the investigated oxidant systems to destroy mass present in impacted aquifer materials under ideal conditions (i.e., well mixed, excess oxidant, long contact time) and hence are the most optimistic.

## 2.3.2 Physical Models

After 1 to 2 PVs of NaBr injection, the effluent concentration of bromide reached ~50% of the injected concentration (100 mg/L), and after 3 to 4 PVs reached 100% for all physical models. Based on the tracer test breakthrough profiles the effective porosity for CO-bleb and CO-lense was 0.26, and 0.38 respectively, and ranged from 0.27 to 0.38 for the treatment bleb physical models, and from 0.33 to 0.36 for treatment lense physical models.

For the control systems (CO-bleb and CO-lense) the effluent pH was steady between 7.5 and 8, and the EC was minimal (< 300 µS/cm) as expected. The concentrations of the detectable organic compounds in the effluent from both control systems were relatively constant except for a notable decrease in the concentration of benzene. The final bulk soil concentrations were essentially

unchanged from the initial soil concentrations except for benzene. Benzene was quickly depleted from the system as a result of a higher solubility and lower initial soil concentration compared to other compounds in the system.

For both permanganate systems (PM-bleb and PM-lense) the average naphthalene and acenaphthene effluent concentrations following each oxidant injection episode (~2 PVs/episode) decreased (Figure 2.4(a, b)). In contrast, the average naphthalene and acenaphthene effluent concentrations following each oxidant injection episode (~2 PVs/episode) for the persulfate systems either remained relatively constant (PS-bleb) or increased (PS-lense) (Figure 2.4(c, d)). These trends were generally consistent for the other monitored compounds except for benzene which remained relatively constant following each persulfate injection episode in the PS-bleb and PS-lense systems.

The average maximum permanganate effluent concentration was ~15 g/L during the first injection episode and increased to ~17 g/L during the second and third injection episodes for the PM-bleb physical models, and was ~17 g/L during the first injection episode and ~20 g/L during the second and third injection episodes for the PM-lense systems. The average maximum persulfate effluent concentration for the PS-bleb physical models was ~23 g/L during the first injection episode and increased to ~25 g/L during the second and third injection episodes. For the PS-lense physical models the average maximum persulfate effluent concentration was ~25 g/L for all injection episodes. The significant reduction of the effluent permanganate or persulfate concentration to near the MDL during the injection of ~3 PVs of de-gassed Milli-Q water (see Figure A.4 in Appendix A) indicated that remnant oxidant was removed from the experimental system prior to collection of an effluent sample for analyses of organic compounds. The effluent EC profiles were consistent with the permanganate or persulfate effluent profiles.

The effluent pH for the PM-bleb physical models increased from 7.3 to 9.5 with minor decreases when permanganate was present in the system. In contrast, the effluent pH for the PM-lense physical models oscillated between 7.6 and 9.4. The effluent pH remained relatively stable at 7.9 for the PS-belb and 7.6 for the PS-lense systems.

An evaluation of the initial and final bulk soil concentration data indicated that for the PM-bleb system there was a statistically significant reduction in the total quantifiable mass of ~30%. This reduction was a result of significant reductions in the concentration of naphthalene, 1-methylnaphthalene, 2-methylnaphthalene, and acenaphthene. While the PS-bleb system also experienced a decrease in the total quantifiable mass (~10%), this observed magnitude was not

statistically significant at the 5 % level of significance. The high variability in both the initial and final bulk soil concentration data for the PM-lense and PS-lense systems prevented any conclusions relating to the mass degraded to be drawn. It is suspected that the inherent variability in the soil sub-sampling procedure used and the contaminant heterogeneity present in the lense physical models was the root cause.

Oxidant mass balance calculations for the bleb systems indicated that 50 and 17 % of the permanganate and persulfate mass injected was consumed, respectively; while for the lense systems 35 and 19 % of the permanganate and persulfate mass injected was consumed, respectively. Hence, while persulfate consumption was similar in the bleb and lense systems, permanganate consumption in the bleb systems was more significant and can be attributed to higher NAPL-aqueous phase contact area. During the 3 oxidant injection episodes (6 PVs total), elevated oxidant concentrations (> 5 g/L) were present for a total residence or contact time of ~8 days. The oxidant resident time was controlled by the flow rate which was established to yield a moderate linear velocity of 10 cm/day. It was not the objective of these physical model experiments to degrade all the mass present but rather to determine treatment expectations under realistically aggressive conditions. If the intent was to degrade all the mass present then ~50 g of oxidant would have been required to degrade 100 % of the initial quantified mass in either the bleb or lenses system. This oxidant demand estimate is based on a stoichiometry ~100 g-oxidant/g of the initial quantified mass estimated from the slurry experiments. The bulk soil concentration of the aquifer material used in the lense system was about 100 % larger than that using in the bleb system but only half of the physical model was filled with impacted material. Each physical model received a total of ~5 g of oxidant, or about 10 % of the stoichiometric requirement delivered in 6 PVs. A typical injection event at the field-scale is less than 1 PV (Crimi et al., 2011) so it would be a significant effort involving multiple mobilizations over several months to deliver this stoichiometric requirement.

Overall the data from these experiments indicate that the behavior of the physical models with the lense architecture was similar to those with the bleb architecture. Permanganate outperformed persulfate in terms of impacting a change to the system effluent concentration and bulk soil concentration; albeit this change was minor (there was an insignificant change for persulfate). Despite the observation of better efficiency in the permanganate systems, the total mass removal was low for both systems and hence the benefit of flushing 6 PVs of permanganate or persulfate at a concentration of 30 g/L under the physical model operating conditions was minimal.

## 2.3.3 Screening Model Simulations

2.3.3.1 Parameterization

Consistent with the physical model dimensions, the system length and cross-sectional area were set equal to 7.7 cm and 8.37 $cm^2$ respectively. Overall this screening model was able to capture the hydraulic and solute transport behaviour observed in the small-scale physical model systems well (see Figure A.5 in Appendix A). The effective porosity values estimated were: 0.28 for PM-bleb, and 0.35 for PM-lense, PS-bleb, and PS-lense. These porosity values are close to the assumed value of 0.3 which was used for the initial nominal PV calculation. The system velocity was assigned a value of 10 cm/day which is consistent with the average flow rate, cross-sectional area and effective porosity used for the physical model systems.

To reduce model complexity, 22 representative organic compounds (Table 2.2) were extracted from the NAPL analytical results (Table A.1 in Appendix A) and used to represent the initial NAPL composition. These 22 compounds represent 29% of the NAPL mass and the remaining bulk NAPL mass include some identified compounds (~5%) and the unidentified fraction (~66%). NAPL saturation for each physical model system was estimated from the initial bulk soil concentration data, bulk density and NAPL composition. The average NAPL saturation values estimated were: 6.4% for PM-bleb, 6.6% for PM-lense, 4.3% for PS-bleb, and 7.9% for PS-lense. Representative NAPL constituent solubility and fugacity data were obtained from the literature (Lide 1999; Eberhardt & Grathwohl 2002; Thomson et al. 2008; Peters et al. 1997).

Since higher treatment efficiency was observed in the physical model systems using permanganate, we choose to focus exclusively on permanganate in these screening model simulations. Literature values (Forsey et al., 2010; Forsey, 2004; Thomson et al., 2008) for the second-order oxidant reaction rate coefficients for permanganate were used for most of the 22 representative organic compounds (Table 2.2). Missing second-order oxidant rate coefficient values were assumed based on structure and trends observed from the aqueous batch experiments. Theoretical values were used for the permanganate/organic compound stoichiometry mass ratio (β) (Table 2.2).

The lumped mass transfer rate coefficient (λ) captures the complex dissolution process within the system reflecting, among other factors, the NAPL architecture. This parameter was determined through a calibration procedure that involved the minimization of the sum-of-squares of the difference between the observed and simulated baseline concentrations for first sampling episode

(Step 3) for the four physical model systems explored (see Figure A.6 in Appendix A for an example scatter plot). The average estimated value for λ was 0.09/day for the PM-bleb systems, and 0.14/day for PM-lense system. The higher λ value for the lense system is presumably due to the higher NAPL saturation which results in more NAPL-water contact area and higher dissolution rate.

The observed tracer test behaviour in conjunction with the initial NAPL saturation estimates and the lumped mass transfer coefficient values indicate that, despite all attempts to create two distinct NAPL architectures, both the bleb and lense systems were very similar. This is consistent with the experimental observations.

2.3.3.2 Benchmarking

The parameterized model was used to simulate the two permanganate physical model systems (PM-bleb, and PM-lense). The overall mass of permanganate consumed required adjustment so that the simulated effluent permanganate concentration profiles matched the observed effluent permanganate concentration profiles. This adjustment involved scaling the mass of oxidant consumed at each model time step by a factor of 180. This scaling resulting in ~1.3 g of additional permanganate being consumed likely as a result of NOD reactions (~0.8 g), unsuitable permanganate/organic compound stoichiometry mass ratios used, and oxidation of other organic compounds that were not considered in the model. Figures 2.5 and 2.6 show the simulated effluent concentrations for permanganate and five representative organic compounds (benzene, naphthalene, 1-methylnaphthalene and 2-methylnaphthalene, and acenaphthene) for the PM-bleb and PM-lense systems, respectively. The concentration of all the organic compounds initially decrease from equilibrium conditions as mass is being removed from the system by washout until the first permanganate injection episode occurs at 6 PVs. When permanganate is present in the system all the reactive compounds are degraded to < MDL and then rebound once the injection solution is switched to Milli-Q water. Benzene is not reactive with permanganate and hence follows a steady dissolution profile. Since average parameter values were used for the bleb and lense systems there is a slight mismatch in timing compared to the effluent observations. The developed screening model was able to capture the general behavior (trends and concentration magnitude) observed in the small-scale physical model experiments.

2.3.3.3 Long-Term Simulations and Sensitivity

To investigate long-term treatment expectations the constrained screening model was used to simulate system behaviour over a 10-year period following treatment. The following scenarios were performed:

i. *Baseline Scenario* - representative of the PM-bleb system with 6 PVs of permanganate (30 g/L) injected in 3 episodes.
ii. *No-treatment/Natural Dissolution Scenario* - representative of the CO-bleb system.

In addition, the sensitivity of the *Baseline Scenario* to changes in pore velocity, injected oxidant concentration, mass transfer rate coefficient, and NAPL saturation were investigated. In particular, the following simulations were performed (the underlined values represent baseline conditions):

i. Pore velocity variation (1, 10 and 100 cm/day)
ii. Oxidant concentration variation (30 vs 100 g/L)
iii. Mass transfer rate coefficient ($\lambda$) variation (0.09, 0.18, 1.8 /day)
iv. NAPL saturation ($S_n$) variation (0.1, 1, 6.4 %)

Figure 2.7 shows the long-term simulation results for the PM-bleb system with and without treatment. As expected the organic compound concentrations are reduced temporality as a result of the injection of 6 PVs of permanganate and then rebound to a profile that is essentially coincident with a no-treatment/natural dissolution scenario. These results indicate that injecting 6 PVs of permanganate which is considered an aggressive approach will not materially affect the long-term behavior of dissolved phase concentrations relative to the *No-treatment Scenario*.

The sensitivity of the *Baseline Scenario* effluent concentrations to changes in pore velocity (1, 10 and 100 cm/day) is presented in Figure 2.8. The mismatch in timing of the oxidant injection episodes results from the different durations for each PV (i.e., 7.7, 0.77, and 0.077 day). The pore velocity directly affects the contact or system residence time. For the lower velocity of 1 cm/day the permanganate effluent concentration reaches a maximum of ~0.04 g/L indicating that most of the permanganate mass has been consumed. However, as a result of the increased residence time the effluent concentrations of the organic compounds for the velocity of 1 cm/day are ~5 times higher than those generated from the *Baseline Scenario*. The pore velocity of 100 cm/day yielded the highest effluent permanganate concentration and the lowest effluent organic compound concentrations as a result of the lower residence time. The mass degraded by

permanganate for a velocity of 1 cm/day is 2 and 22 times larger than the mass degraded for a velocity of 10 and 100 cm/day, respectively. The total PVs flushed during 10 years for a velocity 100 cm/day is 10 and 100 times higher than for a velocity of 10 and 1 cm/day. However, after 10 years, the effluent organic compound concentrations have not changed significantly with 35, 33, and 24% of the initial mass quantified removed for a velocity of 100, 10, and 1 cm/day, respectively. Only 0.04, 0.3, and 1.2% of the total mass loss from the system was degraded by permanganate for a velocity of 100, 10, and 1 cm/day, respectively. Hence, changes in the system residence time did not significantly increase the mass removed.

The sensitivity of the of the *Baseline Scenario* effluent concentrations to changes in the injected permanganate concentration is presented in Figure 2.9. While the effluent permanganate concentrations are significantly different, the effluent organic compound concentrations are similar over the 10-year simulation period. This confirms that the *Baseline Scenario* was not permanganate mass depleted nor would a higher permanganate concentration increase mass removal. The simulation results show that if oxidizable organic compounds are present in the aqueous phase that there is sufficient permanganate mass in the system to degrade them.

As expected, by increasing the lumped mass transfer rate coefficient the effluent permanganate concentration decreases and the effluent organic compound concentrations increase (Figure 2.10). Increasing the lumped mass transfer rate coefficient increases the dissolution rate and allows more mass of organic compounds to be transferred into the aqueous phase. A lumped mass transfer rate coefficient of 1.8 /day significantly influences the long-term behavior of dissolved phase concentrations and after 1000 days the effluent concentrations of organic compounds significantly decrease except for benzene which is depleted much faster. After 10 years, 33, 48, and 76% of the initial mass quantified was removed for a lumped mass transfer rate coefficient of 0.09, 0.18, and 1.8 /day, respectively. Only 0.3, 0.4, and 0.5% of the total mass loss from the system was degraded by permanganate for a lumped mass transfer rate coefficients of 0.09, 0.18, and 1.8 cm/day, respectively.

The sensitivity of the *Baseline Scenario* effluent concentrations to the changes in the initial NAPL saturation is presented in Figure 2.11. The effluent permanganate concentration is identical; however, the long-term effluent organic compound concentrations are influenced for the initial NAPL saturation < 1%. After 10 years, 33, 71, and 94% of the initial mass quantified was removed for a NAPL saturation of 6.4, 1.0, and 0.1%, respectively. Approximately 0.3, 1.0, and 7.2 % of

the total mass loss is degraded by permanganate for an initial NAPL saturation of 6.4, 1.0, and 0.1% respectively.

These sensitivity results indicate that scenarios that involved a lower velocity (1 cm/day compared to 10 cm/day) and a higher oxidant concentration (100 g/L compared to 30 g/L) were unable to significantly alter the long-term effluent profiles of the organic compounds. Alternatively, increasing the lumped mass transfer rate coefficient from 0.09 to 1.8 can affect the long-term behavior of dissolved phase concentrations. These results provide additional evidence that treatment efficiency is mass transfer limited in this system. The scenarios investigated clearly indicate that chemical oxidant treatment (6 PVs at 30 g/L) may be effective for regions where mass is present at low NAPL saturations (< 1%).

## 2.4 SUMMARY

The focus of the research effort reported in the paper was to investigate the performance of persulfate and permanganate to degrade FMGP residuals in a dynamic flow system representative of *in situ* conditions, and to explore treatment expectations and the potential long-term system behavior. The key findings determined are:

- Approximately 29% of the NAPL mass was quantified (72% unidentified, labeled as bulk NAPL); hence our understanding of the behavior of the bulk NAPL mass is uncertain. However, based on analytical data collected the bulk NAPL is generally considered to consist of low solubility components and as a result is not readily treated by chemical oxidants.
- The dissolved phase components were readily treatable with persulfate or permanganate (except for benzene) in well-mixed aqueous and slurry batch systems. This demonstrates that when organic components are dissolved and in contact with the oxidant they can be readily degraded.
- As a result of the well-mixed conditions employed, the batch experiment results provide the most optimistic outcome and can be used to bound the expectations for the effectiveness of chemical oxidation of MGP residuals.
- The physical model experiments were performed to evaluate the effects of 6 PVs of oxidant treatment (3 injection episodes at 2 PVs/episode) by a chemical oxidant. This is considered an aggressive ISCO approach. Permanganate outperformed persulfate in terms of impacting a change to the system effluent concentration and bulk soil concentration. Despite this observation, the total mass removal was low for both systems and hence the benefit of flushing

6 PVs of permanganate or persulfate at a concentration of 30 g/L under the physical model operating conditions was minimal.

- The screening model was used to estimate long-term expectations of dissolved phase concentrations following ISCO treatment. The model input parameters were constrained by literature data and the physical model experimental results. The model projected the following, after treatment of blebs or lenses of NAPL with 6 PVs of oxidant:
  - The results from scenarios that involved a NAPL saturation of between approximately 4 and 8% illustrated that, following the oxidant injection episodes, the long-term effluent profile of representative organic compounds were unaffected.
  - Long-term simulation results over a 10-year period indicate that representative organic compounds are reduced temporality as a result of the oxidant applications and then rebound to a profile that is coincident with a natural dissolution / no-treatment scenario.
  - Scenarios that involved a slower velocity (1 cm/day compared to 10 cm/day) and higher oxidant concentration (100 g/L compared to 30 g/L) were unable to significantly alter the long-term concentrations of representative organic compounds.
  - The results from scenarios that involved a lower initial NAPL saturation of <1% illustrated that the long-term effluent profiles of the representative organic compounds were affected.
  - By increasing the lumped mass transfer rate coefficients (from 0.09 to 1.8 /day) the long-term effluent profiles of the representative organic compounds were affected and after ~3 years were < MDL. This evidence is strongly suggestive that successful treatment with chemical oxidants is mass transfer limited.

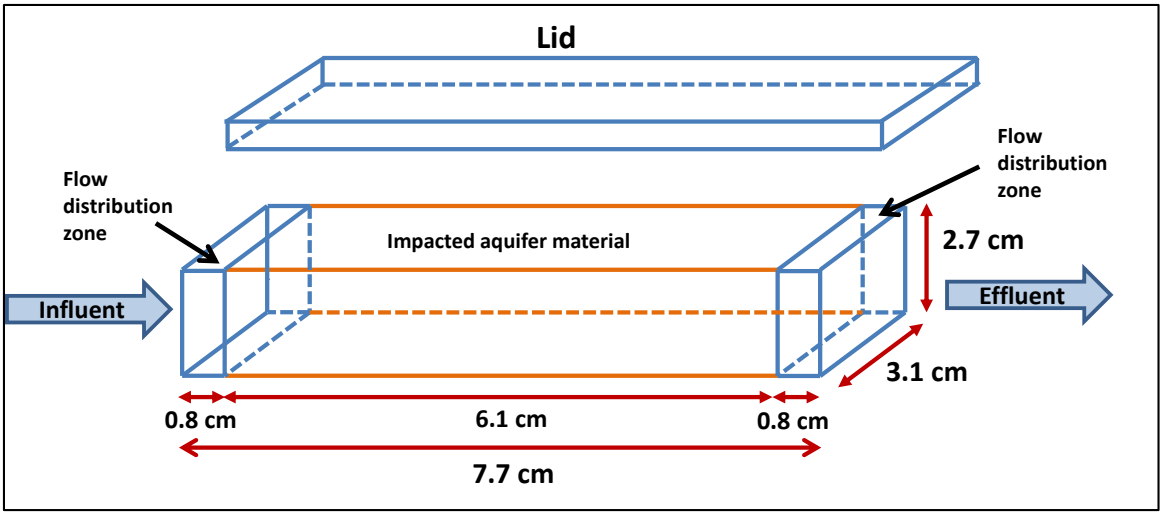


**Figure 2.1:** Schematic of physical model chamber with a length of 7.7 cm and cross-sectional area of 8.37 $cm^2$ (3.1 cm x 2.7 cm). The influent and effluent ends were packed with a 0.8 cm long zone of glass beads. The interior 6.1 cm long zone was packed with impacted aquifer materials.

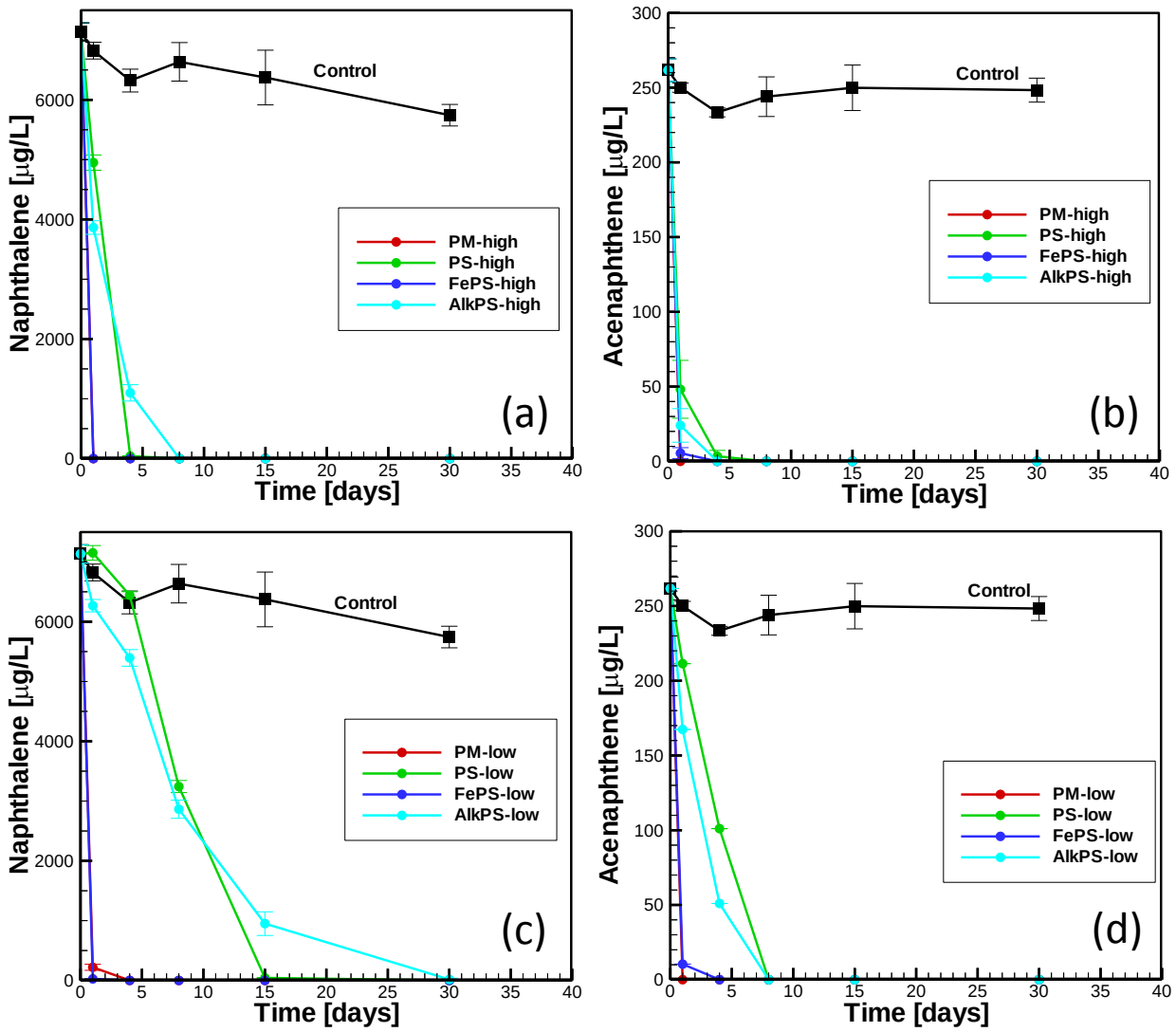


**Figure 2.2:** Temporal concentration profiles of (a, c) naphthalene and (b, d) acenaphthene in impacted groundwater exposed to various oxidant systems (permanganate (PM), persulfate (PS), iron activated persulfate (FePS), and alkaline activated persulfate (AlkPS)) at high (30 g/L) and low (5 g/L) concentrations. The error bars represent the standard deviation from triplicate reactors.

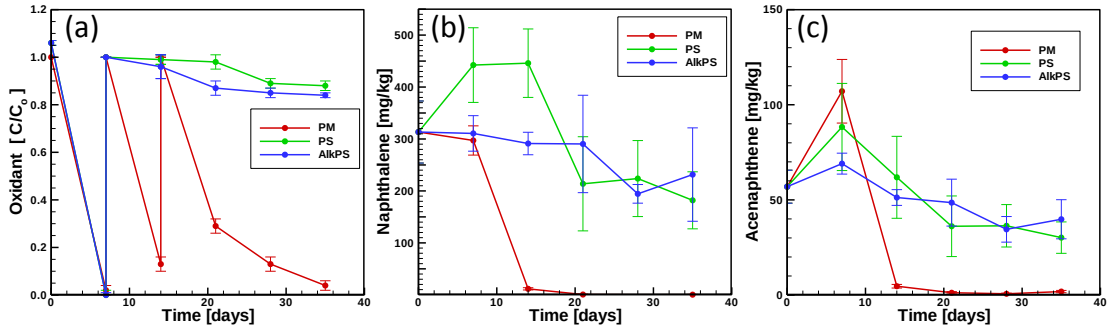


**Figure 2.3:** Temporal concentration profiles of (a) oxidant, (b) naphthalene, and (c) acenaphthene from the slurry experiments. The initial oxidant mass to solids ratio was 30 g/kg for the persulfate (PS), permanganate (PM), and alkaline activated persulfate (AlkPS) systems. The initial oxidant concentration was 30 g/L for all systems. The error bars represent the standard deviation from four replicates.

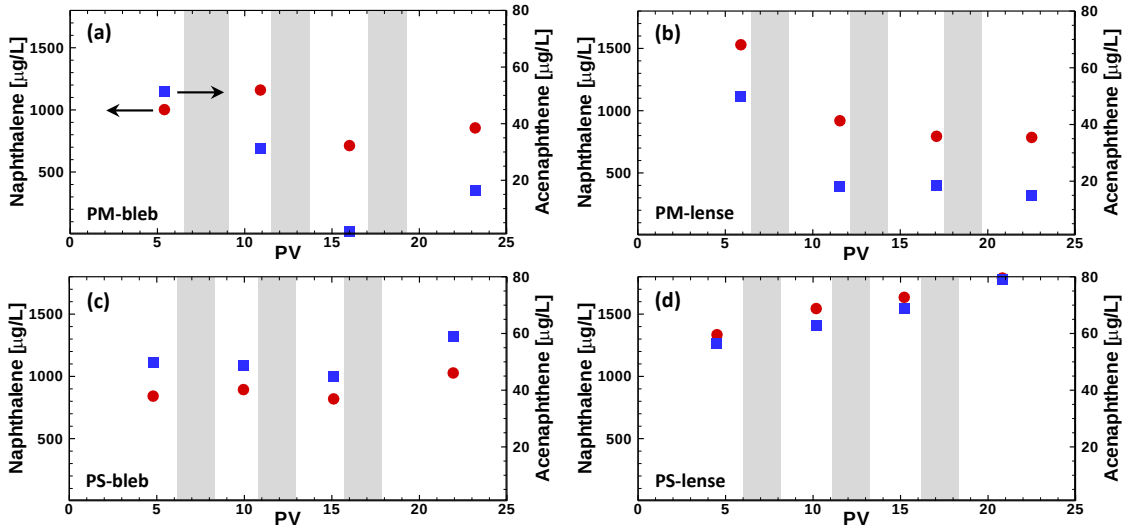


**Figure 2.4:** Effluent concentrations for naphthalene (●; left axis) and acenaphthene (■; right axis) from the (a) PM-bleb, (b) PM-lense, (c) PS-bleb and (d) PS-lense physical model experiments. Each data point represents the average from the duplicate physical models. The shaded bands represent the average PV intervals when permanganate or persulfate was injected into each physical model.

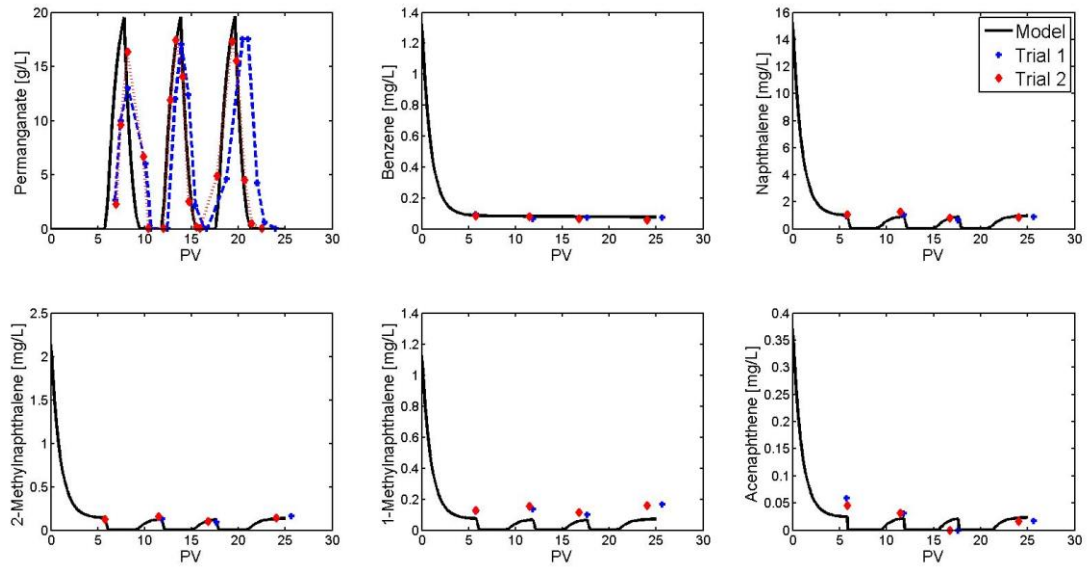


**Figure 2.5:** Simulated effluent concentrations for permanganate and five representative organic compounds (benzene, naphthalene, 1-methylnaphthalene and 2-methylnaphthalene, and acenaphthene) for PM-bleb systems. Also shown are observed effluent concentrations. (Note: initial equilibrium concentrations were assumed in the simulations).

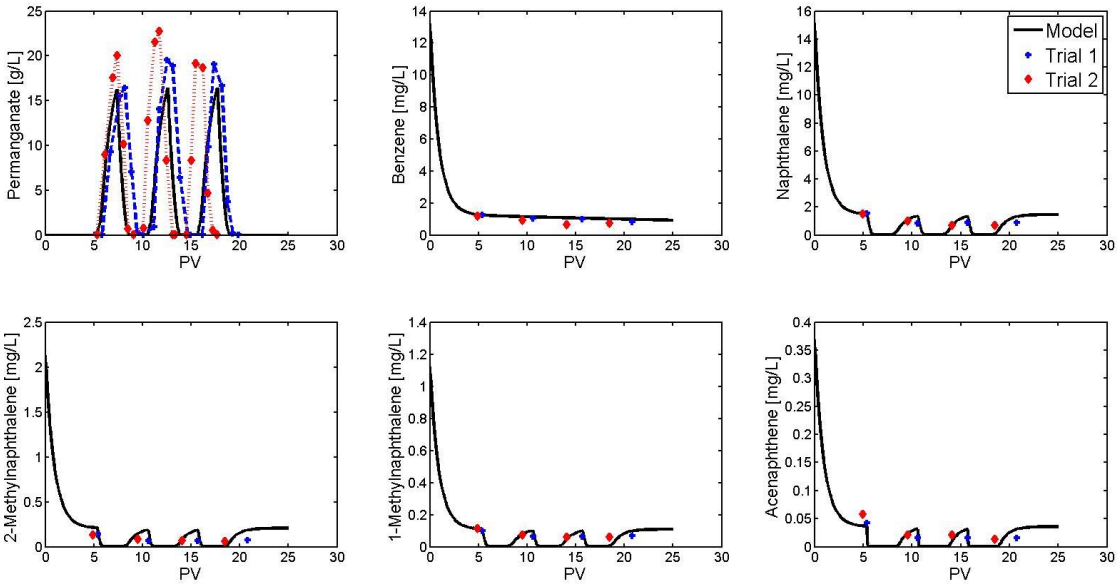


**Figure 2.6:** Simulated effluent concentrations for permanganate and five representative organic compounds (benzene, naphthalene, 1-methylnaphthalene and 2-methylnaphthalene, and acenaphthene) for PM-lense systems. Also shown are observed effluent concentrations. (Note: initial equilibrium concentrations were assumed in the simulations).

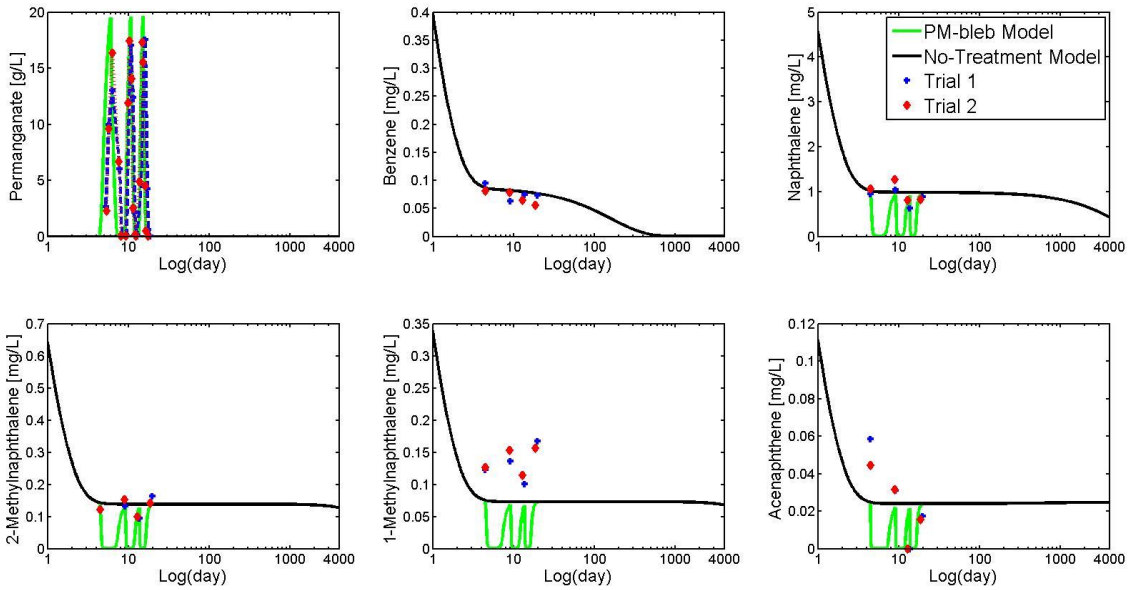


**Figure 2.7:** Simulated long-term effluent concentrations for permanganate and five representative organic compounds (benzene, naphthalene, 1-methylnaphthalene and 2-methylnaphthalene, and acenaphthene) for the PM-bleb system with and without treatment. Also shown are observed concentrations. (Note: initial equilibrium concentrations were assumed in the simulations).

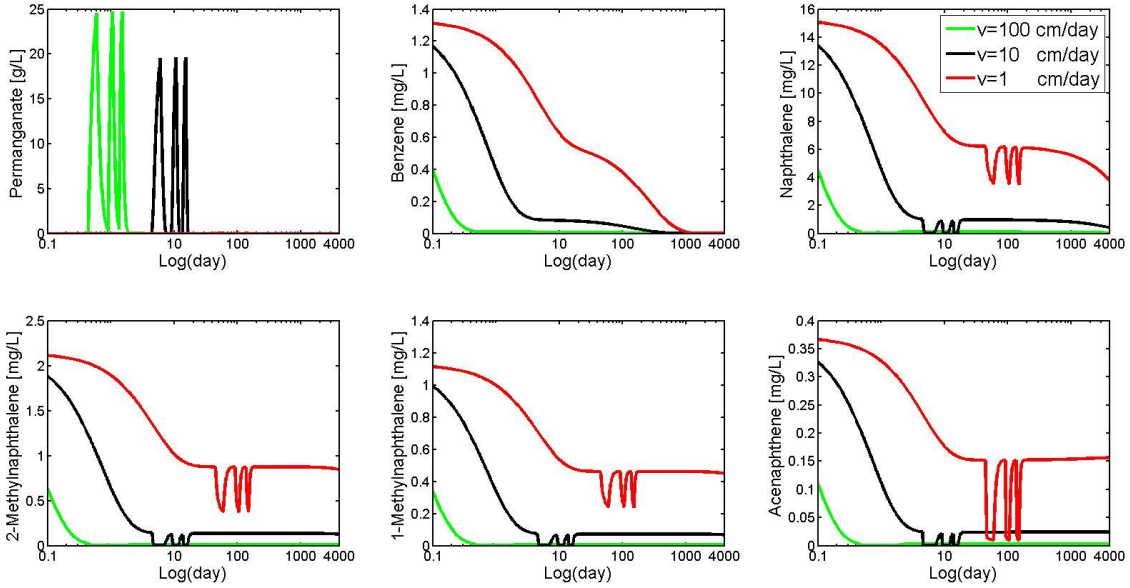


**Figure 2.8:** Sensitivity of the simulated long-term effluent concentrations for permanganate and five representative organic compounds (benzene, naphthalene, 1-methylnaphthalene and 2-methylnaphthalene, and acenaphthene) for the PM-bleb system to changes in pore velocity. (Note: initial equilibrium concentrations were assumed in the simulations).

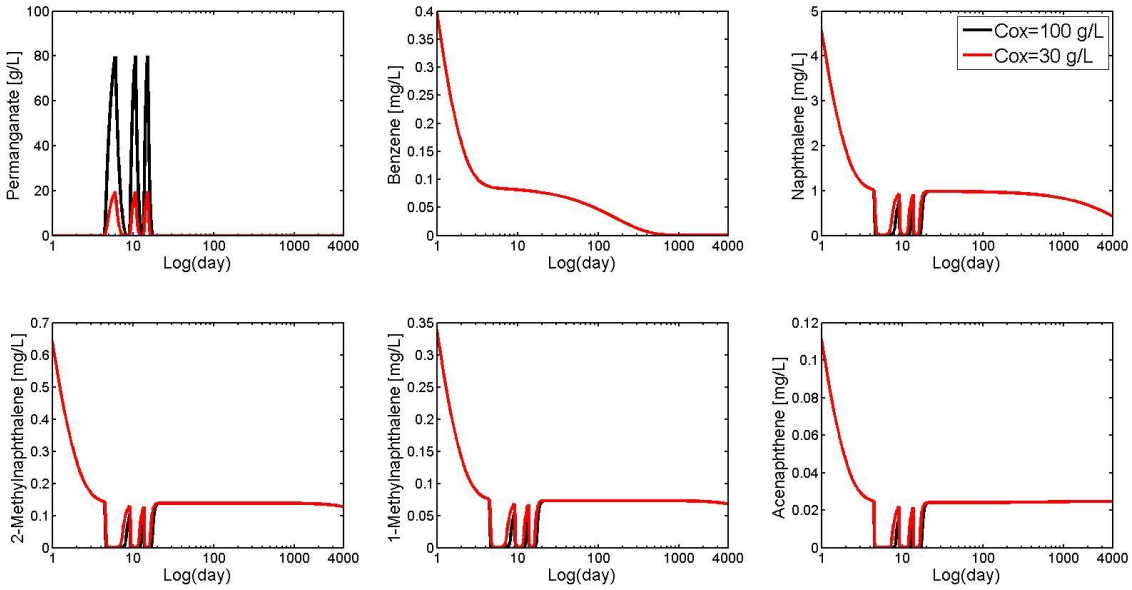


**Figure 2.9:** Sensitivity of the simulated long-term effluent concentrations for permanganate and five representative organic compounds (benzene, naphthalene, 1-methylnaphthalene and 2-methylnaphthalene, and acenaphthene) for the PM-bleb system to changes in oxidant (Note: initial equilibrium concentrations were assumed in the simulations).

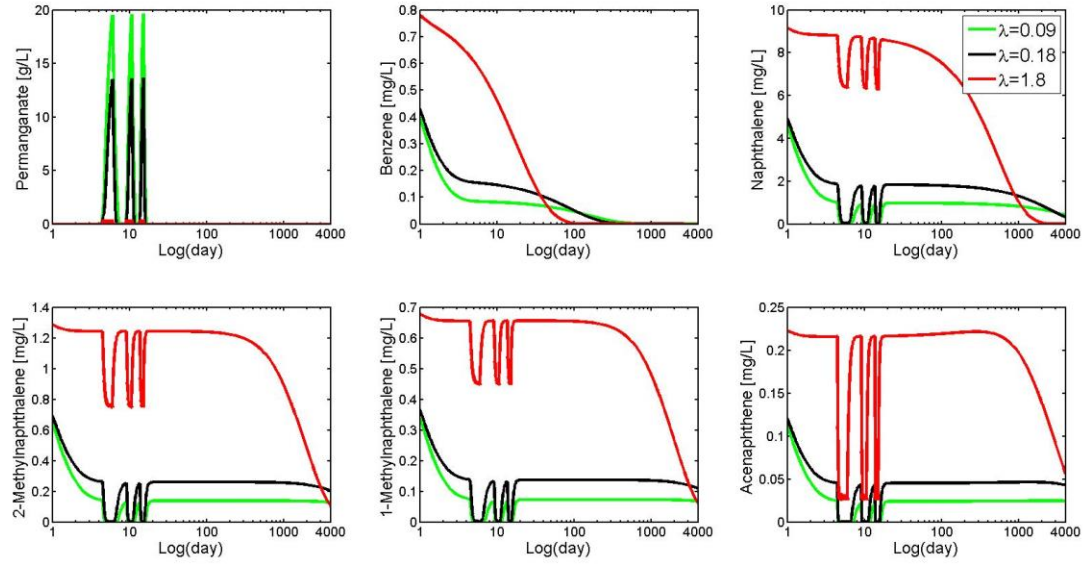


**Figure 2.10:** Sensitivity of the simulated long-term effluent concentrations for permanganate and five representative organic compounds (benzene, naphthalene, 1-methylnaphthalene and 2-methylnaphthalene, and acenaphthene) for the PM-bleb system to changes in mass transfer rate coefficient. (Note: initial equilibrium concentrations were assumed in the simulations).

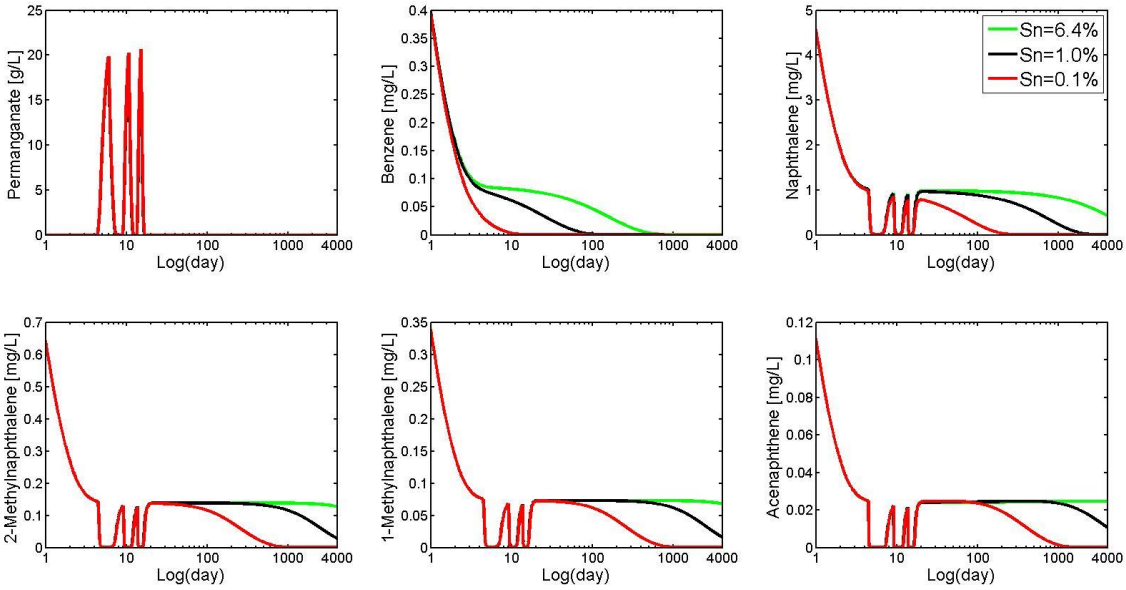


**Figure 2.11:** Sensitivity of the simulated long-term effluent concentrations for permanganate and five representative organic compounds (benzene, naphthalene, 1-methylnaphthalene and 2-methylnaphthalene, and acenaphthene) for the PM-bleb system to changes in NAPL saturation. (Note: initial equilibrium concentrations were assumed in the simulations).

**Table 2.1:** Summary of published bench-scale studies which have used either persulfate or permanganate to degrade FMGP residuals.

| Source | Experimental System | Reaction time or PVs | Material | Organic Concentration | Oxidant System(s) | Oxidant Dose | Removal in soil [%] |
|---|---|---|---|---|---|---|---|
| This study | batch[1], physcial model | batch: 5 weeks, physcial model: 6 PVs | FMGP impacted aquifer material | BTEX = 0.02 & $PAH_T$ = 3.54 g/kg soil (23 compounds)[10] | 30 g/L permanganate, 30 g/L persulfate and 30 g/L alkaline activated persulfate | batch:~8.5 g oxidant/g PAH, physical model:~10 g oxidant/g PAH | permanganate batch:~95% of $PAH_T$, persulfate batch:~70% of $PAH_T$, physical model: no significant PAH removal |
| Peng et al. (2016) | batch[2] | 120 min | spiked soil | $PAH_T$[11] = 6.87 g/kg (20 compounds) | 50 g/L ultrasound-heat-activated persulfate (80 °C) | ~29 g oxidant/g PAH | ~85% of $PAH_T$ |
| Cassidy et al. (2015) | batch[3] | 1 week | FMGP impacted soil | BTEX = 0.58 & $PAH_T$ = 3.06 g/kg soil (18 compounds) | 36.6 g/L alkaline activated persulfate | ~5 g oxidant/g PAH | 55% of BTEX & 64% of $PAH_T$ |
| Wang et al. (2015) | batch[4] | 3 hr | coal tar pitch | $PAH_T$ = 76.50 g/kg (7 compounds) | 31.6 g/L permanganate | ~2 g oxidant/g PAH | 62.5% of carcinogenicity removed |
| Hauswirth et al. (2014) | column | 52 PVs | FMGP impacted soil | $PAH_T$[12] = 1.99 g/kg (25 compounds) | 50 g/L persulfate & 0.2 M NaOH | ~330 g oxidant/g PAH | 53% of $PAH_T$ |
| Usman et al. (2012) | batch[5] | 1 week | FMGP impacted soil | $PAH_T$ = 1.3 g/kg soil (16 compounds) | iron-activated persulfate (molar ratio 1:1) | not reported | no PAH removal |
| Richardson et al. (2011) | batch[6], column | batch: 16 days, column: 6 PVs | FMGP impacted soil | $PAH_T$ = 0.295 g/kg soil (14 compounds) | 20 g/L heat-activated persulfate (40 °C) | ~91 g oxidant/g PAH | batch: 47% of $PAH_T$, column: no significant PAH removal |
| Ferrarese et al. (2008) | batch[7] | until consumption of oxidant | canal sediment | $PAH_T$ = 2.8 g/kg soil (16 compounds) | 158 g/L permanganate, and 120 g/L Fe activated persulfate (Fe:oxidant molar ratio of 1:25) | 188 g permanganate/g PAH; 142 g persulfate/g PAH | permanganate: 96% of $PAH_T$, persulfate: 88% of $PAH_T$ |
| Nadim et al. (2005) | batch[8] | 24 hr | FMGP impacted soil | $PAH_T$ = 0.01 g/kg soil (7 compounds) | 5 g/L persulfate + 0.124 g/L Fe-EDTA | ~1500 g oxidant/g PAH | 75 to 100% of $PAH_T$ |
| Brown et al. (2003) | batch[9] | 30 min | spiked soil | $PAH_T$ = 0.73 g/kg soil (6 compounds) | 25 g/L permanganate | ~68.5 g oxidant/g PAH | 8 to 72% of $PAH_T$ |

Notes:

1. 125 mL reactors filled with 75 g of impacted material and 75 mL oxidant solution, mixed and left in the dark.
2. 5 g surficial soil with 100 mg of laboratory grade coal tar added to a 40 mL vial and mixed with 20 mL oxidant solution.
3. 2.5 L reactors filled with 3 kg soil and mixed with a blender.
4. 20 g crushed coal tar pitch and 100 mL oxidant solution placed in 250 mL reactor and mixed on a shaker.
5. 2 g soil in 20 mL oxidant solution.
6. Batch data not reported.
7. 30 g sediment mixed with 100 mL solution, reactors periodically shaken.
8. 250 mL reactor mixed on a shaker (liquid : soil ratio = 3.33)
9. 250 mL reactor filled with 50 g soil and 100 mL of oxidant solution; continuously stirred.
10. Number of quantified PAH compounds.
11. Estimated from data provided.
12. Estimated from data provided, and assuming a NAPL density of 1.1 g/mL and a bulk density of 1.7 g/mL.

**Table 2.2:** NAPL composition, molecular weight (MW), solubility, fugacity ratio ($f^S/f^L$), permanganate second-order reaction rate coefficient (*k*), and permanganate/constituent stoichiometry (β) for the representative organic compounds using in the model simulations.

| Organic Compound | Concentration [mg/kg] | MW [g/mol] | Solubility [mg/L] | $f^S/f^L$ [-] | *k* [L/g/day] | β [g/g] | Comment |
|---|---|---|---|---|---|---|---|
| **BTEX** | | | | | | | |
| Benzene | 2640 | 78.1 | 1780 | 1.00 | 0 | 20.2 | from Forsey et al. (2010) |
| Ethylbenzene | 4480 | 106.2 | 161.2 | 1.00 | 3.31 | 20.8 | from Forsey (2004) |
| Xylene(s) | 2618 | 106.0 | 173.5 | 1.00 | 0.389 | 20.8 | estimate based on toluene |
| Toluene | 32.3 | 92.1 | 534.8 | 1.00 | 0.389 | 20.6 | estimate based on ethylbenzene |
| **Trimethylbenzenes** | | | | | | | |
| Trimethylbenzene(s) | 3750 | 120.2 | 57.4 | 1.00 | 0.288 | 21.0 | estimate based on methylethylbenzene |
| **Methylethylbenzene** | | | | | | | |
| Methylethylbenzene(s) | 2275 | 120.2 | 94 | 1.00 | 0.288 | 21.0 | from Forsey (2004) |
| **PAHs** | | | | | | | |
| 1-Methylnaphthalene | 25500 | 142.2 | 28.5 | 1.00 | 7.34 | 20.0 | from Forsey (2004) |
| 2-Methylnaphthalene | 46700 | 142.2 | 25.4 | 0.86 | 10.5 | 20.0 | from Forsey (2004) |
| 2,6-Dimethylnaphthalene | 11500 | 156.2 | 2.0 | 1.00 | 14.4 | 20.2 | estimate based on methylnaphthalene |
| Acenaphthene | 13300 | 154.2 | 3.9 | 0.20 | 115 | 19.8 | from Forsey (2004) |
| Acenaphthylene | 4050 | 152.2 | 9.8 | 0.22 | 6.05 | 19.4 | estimate based on naphthalene |
| Anthracene | 6280 | 178.2 | 0.05 | 0.01 | 288 | 16.2 | estimate based on phenanthrene |
| Biphenyl | 4990 | 154.2 | 7.5 | 1.00 | 0 | 0.0 | from Forsey et al. (2010) |
| Chrysene | 2810 | 228.2 | 0.002 | 0.01 | 6.78 | 19.4 | from Forsey (2004) |
| Dibenzofuran | 1500 | 168.2 | 10.0 | 0.25 | 0 | 16.9 | from Forsey et al. (2010) |
| Fluoranthene | 7930 | 202.3 | 0.26 | 0.21 | 475 | 19.2 | from Forsey (2004) |
| Indane | 11200 | 118.0 | 109.1 | 1.00 | 14.4 | 20.5 | estimate based on methylnaphthalene |
| Indene | 1700 | 116.2 | 390 | 1.00 | 14.4 | 20.0 | estimate based on methylnaphthalene |
| Fluorene | 7720 | 166.2 | 2.0 | 0.16 | 230 | 19.3 | from Forsey (2004) |
| Naphthalene | 83800 | 128.2 | 31.7 | 0.30 | 6.05 | 19.7 | from Forsey (2004) |
| Phenanthrene | 26400 | 178.2 | 1.18 | 0.28 | 230 | 16.5 | from Forsey (2004) |
| Pyrene | 12900 | 202.3 | 0.13 | 0.11 | 864 | 19.2 | from Forsey (2004) |
| Bulk | - | 280.0 | 0 | 1.00 | 0 | 0.0 | not reactive |

# Chapter 3

# The Role of Intra-NAPL Diffusion on Mass Transfer from Multi-Component NAPLs

## OUTLINE

An experimental and computational study was performed to investigate the role of multi-component intra-NAPL diffusion on NAPL-water mass transfer under static conditions. Molecular weight and the NAPL component concentrations were determined to be the most important parameters affecting intra-NAPL diffusion coefficients. For a spherical NAPL body, a combination of NAPL properties and interphase mass transfer rate can result in internal diffusion limitations. When the main intra-NAPL diffusion coefficients are in the range of self-diffusion coefficients, dissolution is not limited by internal diffusion except for high mass transfer rate coefficients. For a complex and relatively high viscous NAPL, smaller intra-NAPL diffusion coefficients are expected and even low mass transfer rate coefficients can result in diffusion-limited dissolution.

Key Words: Intra-NAPL diffusion, Rate-limited mass transfer, MGP residuals, Higher viscosity layer.

## HIGHLIGHTS

- Inverse dependency between mass transfer rate coefficient and molecular weight
- Model developed to estimate intra-NAPL diffusion within complex NAPLs
- Molecular weight and NAPL concentration impact intra-NAPL diffusion coefficients
- NAPL composition, viscosity, and mass transfer rate can limit intra-NAPL diffusion

# 3.1 INTRODUCTION

The remediation of soil and groundwater contaminated with multi-component non-aqueous phase liquids (NAPLs) such as crude oil, creosote, or coal tars from former manufactured gas plants (MGP) is associated with a number of challenges (Birak & Miller, 2009). One of the primary factors that restricts the performance of remedial technologies for multi-component NAPLs is the extent and rate of NAPL dissolution (Luthy et al., 1994). Mass transfer kinetics at the NAPL-water interface is usually described by a stagnant film model (Miller et al., 1990) wherein the dissolution of organic components from the NAPL into the aqueous phase is comprised of several mass transfer steps (Seagren et al., 1993; Heyse et al., 2002;). The first step involves the diffusion of organic molecules towards the NAPL-water interface boundary layer, while the second step is diffusion through a rigid or emulsion interface between the water and NAPL. This interface is formed due to depletion of more soluble compounds at the NAPL boundary, and can completely separate the bulk-aqueous and bulk-NAPL phases by a film composed of either an aqueous film, or an interfacial organic film, or both (Peters et al., 2000; Wehrer et al., 2013a). In the third step, the organic molecules will dissolve in the bulk-aqueous phase after passing through the aqueous film. Each of these mass transfer steps can be limiting since they act in series, and the one with the highest resistance will control the overall dissolution of an organic compound into the aqueous phase (Ortiz et al., 1999; Wehrer et al., 2013a).

A substantial body of field and laboratory data (e.g., Hunt et al., 1988; Mercer & Cohen, 1990; Powers et al., 1992; Seagren et al., 1999; Mobile et al., 2016) has shown that the concentration of organic compounds in groundwater is usually less than their corresponding equilibrium concentration at various observation scales. This implies that NAPL architecture, flow bypassing, low residual saturation (Powers et al., 1998; Soga et al., 2004), and diffusional transport limitations (Luthy et al., 1993; Luthy et al., 1997; Ortiz et al., 1999; Wehrer et al., 2013; Lekmine et al., 2014) can impact dissolution. Consequently, dissolution of organic components is usually modeled as a rate-limited process with diffusion governing the mass transfer through the NAPL-water interface.

Due to thermodynamics, the presence of more than one component within a multi-component NAPL may restrict intra-NAPL diffusion (Cussler, 1997; Ortiz et al., 1999). This occurs since the diffusion of each component is influenced by its own concentration gradient as well as the concentration gradients of the other components present in the organic mixture (Cussler, 1997; Zielinski & Hanley, 1999). For example, Mukherji et al. (1997) investigated the aqueous

equilibrium concentrations of a continuously-stirred mixture of four synthetic dense NAPLs (DNAPLs) composed of structurally similar components that were in direct interaction with an aqueous phase. The results demonstrated that experimental equilibrium concentrations were within a factor of two compared to values predicted by modified Raoult's law (Lee et al., 1992) for an ideal mixture indicating that non-ideal interactions were not observed between components. However, the assumption of a well-mixed ideal mixture with structurally similar components is not always applicable in most subsurface systems (Khachikian & Harmon, 2000). Miller et al. (1985) reported that non-ideal behaviour will escalate when the molecular size of components are larger than octanol, and Banerjee et al. (1984) indicated that the presence of dissimilar molecules in organic mixtures resulted in deviation from ideal behaviour. By extension, it is expected that the effects of intra-NAPL diffusion will be more significant in multi-component NAPLs such as MGP residuals which are composed of hundreds to thousands of structurally dissimilar organic components (Luthy et al., 1993; Brown et al., 1999; Birak & Miller, 2009). When multi-component NAPLs are exposed to groundwater, the more soluble components will dissolve leaving the less soluble components at the interface (Liu et al., 2009; Peters et al., 2000). Diffusional resistance within a multi-component NAPL may then limit the movement of organic molecules toward the interface (Ortiz et al., 1999), and hence a new emulsion-like and high viscous interfacial film or a skin can be formed on the NAPL surface. This phenomenon is called weathering or aging, and affects diffusion across the NAPL-water interface, and consequently the dissolution of organic compounds will be reduced (Liu et al., 2009; Wehrer et al., 2013a,b).

Previous research indicates that coal tar, creosote, and crude oil weathering effects have been experimentally observed and attributed to either NAPL composition or inter-molecular interactions at the NAPL-water interface (Luthy et al., 1993; Nelson et al., 1996; Mahjoub et al., 2000; Alshafie & Ghoshal, 2004; Ghoshal et al., 2004). Luthy et al. (1993) observed the formation of a semi-rigid, skin-like layer at the interface of a coal tar drop suspended in water after three days, and this layer led to reduced NAPL-water mass transfer and a disequilibrium condition after seven days. Ghoshal et al. (2004) reported that a skin layer at a crude oil-water interface reduced the mass transfer coefficient by up to 80 percent after 35 days. It has been suggested that crude oil-water interfacial films are mostly comprised of asphaltenes and polar resins (Strassner, 1968; Jada & Salou, 2002; Ghoshal et al., 2004; Varadaraj & Brons, 2012). Nelson et al. (1996) hypothesized that inter-molecular interactions at a coal tar-water interface resulted in the formation of a semi-gelatinous film. Barranco and Dawson (1999) reported that even a small fraction of asphaltenic components in coal tar can affect interfacial properties. Barranco and Dawson (1999) also

indicated that film formation at a coal tar-water interface occurred under acidic to neutral pH rather than alkaline conditions. Also at temperatures > 45 °C interfacial film formation is less likely (Mohammed et al., 1993). Finally, Powers et al. (1996), and Brown and Neustadter (1980) observed that film formation at a crude oil-water interface affected mineral wettability.

Surprisingly, the role of intra-NAPL diffusion on the dissolution of organic components from NAPL sources has received little attention. Holman and Javandel (1996) employed a simplified two-dimensional intra-NAPL diffusive flux expression with a constant diffusion coefficient to represent the dissolution from a light NAPL (LNAPL) pool. In this model the dissolution of each organic component was independent of others, and the local equilibrium assumption was considered at the LNAPL-water interface. Brahma and Harmon (2003) assessed multi-component diffusion within two organic mixture composed of three organic liquids. While this work provides valuable insight, the peer-reviewed literature in this area has investigated organic mixtures comprised of only a few components. In addition, film formation, concentration profiles, and diffusion limitations within a NAPL body have not been thoroughly explored.

The objective of this study was to determine the role of multi-component intra-NAPL diffusion on NAPL-water mass transfer and interfacial depletion of the more soluble compounds, and to identify some of the conditions where this process needs to be considered. To support this evaluation, a diffusion-based numerical model was developed to simulate mass discharge and intra-NAPL concentration gradients under static aqueous conditions. A series of static experiments were conducted using coal tar collected from a former MGP site to capture multi-component diffusion-limited mass transfer behavior. These experiments were designed to generate relevant model parameters (e.g., mass transfer rate coefficients, equilibrium concentrations, activity coefficients, and NAPL characteristics) for simulation purposes.

## 3.1.1 Intra-NAPL Diffusion Theory

Diffusive flux within a multi-component NAPL depends on the molecular interactions and relative abundance of components present in the system (Cussler, 1997; Weber & DiGiano, 1995). According to Fick's law, a multi-component diffusive flux can be represented as (Cussler, 1997):

$$-J_i = \sum_{j=1}^{n-1} D_{ij} \nabla C_j \tag{3.1}$$

where $n$ is the total number of components with component $n$ arbitrarily chosen as the solvent, and $D_{ij}$ represents multi-component diffusion coefficients employed to approximate diffusivity

within a system of $n$ components. The array, $D_{ij}$, includes $(n-1)^2$ diffusion coefficients where the diagonal terms, $D_{ii}$, represent the effects of the concentration gradient of component $i$ on its own flux, and off-diagonal or cross-coefficients, $D_{ij}$, reflect the effects of the concentration gradients of other components present in the mixture on the flux of component $i$ (Zielinski & Hanley, 1999). The off-diagonal diffusion coefficients can be positive or negative indicating that diffusion of one component can be enhanced or hindered by other components present in the organic mixture (Brahma & Harmon, 2003).

Few theoretical models have been developed to predict the diffusion coefficients in multi-component mixtures (Cussler, 1997; Kett & Anderson, 1969a; Leahy-Dios & Firoozabadi, 2007). In this study, the multi-component intra-NAPL diffusion coefficients were estimated by the model developed by Kett and Anderson (1969a). In this model the hydrodynamic theory of Hartley and Crank (1949) was applied to the multi-component Fickian diffusion process in non-associating, non-electrolyte solutions of any number of components. The generalized expressions to estimate multi-component diffusion coefficients in non-associating solutions were developed (Kett & Anderson, 1969a) and validated by experimental evidence (Kett & Anderson, 1969b) using two non-associating ternary systems (dodecane-hexadecane-hexane, and toluene-chlorobenzene-bromobenzene).

According to hydrodynamic theory (Hartley & Crank, 1949), the diffusive flux consists of two different types of motion: intrinsic diffusion (molecular motion), and bulk motion of the medium. Intrinsic diffusion is related to the energy of each molecule to move compared to the surrounding molecules, and bulk motion results from the flow of other components present in the mixture to compensate the accumulation of mass in one section. Kett and Anderson (1969a) described the intrinsic diffusion flux by equating the driving and resisting forces imparted on a diffusing molecule as:

$$J_i = -\frac{C_i}{\sigma_i \eta}\frac{\partial \mu_i}{\partial x} \tag{3.2}$$

where $J_i$ is the flux of component $i$ relative to the medium resulting from intrinsic diffusion, $C_i$ is the concentration in the NAPL, $\frac{\partial \mu_i}{\partial x}$ is the chemical potential gradient, $\eta$ is mixture viscosity, and $\sigma_i$ is a proportionality coefficient called the friction factor representing the effects of the shape and size of the diffusing molecule. To consider the effects of bulk motion, Eq. 3.2 can be modified by incorporating the expressions for the velocity of the medium to yield (Kett & Anderson, 1969a):

$$J_i = -\frac{C_i}{\sigma_i \eta}\frac{\partial \mu_i}{\partial x} + C_i \sum_{j=1}^{n-1}\frac{V_j C_j}{\sigma_j \eta}\frac{\partial \mu_j}{\partial x} \tag{3.3}$$

where $n$ is the total number of components, and $V_j$ is the molar volume. Eq. 3.3 represents the flux of component $i$ within a mixture with respect to a fixed coordinate system when the molar volumes are constant for $(n-1)$ independent intra-NAPL fluxes (Kett & Anderson, 1969a). At constant pressure and temperature, the chemical potential gradient in Eq. 3.3 can be related to the concentration gradient. Consequently, the diffusive flux (Eq. 3.3) is equivalent to the multi-component version of Fick's law, and the general expressions for the multi-component diffusion coefficients ($D_{ij}$) can be derived. While Kett and Anderson (1969b) derived the $D_{ij}$ expressions for a ternary system, in this study the general form of $D_{ij}$ for a system of $n$ components was derived to estimate the intra-NAPL diffusion coefficients within a multi-component NAPL. The diagonal terms ($D_{ii}$) can be represented as:

$$D_{ii} = \frac{RTC_i}{\eta}\left\{\left(\frac{1-V_iC_i}{\sigma_i} + \frac{V_nC_i}{\sigma_n}\right)\left[\left(\frac{\partial ln\gamma_i}{\partial C_i}\right) + \frac{1}{C_i} - \frac{1}{C_T}\left(1-\frac{V_i}{V_n}\right)\right] + \sum_{k=1,(k\neq i)}^{n-1} C_k\left(\frac{V_n}{\sigma_n} - \frac{V_k}{\sigma_k}\right)\left[\left(\frac{\partial ln\gamma_k}{\partial C_i}\right) - \frac{1}{C_T}\left(1-\frac{V_i}{V_n}\right)\right]\right\} \tag{3.4a}$$

and the off-diagonal coefficients ($D_{ij,i\neq j}$) can be written as:

$$D_{ij} = \frac{RTC_i}{\eta}\left\{\left(\frac{1-V_iC_i}{\sigma_i} + \frac{V_nC_i}{\sigma_n}\right)\left[\left(\frac{\partial ln\gamma_i}{\partial C_j}\right) - \frac{1}{C_T}\left(1-\frac{V_j}{V_n}\right)\right] + C_j\left(\frac{V_n}{\sigma_n} - \frac{V_j}{\sigma_j}\right)\left[\left(\frac{\partial ln\gamma_j}{\partial C_j}\right) + \frac{1}{C_j} - \frac{1}{C_T}\left(1-\frac{V_j}{V_n}\right)\right] + \sum_{k=1,(k\neq i,j)}^{n-1} C_k\left(\frac{V_n}{\sigma_n} - \frac{V_k}{\sigma_k}\right)\left[\left(\frac{\partial ln\gamma_k}{\partial C_j}\right) - \frac{1}{C_T}\left(1-\frac{V_j}{V_n}\right)\right]\right\} \tag{3.4b}$$

where $C_T$ is the sum of molar concentrations of components present in the mixture, $\gamma$ is the activity coefficient, $R$ is the universal gas constant, and $T$ is the absolute temperature. The derivative of the activity coefficient with respect to the concentration of each component ($\frac{\partial \ln\gamma}{\partial C_i}$), can be estimated using the activity coefficient data by assuming that the concentrations of other components present in the system are constant. Kett and Anderson (1969a) suggested that if the self-diffusion ($D_i$) and infinite dilution diffusion coefficients ($D_{ij}^o$) for each component are available, the local friction factor can be estimated as:

$$\sigma_i = RT\left(\frac{X_i}{D_i\eta_i} + \sum_{j=1,j\neq i}^{n}\frac{X_j}{D_{ij}^{o}\eta_j}\right) \quad (3.5)$$

where $X_i$ is the mole fraction of each component within the NAPL mixture, and $\eta_i$ is the viscosity of each pure component. Self-diffusion represents the diffusion process of each component in its own pure state and is defined by Albright and Miller (1965) as "the special case of intra-diffusion for systems that contain no other components than two isotopic forms of a chemical species". Infinite dilution diffusion represents the interactions between two components in a mixture and was defined by Kett and Anderson (1969a) as "the mutual-diffusion coefficient of the *i j* binary at infinite dilution of *i* ".

# 3.2 EXPERIMENTAL INVESTIGATION

## 3.2.1 Materials and Methods

To examine the direct interaction of a multi-component NAPL and an aqueous phase, and to investigate diffusion-limited mass transfer and dissolution behavior of organic components, a series of static experiments using 10 mL (nominal) Pyrex graduated conical centrifuge vials was performed.

The MGP residuals used in this study were obtained from the former West Florida Natural Gas Company Site located in Ocala, Florida. From the late 1890s until about 1953, water gas or carbureted water gas was manufactured at this location by the "Lowe" carbonization process or destructive distillation of bituminous coal and coke. According to Brown's Directory, gas production was ~48 x $10^3$ $m^3$/yr in 1900 and steadily increased to 900 x $10^3$ $m^3$/yr by 1950. In 1952, manufacturing stopped at the plant and the facility converted to the sale of butane-propane-air. Residues from the MGP process, including tars and oily wastewaters, were deposited in the area of the former gas plant facilities during operations. There was an historic coal tar pit or area where residual tars were stored prior to sale for off-site use as roofing materials. The MGP residual received was obtained from a NAPL collection well screened from 24 to 27 m below ground surface in weathered limestone, and was a non-homogeneous mixture composed of a LNAPL and DNAPL portion with minor sediment. For the purpose of this experiment, our focus was on the DNAPL portion. Thus, 10 mL of the MGP residual was mixed with 10 mL Milli-Q water in a 40 mL vial and centrifuged at 10,000 rpm for 15 min. The DNAPL portion was collected after centrifuging and again mixed with water and centrifuged. This process was repeated multiple times to separate a sufficient mass of DNAPL which was then used. The final DNAPL volume was

assumed to be a homogeneous mixture, and the viscosity was determined to be 1.22 g/(cm s) using a dilution viscometer (Cannon-Ubbelhode) and the density of NAPL was determined to be 1.08 g/mL. Table 3.1 provides a summary of the most abundant and soluble components detected within the DNAPL portion along with some associated properties. The identified 19 components account for ~40 % of the total NAPL mass. The remainder of the NAPL mass was unidentified and assumed to be composed of higher molecular weight and lower soluble components.

Each 10 mL conical vial was partially filled with Milli-Q water and then 0.1 mL of the homogenised NAPL was gradually injected into the bottom of each vial through the water using a 100 µL glass syringe (Hamilton, Sigma Aldrich). The vials were then completely filled with Milli-Q water (total volume of water was 11.2 mL). The NAPL-water surface area was ~0.10 $cm^2$. A total of 18 vials were constructed and left in the dark at an ambient temperature of 20 $^oC$. The vials were not disturbed to ensure that NAPL-water mass transfer was limited only to diffusional transport of organic components. Duplicate reactors were sacrificed at each time increment (e.g., 2, 7, 12, 15, 22, 28, 36, 49, and 61 days). Aliquots of the aqueous solution were taken by a 10 mL glass syringe (Hamilton, Sigma Aldrich), and then centrifuged for 15 minutes at 6000 rpm to separate possible undissolved MGP residual. The concentration of organic compounds (Table 3.1) present in the aqueous sample along with the solution pH (Orion pH meter, model 290A) was determined.

For analysis of the organic components in the aqueous phase, a 5 mL sample was mixed with 14 mL of water in a 20 mL vial. This was followed immediately by the addition of 1.0 mL of methylene chloride (containing internal standards metafluoro-toluene (MFT) and fluoro-biphenyl (FBP) at 25 mg/L). The vial was quickly resealed and agitated on its side at 350 rpm on a platform shaker for 20 min. After shaking, the vial was inverted and the phases were allowed to separate for 30 min. Approximately 0.7 mL of the dichloromethane phase was removed from the inverted vial with a gas tight glass syringe through the Teflon septum. The solvent was placed in a 2.0 mL Teflon sealed autosampler vial for injection into the gas chromatograph (GC). For the analysis of the DNAPL portion, a sub-sample was added directly to methylene chloride and transferred to a 2.0 mL autosampler vial and crimp sealed with a Teflon cap. All NAPL and aqueous samples were analyzed using a HP 5890 capillary GC, a HP7673A autosampler, and a flame ionization detector. Three (3) mL of methylene chloride was injected in splitless mode (purge on 0.5 min, purge off 10 min) onto a 0.25 mm x 30 m length, DB5 capillary column with a stationary phase film thickness of 0.25 µm. The helium column flow rate was 2.0 mL/min with a make-up gas flow rate of 30 mL/min. The injection temperature was 275 $^oC$, detector temperature was 325 $^oC$ and initial column oven temperature was 35 $^oC$ held for 0.5 min, then ramped up at 15 $^oC$/min to a final

temperature of 250 °C and held for 2 min. A GC run time was 16 min. Data integration was completed with a SRI Model 302 Peak Simple chromatography data system. The method detection limit (MDL) was 20 µg/L for aqueous samples, and 5 mg/kg for NAPL samples.

### 3.2.2 Results and Discussion

A total of nine components were detected in the aqueous phase including BTEX (benzene, toluene, ethylbenzene, and xylene), trimethylbenzene, and four polycyclic aromatic hydrocarbons (PAHs) (naphthalene, 1-methylnaphthalene, 2-methylnaphthalene, and acenaphthene). The other components were < MDL. The average pH value of the aqueous phase was 5.3 at the start of the experiment and decreased gradually to 4.5 by Day 61 likely due to the dissolution of organic acids. No physical changes (i.e., color, temperature, precipitate formation) were observed. The diffusion-limited dissolution of this MGP residual in water manifested in these static experiments as an initial rapid increase of dissolved phase concentrations from Day 2 to Day 10 followed by minor fluctuations until Day 61 (Figure 3.1). Except for naphthalene, xylene and ethylbenzene, the detected components appear to reach an equilibrium concentration by Day 61 (Table 3.2).

Lee et al. (1992) indicated that the aqueous equilibrium concentration of PAHs within coal tars can be estimated by employing a modified form of Raoult's law given by:

$$C_{eq,i}^{w} = X_i^N \gamma_i^N \frac{S_i}{(f_i^s / f_i^l)} \tag{3.6}$$

where $C_{eq,i}^{w}$ is aqueous equilibrium concentration of each component, $N$ and $w$ superscripts refer to NAPL and water phase respectively, $S_i$ is the aqueous solubility, and $f_i^s$ and $f_i^l$ are fugacities in the pure solid and pure liquid states respectively (Table 3.1). Naphthalene and benzene due to the high mole fraction and solubility values, respectively, have the highest aqueous phase concentrations. While ethylbenzene, xylene, toluene, and trimethylbenzene have a higher solubility compared to naphthalene, they have lower equilibrium concentrations due to lower mole fractions and higher fugacity ratios. Toluene has the lowest aqueous concentration which is proportional to its low mole fraction within the NAPL. 1-methylnaphthalene and 2-methylnaphthalene show similar behaviour and reach an equilibrium concentration in < 30 days.

The aqueous phase mass balance can be written by employing the stagnant film model for each organic component as (Miller et al., 1990):

$$\frac{dC_i^w}{dt} = k_{w,i}(C_{eq,i}^w - C_i^w) \quad (3.7)$$

where $C_i^w$ is aqueous concentration, $t$ is time, $k_{w,i}$ is lumped mass transfer rate coefficient (1/T), and $C_{eq,i}^w$ is the aqueous equilibrium concentration. To determine the lumped mass transfer rate coefficient for each component, Eq. 3.7 can be solved analytically with the initial condition specified as an aqueous concentration of zero at $t = 0$, to yield:

$$\ln\left(1 - \frac{C_i^w}{C_{eq,i}^w}\right) = -k_w t \quad (3.8)$$

Eq. 3.8 was applied to the experimental data (Figure 3.1) and the lumped mass transfer rate coefficient for each component was determined using linear regression. The resulting values ranged from 0.036 to 0.1 /day. For naphthalene, xylene and ethylbenzene, the equilibrium concentrations were also estimated and presented along with the estimated lumped mass transfer data in Table 3.2. The lumped mass transfer rate coefficients were multiplied by the experimental aqueous volume (11.2 mL) and divided by the NAPL-water surface area (0.1 $cm^2$) to estimate mass transfer rate coefficients which varied from 4 to 11.2 cm/day with 1-methylnaphthalene and 2-methylnaphthalene having the highest values (~11.2 cm/day), and toluene and naphthalene the lowest values (4 cm/day).

Ghoshal et al. (1996) reported that the naphthalene mass transfer coefficient from a coal tar globule in a gently stirred continuous flow reactor varied from 21 to 26 cm/day. Mukherji et al. (1997) showed that the mass transfer rate coefficients for organic components within four synthetic NAPLs were similar, and in the range of 69 to 259 cm/day which is ~20 times higher than those determined from this experimental investigation. They also observed an equilibrium period that was 5 to 7 days which is significantly shorter than the 30 to 60-day equilibrium period observed in this study. The higher mass transfer rate coefficients and shorter equilibrium period is a reflection of the continuous stirred system (both NAPL and aqueous phase) employed by Mukherji et al. (1997) compared to the static system used in this study to capture the diffusion-limited NAPL-water mass transfer. Diffusion-limited dissolution, which can be a predominant phenomenon in subsurface systems, results in rate limited mass transfer and longer equilibrium times.

Mukherji et al. (1997) also observed that higher molecular weight compounds have larger mass transfer rate coefficients. Wehrer et al. (2013a) placed fresh and aged NAPLs into dialysis tubing

and, in contrast to Mukherji et al. (1997), did not mix the NAPL. They determined an inverse dependency between molecular weight and intra-NAPL diffusion coefficients by fitting a spherical diffusion model to experimental NAPL concentration data implying that higher molecular weight and size act as a resisting force for diffusional transport. Wehrer et al.(2013a) also reported that the inverse dependency between diffusion coefficients and molecular weight was much less pronounced for aged MGP residuals compared to fresh MGP tars. Similarly, for the MGP residual used in this study, no overall trend was observed between molecular weight and mass transfer rate coefficient (Figure 3.2). Rather an inverse dependency of the mass transfer rate coefficient on molecular weight is evident for the BTEX components. A similar but separate trend is apparent between the mass transfer rate coefficients and the molecular weight for the PAHs (1-methylnaphthalene, 2-methylnaphthalene and acenaphthene) except for naphthalene (MW = 128.2 g/mol) which has a smaller $k_w$ compared to 1-methylnaphthalene and 2-methylnaphthalene (MW = 142 g/mol). The distinct inverse dependency of mass transfer rate coefficient on molecular weight for BTEX and PAHs suggests that BTEX and PAHs have different mass transfer behavior.

# 3.3 MULTI-COMPONENT INTRA-NAPL DIFFUSION MODEL

## 3.3.1 Model Description

To explore the role of intra-NAPL diffusion on the NAPL-water mass transfer, a temporal-spatial diffusion-based mathematical model was developed. For the purpose of this evaluation, an isolated initially homogeneous spherical NAPL blob with the total surface area available for mass transfer was considered to be suspended in a well-mixed volume of water (Figure 3.3). The mass balance for each component within the NAPL in a spherical NAPL blob can be written as (Bird et al., 2002):

$$\frac{\partial \mathrm{C_i}}{\partial \mathrm{t}} = \frac{1}{r^2}\frac{\partial}{\partial \mathrm{r}}\left(r^2 \sum_{j=1}^{n-1} \mathrm{D_{ij}} \frac{\partial \mathrm{C_j}}{\partial \mathrm{r}}\right) \tag{3.9}$$

where $r$ is the radial coordination and changes in the mixture density are negligible. If the volume of water surrounding the spherical NAPL blob is small, the system will reach to an equilibrium condition quickly, while if the volume of water is large, a longer period of time is required to reach equilibrium condition and thus the NAPL blob may be depleted. Eq. 3.9 was subjected to the boundary conditions of symmetry ($\frac{\partial C}{\partial r} = 0$) at the centre of the NAPL sphere, and the flux ($J_i$) at

the external sphere NAPL-water boundary was equated to the first-order mass transfer expression (Miller et al., 1990; Weber & DiGiano, 1995) as given by:

$$J_i = K(C^w_{eq,i} - C^w_i) \tag{3.10}$$

where $K$ is the mass transfer rate coefficient (L/T). The aqueous equilibrium concentration for each component ($C^w_{eq,i}$) was estimated by using the modified form of Raoult's law (Eq. 3.6). To account for the film transfer resistance and compositional changes at the NAPL interface, the mole fractions in Eq. 3.6 were based on the component concentrations at the external NAPL sphere boundary. Activity coefficients ($\gamma_i$) were calculated using the universal Quasi-chemical functional group activity coefficient (UNIFAC) (Poling et al., 2001).

Eq 3.9 was solved using a fully-implicit finite volume scheme, and at each time step the equilibrium concentration and mass flux of each component was estimated using Eq. 3.10. The shrinkage of the NAPL body due to mass loss was handled by assuming that the NAPL sphere shrinks uniformly. Since mass transfer and equilibrium concentrations in Eq. 3.10 are related to the external boundary control volume attributes, and because unequal spatial discretization near the moving boundary results in the loss of accuracy (Crank, 1984), a modified mesh system similar to that used by Crank and Gupta (1972) with uniform discretization (except for the control volume near *r* = 0) and fixed time steps were employed. At each time step, mass loss and shrinkage length were determined using the estimated mass flux at the interface (Eq. 3.10), and then the length and concentrations within the external boundary control volume were modified. Subsequently, by assuming a wall boundary condition ($J_i = 0$) at the interface, the system of equations was solved by incorporating Eq. 3.4 and Eq. 3.9 to update concentration profiles within the NAPL sphere. At the end of each time step, the mesh system was modified by shifting the mesh toward the centre (*r* = 0) a distance equal to the shrinkage length and then the concentrations at the centroids of new control volumes were interpolated using a cubic spline method (Crank & Gupta, 1972). Finally, the average aqueous concentrations ($C^w_i$) in Eq. 3.10 were calculated using the NAPL-water interface mass flux.

The numerical algorithm used to solve the intra-NAPL diffusional flux mass balance equation (Eq.3.9) was verified by comparing the numerical solution with an analytical solution for spherical diffusion with a constant flux (*F*) and diffusion coefficient (*D*) without shrinkage as given by (Crank, 1975):

$$\frac{D(C_o - C\ (t,r))}{F\ R} = \frac{3Dt}{R^2} + 0.5\frac{r^2}{R^2} - 0.3 - 2\frac{R}{r}\sum_{n=1}^{\infty}\frac{\sin(\propto_n r)}{\propto_n^2 R^2 \sin(\propto_n R)} exp(-D\ \propto_n^2\ t) \quad (3.11)$$

where $C_o$ is initial concentration, $R$ is the radius of the sphere, and $\propto_n$ are the positive roots of

$$(\propto_n R)\cot(\propto_n R) = 1 \quad (3.12)$$

A visual comparison of the numerical and analytical results is presented in Figure B.1 in Appendix B. Estimation of multi-component diffusion coefficients by the Kett and Anderson model (1969a) (Eq. 3.4) was verified by comparing the generated values to the experimental diffusion coefficients (Kett & Anderson, 1969b) for a ternary mixture composed of dodecane, hexadecane, and hexane (Table B.1 in Appendix B). The estimated values are in agreement with both the experimental and model results reported by Kett and Anderson (1969b) in the range of ± 62%.

### 3.3.2 Model Parameterization and Investigated Scenarios

The results from the experimental investigation indicated that diffusion-controlled dissolution behavior under static conditions occurred. In addition, the data from the static experiments were used to derive mass transfer rate coefficients, and aqueous equilibrium concentrations for the nine detected components associated with the former MGP NAPL employed. It was not our intent here to simulate the experimental conditions, but rather to use the data set assembled to inform model parameters so that representative physical and chemical properties are used.

For the initial condition for Eq. 3.9, a 0.5 g homogenous spherical NAPL blob (radius of ~ 0.48 cm) surrounded by an aqueous phase was specified, and the initial concentration of organic components were assigned to be identical to the former MGP NAPL employed in the static experiments (Table 3.1) which contained 19 representative organic compounds (40% of the NAPL mass). The remainder of NAPL mass was considered to be comprised of an unresolved or bulk portion composed of higher molecular weight and lower soluble components and assigned nominal values (see Table 3.1). Since the focus of this study was to explore intra-NAPL compositional changes, 50 L of water was assumed to surround the NAPL blob. This volume was chosen so that the dissolved phase concentrations did not reach equilibrium over the simulation period allowing compositional changes within the NAPL to be observed.

For the estimation of multi-component intra-NAPL diffusion coefficients ($D_{ij}$) using Eq. 3.4, a temperature of 20 ºC was assumed and the mixture viscosity was estimated using the Yon and Toor relationship (Kett & Anderson, 1969b):

$$\ln(\eta) = \sum_{i=1}^{n} X_i \ln\eta_i \tag{3.13}$$

The viscosity of each compound ($\eta_i$) was obtained from the literature (Lide et al., 1999) or estimated by using the Orrick and Erbar method (Poling et al., 2001) with an average deviation of 15% as:

$$\ln\left(\frac{\eta_i}{100\ \rho_i MW}\right) = A + \frac{B}{T} \tag{3.14}$$

where $MW$ is molecular weight (g/mol), $T$ is absolute temperature, $A$ and $B$ are estimated by a group contribution technique, and the units for viscosity and density are g/(cm s), and g/cm$^3$ respectively. Table 3.1 summarizes the molecular weight, viscosity, and density values of each component. For the bulk portion, the molecular weight was assumed, and the density was assigned a value of 1.14 g/cm$^3$.

To estimate the friction factors (Eq. 3.5), the self and infinite dilution diffusion coefficients for PAHs with a fugacity ratio less than unity were estimated similar to the other components which are liquid at ambient temperature. This approach is plausible since PAHs with a fugacity ratio less than unity can exist as liquid due to melting point depression within multi-component mixtures (Peters et al. 1997). The infinite dilution diffusion coefficients ($D_{ij}^{o}$) were determined using a modified form of the Tyn and Calus relationship (Poling et al., 2001), and the self-diffusion values ($D_i$) were calculated using the Houghton's Cubic Cell model (Houghton, 1964) as given by:

$$D_{ij}^{o} = 8.93 \times 10^{-10} \left(\frac{\overline{V}_{j,b}^{0.267}}{\overline{V}_{i,b}^{0.433}}\right) \frac{T}{\eta_j} \left(\frac{\tau_j}{\tau_i}\right)^{0.15} \tag{3.15}$$

$$D_i = \frac{RT\rho_i}{6\eta_i M_i} \left(\frac{V_i}{N}\right)^{\frac{2}{3}} \tag{3.16}$$

where $D_i$ and $D_{ij}^{o}$ have units of cm$^2$/s, viscosity ($\eta$) has units of g/(cm s), density has units of g/cm$^3$, $M$ is molecular weight (g/mol), $R$ is universal gas constant (8.314x10$^7$ (g cm$^2$)/(s$^2$ K mol)), $N$ is Avogadro's number(6.022x10$^{23}$ 1/mol), $\tau$ is surface tension at boiling temperature (g/s$^2$), $V$ is molar volume (cm$^3$/mol) which can be estimated using density and molecular weight data ($MW/\rho$)

(Table 3.1), and $\bar{V}_b$ is molar volume at boiling temperature (cm$^3$/mol) and was estimated using the Schroeder relationship (Poling et al., 2001) (Table 3.1). The Schroeder relationship is an additive method which accounts for the number of atoms of carbon (C), hydrogen (H), oxygen (O), nitrogen (N), halogens (Cl, F, I), sulfur (S), and also the number of carbon double bonds (DB), and triple bonds (TB):

$$\bar{V}_b = 7(N_C + N_H + N_O + N_N + N_{DB} + 2N_{TB}) + 31.5N_{Br} + 24.5N_{Cl} + 10.5N_F + 38.5N_I + 21N_S - 7 \quad (3.17)$$

where the last term is included only if the component has one or more rings. This method is accurate and except for highly associated liquids, gives an average error of 3-4% (Poling et al., 2001). The surface tension ratio ($\tau_j/\tau_i$) in Eq. 3.15 was assumed to equal one (Poling et al., 2001). All of the estimated self and infinite dilution diffusion values are presented in Table B.2 in Appendix B. $D_i$ and $D_{ij}^o$ values for BTEX and methylethylbenzene(s) are in the range of $10^{-5}$ (cm$^2$/s), and for PAHs are in the range of $10^{-6}$ (cm$^2$/s). Since naphthalene is the most predominant component, $D_i$ and $D_{ij}^o$ values for bulk portion of the NAPL were assumed to be similar to naphthalene.

NAPL viscosity can significantly affect mass transfer and intra-NAPL diffusional behavior. Ortiz et al. (1999) indicated that control on mass transfer can change from aqueous to NAPL resistance for high viscous NAPLs. Birak and Miller (2009) reported that the viscosity of MGP residuals comprised of coal, water-gas, and oil gas tars can range from 0.091 to 6600 g/(cm s). In another study by Wehrer et al. (2013a) the viscosity of various fresh and aged coal tars at 20 $^o$C varied from 0.05 to 2.3 g/(cm s). The viscosity of the former MGP NAPL used in the experiment investigation (Section 2) was 1.22 g/(cm s) which lies in the middle of the viscosity range reported by Wehrer et al. (2013a). To explore the effects of NAPL viscosity on internal diffusion and mass transfer processes, four NAPL viscosities were investigated: low (0.12 g/(cm s)), medium (1.22 g/(cm s), high (15 g/(cm s), and very-high (200 g/(cm s)).

Rather than estimate mass transfer rate coefficients for the 11 organic components that were not detected in the aqueous phase during the experimental results, a single mass transfer rate coefficient (Eq. 3.10) was assigned for all of the components using a least-squares analysis framework in conjunction with the aqueous experimental data for the nine detected components (Figure 3.1). The ramifications of this assumption were deemed minor since the focus of this modeling study is on the compositional changes within the NAPL body. The best-fit lumped mass transfer rate coefficient was equal 0.056 /day and was converted to a mass transfer rate

coefficient ($K$) of 6.16 cm/day using the experimental aqueous volume (11.2 mL) and NAPL-water surface area (~0.1 $cm^2$).

To estimate the activity coefficients using the UNIFAC method, the identified components and bulk portion (Table 3.1) were separated into multiple functional groups. Since it is not possible to identify the functional groups in the bulk portion, experimental activity coefficients for the nine detected components were estimated by dividing the experimental equilibrium concentrations by the ideal concentrations determined by modified Raoult's Law (Table 3.2). The initial experimental and UNIFAC activity coefficients were similar (Table 3.1) assuming that the bulk portion contains an equal number (9) of all the individual functional groups which represents the identified 19 components.

The sphere radius was discretized into 0.005 cm control volumes, and a time step increment of 0.1 day was adopted. A mesh convergence test indicated that the NAPL concentration generated using finer mesh increments and time steps varied by < 1%. All simulations were run for a time of 1000 days which was deemed sufficient to observe changes in intra-NAPL diffusional flux and composition.

## 3.3.3 Results and Discussion

### 3.3.3.1 Medium Viscous NAPL

The temporal dissolved phase concentration behavior of the two most predominant components in the medium viscous NAPL ($\eta = 1.2$ g/(cm s)) are presented on Figure 3.4 (see Figure B.2(a) in Appendix B for the other components). After 1000 days of exposure to water the concentration of naphthalene and 2-methylnaphthalene reached ~1.0 and ~0.28 mg/L, respectively. These values are proportional to their initial NAPL mole fraction and aqueous solubility values (Table 3.1). Although phenanthrene also had one of the largest initial NAPL mole fraction values, its lower solubility resulted in a final aqueous concentration that was < 0.05 mg/L. The final (after 1000 days) radial concentration of NAPL components was homogeneous (see Figures 3.5 and B.3 in Appendix B) suggesting that mass transfer at the interface was not restricted due to intra-NAPL diffusion limitations. The ratio of the final to initial NAPL concentrations are shown in Figure 3.6, and indicate, as expected, that the concentration of the more soluble components such as BTEX, naphthalene, and 2-methylnaphthalene were depleted while the concentrations of the less soluble components such as phenanthrene, pyrene, and the bulk portion were enriched. After 1000 days, the viscosity of the NAPL is ~ 6 times higher than its initial value (Figure 3.7) and is attributed to

the enrichment of the bulk portion which is composed of higher viscous and insoluble components.

While the initial main intra-NAPL diffusion coefficients (diagonal values) were ~1x10$^{-7}$ cm$^2$/s (Figure B.4 in Appendix B) the final values decreased an order of magnitude to ~1.7x10$^{-8}$ cm$^2$/s as a result of the changes that occurred within the NAPL body. Naphthalene which is present at the largest concentration has the highest main diffusion coefficient value. Benzene which has the lowest molecular weight has the second highest main diffusion coefficient value. Toluene, xylene, and ethylbenzene also have high main diffusion coefficient values due to their low molecular weight, density, and viscosity values. 1-methylnaphthalene, 2-methylnaphthalene, and indene after naphthalene have the largest main diffusion coefficient values amongst the PAHs. The large main diffusion coefficients for 1-methylnaphthalene and 2-methylnaphthalene are attributed to their high NAPL concentrations, while for indene its large main diffusion coefficient is due to its lower molecular weight compared to the other PAHs. Chrysene with the largest molecular weight, density, and viscosity value has the lowest diffusion coefficient value. The ratios of the final to initial main intra-NAPL diffusion coefficients (Figure B.5 in Appendix B) indicate that the main diffusion coefficient for naphthalene decreased more than the other components since the concentration of naphthalene was the most depleted (Figure B.3 in Appendix B). In contrast, the main diffusion coefficient for phenanthrene decreased the least as a result of its increase in NAPL concentration at 1000 days (Figure 3.6). The initial off-diagonal diffusion coefficient values were between one to three orders of magnitude lower than the main diffusion coefficient values (Table B.3 in Appendix B).

The main intra-NAPL diffusion coefficient values are not of the same order of magnitude as those reported by others. For example, Ortiz et al. (1999) reported that the diffusion coefficients for naphthalene, phenanthrene, and pyrene within transmission oils (viscosity of 8 - 14 g/(cm s)) were in the range of $10^{-9}$ to $10^{-12}$ cm$^2$/s after being exposed to water for ~1 year. Wehrer et al. (2013a) also reported that diffusion coefficients for some PAHs (e.g., naphthalene, acenaphthene, and pyrene) in MGP residuals were in the range of $10^{-10}$ to $10^{-18}$ cm$^2$/s. The difference can be attributed to the experimental conditions (i.e., NAPL composition, higher viscosity, and larger mass transfer rate coefficient) used compared to the experiments performed in this study.

For a spherical blob composed of a medium viscosity NAPL and with mass < 50 g exposed to water under static conditions, interface film formation and diffusion-limited mass transfer due to intra-NAPL diffusion are not expected to occur. Concentration gradients at the interface due to

dissolution can be quickly compensated by diffusional transport to the interface and the NAPL concentration remains homogenous. A sensitivity analyses was conducted to explore potential conditions when intra-NAPL diffusion limitations would arise. The results of this analysis indicated that when the mass transfer rate coefficient is increased to > 15 cm/day, intra-NAPL concentration gradients can be established and hence intra-NAPL diffusion limitations will occur.

3.3.3.2 Influence of Viscosity

Similar to the medium viscous NAPL, no concentration gradient was established in the low viscous NAPL ($\eta$=0.12 g/(cm s)) and mass transfer was not restricted. Hence, the simulated aqueous (Figures 3.4 and B.2(a) in Appendix B) and radial NAPL concentrations (Figure B.3 in Appendix B) for the low viscous NAPL are essentially identical to those obtained for the medium viscous NAPL. A sensitivity analyses indicated that when the mass transfer rate coefficient (Eq. 3.10) was increased to > 180 cm/day, slight intra-NAPL concentration gradients were established for the low viscous NAPL. Mukherji et al. (1997) demonstrated that this range of mass transfer conditions are possible under non-static conditions without sediment for a well-mixed NAPL and aqueous phase. Therefore, the threshold of the mass transfer rate coefficient which can result in interfacial depletion of the more soluble compounds was 15 and 180 cm/day for the NAPL viscosities of 1.2 and 0.12 g/(cm s), respectively, that indicate the combination of NAPL properties (i.e. viscosity, concentration, temperature) and interphase mass transfer rate can result in internal diffusion limitations. It is possible that under some condition increasing the mass transfer rate results in the interfacial film formation and thus restricts the mass transfer and dissolution process. For example, remediation methods such as pump and treat systems that can increase flow rate and hence, increase mass transfer rate can restrict internal diffusion and enhance mass transfer limitations.

For the low viscous NAPL, the initial main intra-NAPL diffusion coefficients were one order of magnitude higher (~$1.5 \times 10^{-6}$ cm/s) compared to those determined for the medium viscous NAPL. These initial main intra-NAPL diffusion coefficients are of the same order as the self-diffusion coefficients (Eq. 3.16 and Table B.2 in Appendix B), and thus the presence of other organic components within this low viscous former MGP NAPL does not restrict internal diffusional flux. This condition is similar to organic mixtures composed of miscible organic components which are liquids at ambient temperature (similar to the organic mixtures investigated by Kett and Anderson (1969b) and Brahma & Harmon (2003)) where intra-NAPL diffusion coefficients of the order of the self-diffusion coefficients can be expected.

The simulated aqueous concentrations for the high viscous NAPL ($\eta$ = 15 g/(cm.s)) at 1000 days are slightly different than the results from the medium viscous NAPL (Figures 3.4 and B.2(b) in Appendix B). While concentration gradients are established within the high viscous NAPL (Figures 3.8(a) and B.6 in Appendix B), the rate of the internal diffusional flux does not significantly limit dissolution. The simulated NAPL concentration of the bulk portion (Figure 3.5) and lower solubility components (i.e., phenanthrene, pyrene, chrysene, fluoranthene) increased at the interface after 1000 days while the higher soluble components were depleted. The estimated initial main intra-NAPL diffusion coefficients for the high viscous NAPL are of the order of $7x10^{-9}$ $cm^2/s$, and the initial off-diagonal diffusion coefficient values are one to three orders of magnitude lower. The main intra-NAPL diffusion coefficients are 15 times smaller than those determined for the medium viscous NAPL and these smaller values resulted in internal diffusion limitations and concentration gradients within the NAPL body. The main intra-NAPL diffusion coefficients after being exposed to water for 1000 days decreased by an order of magnitude and were on the order of $6x10^{-10}$ $cm^2/s$. This decrease can be attributed to the depletion of the more soluble and lower viscous components (e.g., BTEX) indicating that over the time internal diffusion limitations can become more significant. The final viscosity of the high viscous NAPL is > 10 times larger than the initial value (Figure 3.7). The abundance of the bulk portion and lower solubility components at the interface causes the viscosity at the NAPL/water interface to be ~ 10% higher than in the centre of the NAPL body (Figure 3.7).

The simulated radial NAPL concentrations at 1000 days within the very-high viscous NAPL ($\eta$ = 200 g/(cm s)) for the most predominant components are shown in Figure 3.8 (b) (see Figure B.6 in Appendix B for other components). The changes in the NAPL composition are similar to the high viscous NAPL (Figure 3.8 (a)) with the higher soluble components depleted at the interface. The bulk portion (Figure 3.5) as well as low solubility components (i.e., phenanthrene and pyrene) accumulate at the interface. However, for the very-high viscous NAPL, film formation is more pronounced compared to the high viscous NAPL. For example, the naphthalene concentration at the interface of the very-high viscous NAPL is ~20% of the concentration in the core of the NAPL body (Figure 3.8(b)).

Figure 3.9 shows the temporal variations of the mole fractions at the interface and within the entire very-high viscous NAPL body for the most predominant components (see Figure B.7 in Appendix B for other components). While naphthalene is the most dominant component within the entire very-high viscous NAPL body over the 1000 days simulation period, the interfacial naphthalene mole fraction after ~200 days decreased to less than the interfacial mole fraction of phenanthrene

and 2-methylnaphthalene. As a result of the accumulation of the bulk portion and lower soluble components (phenanthrene and pyrene) at the interface, the aqueous equilibrium concentrations (Eq. 3.6) and mass transfer of the higher soluble components decreased. After 1000 days, the shrinkage (initial radius minus final radius) of the NAPL body for the high and very-high viscous NAPLs are 95 and 65 % of the shrinkage of the medium viscous NAPL body, respectively, indicating smaller mass loss due to the interfacial depletion of the more soluble compounds and hence, rate-limited mass transfer. While the simulated aqueous concentrations of the lowest soluble components (e.g., fluoranthene, chrysene, and pyrene) for the very high-viscous NAPL are 10 to 40 % higher compared to those estimated for the medium viscous NAPL at 1000 days, the aqueous concentration of the remainder of the components are 20 to 50 % lower (Figures 3.4 and B.2(c) in Appendix B).

The estimated initial main intra-NAPL diffusion coefficients for the very-high viscous NAPL are 160 times smaller (~ $6x10^{-10}$ $cm^2/s$) than those estimated for the medium viscous NAPL. The radial main intra-NAPL diffusion coefficients after being exposed to water for 1000 days (Figure 3.10) decreased compared to the initial values. At the NAPL/water interface all of the main intra-NAPL diffusion coefficients are ~10 times smaller than within the core of the NAPL body as a result of the depletion of lower viscous components. The abundance of the bulk portion and higher viscous components at the interface causes the viscosity at the NAPL/water interface to increase ~5 times relative to the centre of the NAPL body (Figure 3.7) at 1000 days, and ~14 times compared to the initial viscosity.

## 3.4 SUMMARY

A comprehensive experimental and computational study was performed to investigate the role of intra-NAPL diffusion on the mass transfer between multi-component NAPLs and water, and to identify some of the controlling situations where this process should be considered. A series of static experiments was conducted to investigate diffusion-controlled dissolution of organic components from former MGP residuals. The results indicated that under the diffusion-controlled mass transfer conditions established, the estimated mass transfer rate coefficients were lower than typical mass transfer rate coefficients determined under continuous mixed conditions. Although, no overall trend was observed between the mass transfer rate coefficients for the various organic compounds identified, an inverse dependency between the mass transfer rate

coefficient and molecular weight was clear but different for BTEX and some PAHs compounds suggesting that the intra-NAPL diffusion behavior of these two organic compound classes are different.

To examine the role of intra-NAPL diffusion on NAPL-water mass transfer, we simulated a physical system where an isolated spherical NAPL blob was surrounded by a finite volume of water. In this system the initial composition of the NAPL blob was assumed to be homogeneous, and the total surface area was available for mass transfer. The experimental data set assembled was used to inform the model parameters so that representative physical and chemical properties were used. The results indicated that molecular weight and concentration of each component are the most important parameters affecting intra-NAPL diffusion coefficients. Four NAPLs with different viscosities but the same quantified mass were simulated. For a spherical NAPL body of < 50 g under static conditions, the combination of NAPL properties and interphase mass transfer rates can result in internal diffusion limitations. If the main intra-NAPL diffusion coefficients are in the range of the self-diffusion coefficients ($10^{-5}$ to $10^{-6}$ $cm^2/s$), intra-NAPL diffusion is not limiting since NAPL concentration gradients cannot be established except when high mass transfer rates are present (>180 cm/day). In the case of complex and highly viscous NAPLs, smaller intra-NAPL diffusion coefficients are expected and even the low range of mass transfer rates can result in the interfacial depletion of the more soluble compounds and diffusion-limited dissolution.

In this study we investigated the effect of just one phenomenon (intra-NAPL diffusion) which can result in restrict interfacial mass transfer; however, other phenomena such as inter-molecular interactions and biofilm formation can also result in film formation and influence NAPL-water mass transfer. For example, Mukherji and Weber (1998) reported that interfacial biofilm formation limited NAPL-water mass transfer. Possible compositional changes, solidification, and precipitation (Peters et al. 1999) as well as interfacial weak bonds between organic components and water (Nelson et al., 1996) can also result in skin layer formation and diffusional limitations.

The diffusion-based model developed in this study provides a suitable platform to capture the temporal and spatial compositional changes within complex NAPLs. The simulation results showed that intra-NAPL diffusion can significantly affect mass transfer and dissolved phase concentrations, and that increasing the NAPL-water mass transfer rate may result in intra-NAPL diffusion limitation and restricted dissolution. As a result, consideration should be given to the role of intra-NAPL diffusion in risk assessment evaluations, and during the design and implementation of remediation strategies.

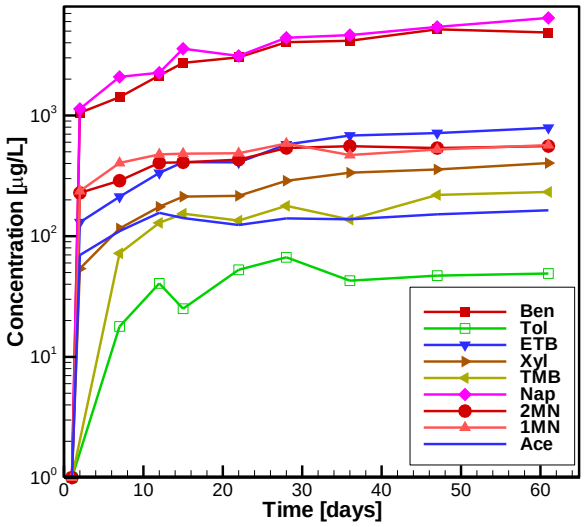


**Figure 3.1:** Temporal concentration profiles of the nine detected components observed in the bulk solution in the static diffusion experiments.

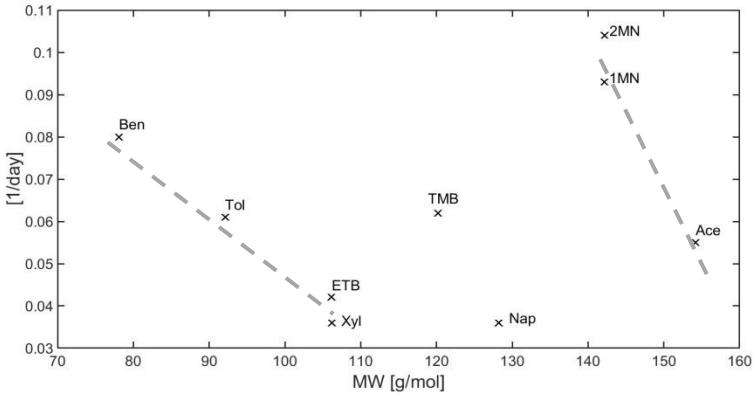


**Figure 3.2:** Lumped mass transfer rate coefficients for each detectable component in the aqueous phase versus molecular weight. The dashed lines represent observed trends for BTEX and some PAH compounds.

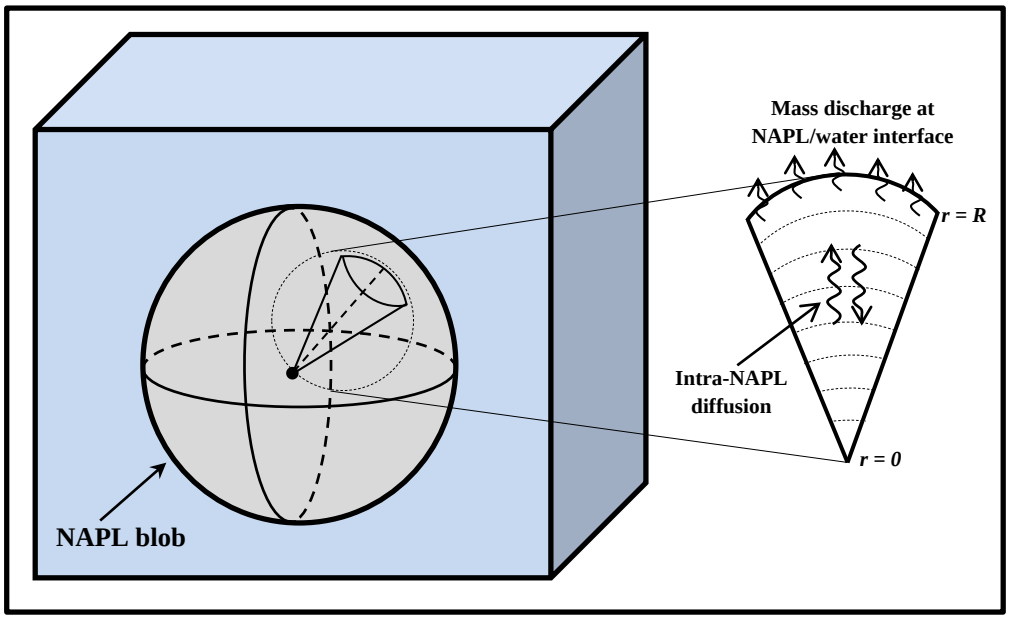


**Figure 3.3:** Schematic of the physical system simulated. A spherical NAPL blob suspended in a well-mixed volume of water. Also shown is the numerical representation associated with Eq. 3.9.

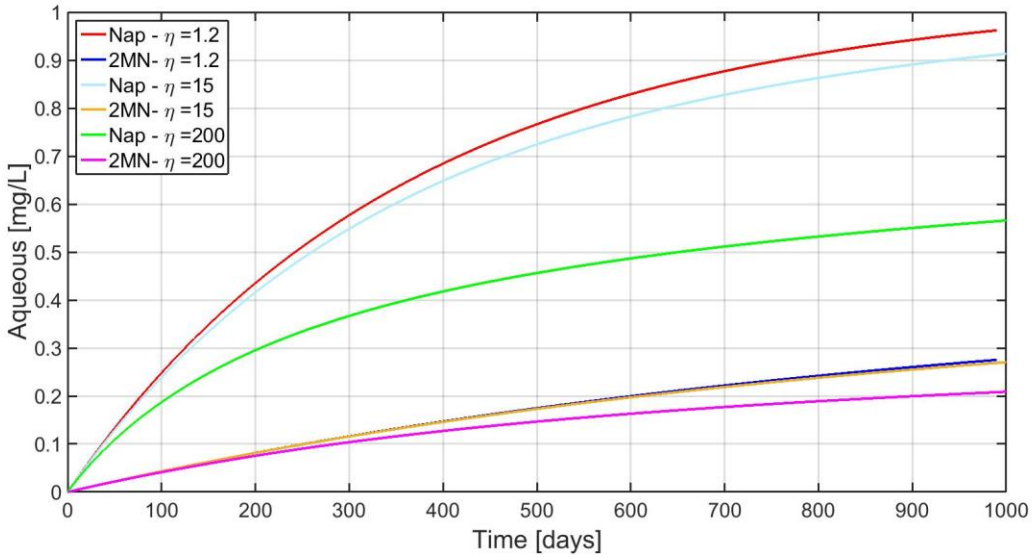


**Figure 3.4:** Aqueous concentration of naphthalene (Nap) and 2-methylnaphthalene (2MN) for different initial NAPL viscosities.

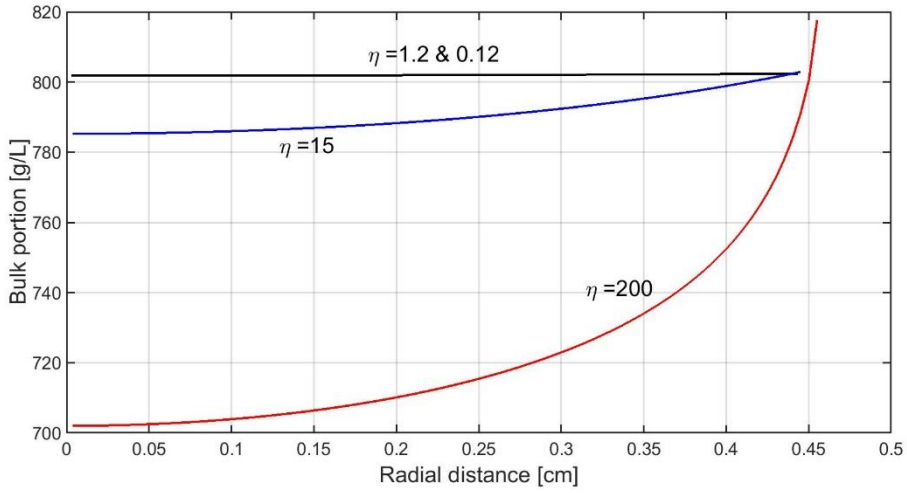


**Figure 3.5:** Radial concentration of the bulk portion for different initial NAPL viscosities at 1000 days.

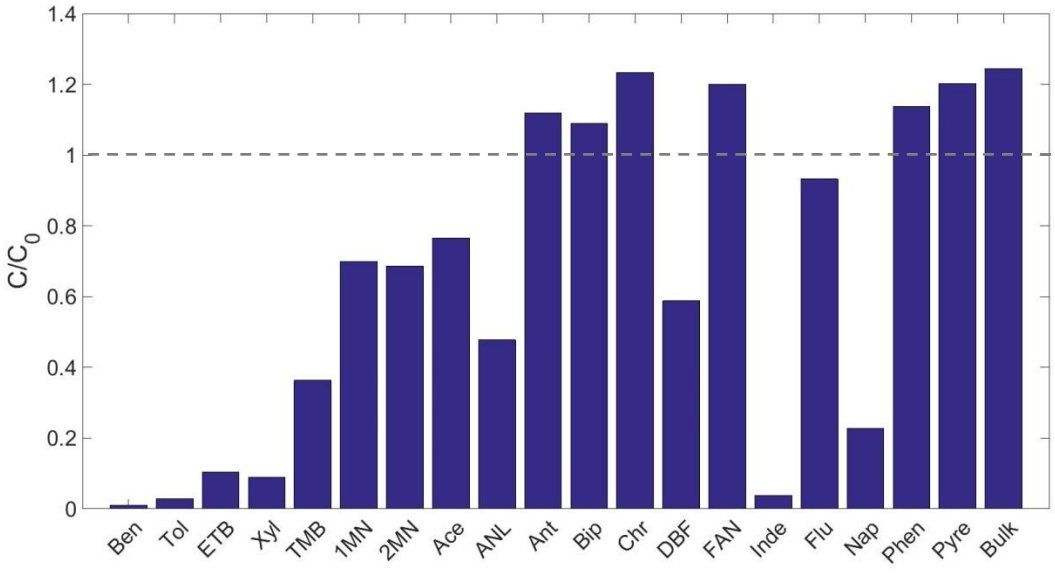


**Figure 3.6:** Ratio of final (1000 days) to initial component concentration within the medium viscous NAPL. From left to right: BTEX, TMB, PAHs in alphabetical order, and bulk portion.

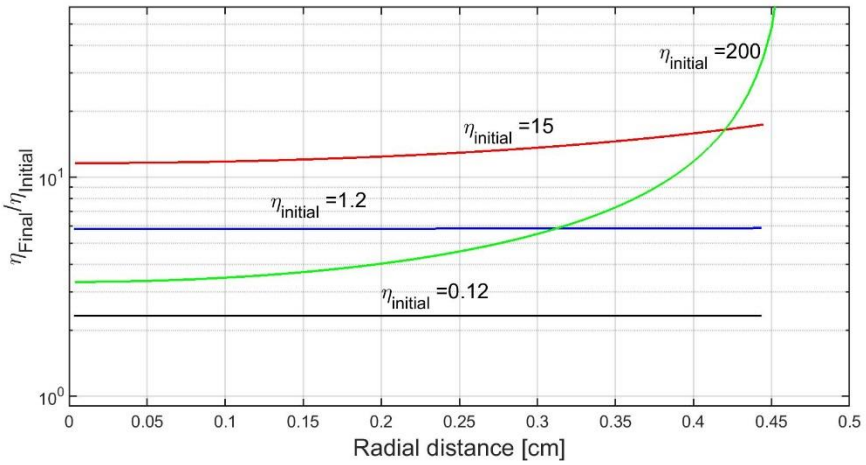


**Figure 3.7:** Ratio of final (1000 days) to initial viscosity for the different initial NAPL viscosities investigated.

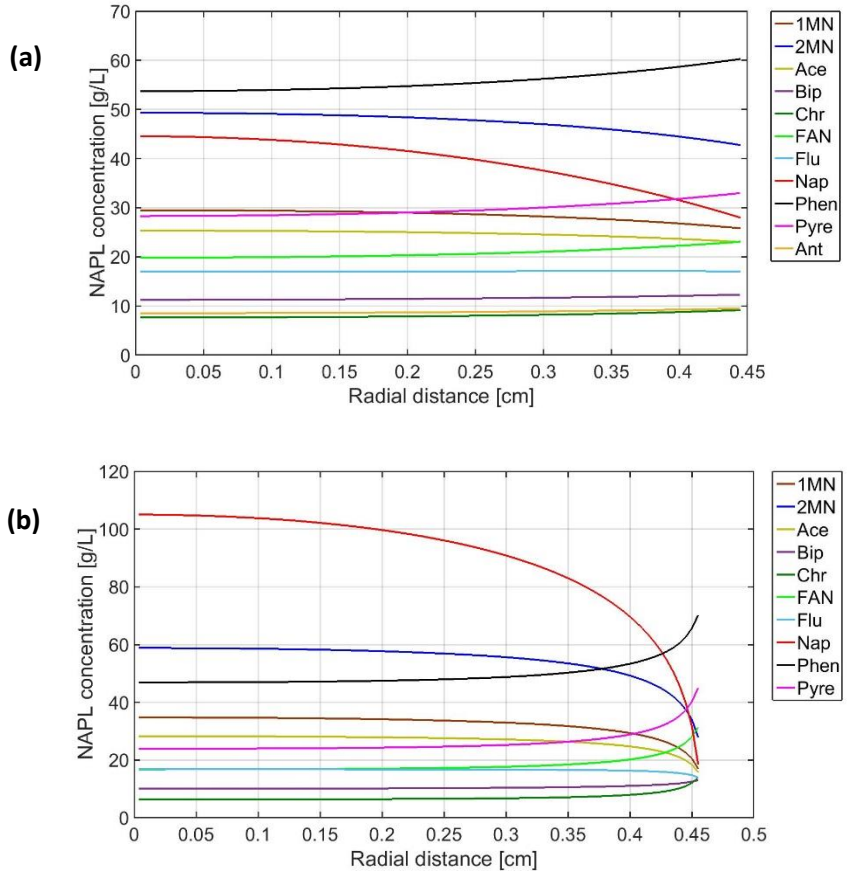


**Figure 3.8:** Simulated NAPL radial composition of the most predominant components at 1000 days for (a) the high viscous NAPL ($\eta_{initial}$ = 15 g/(cm s)), and (b) the very-high viscous NAPL ($\eta_{initial}$ = 200 g/(cm s)).

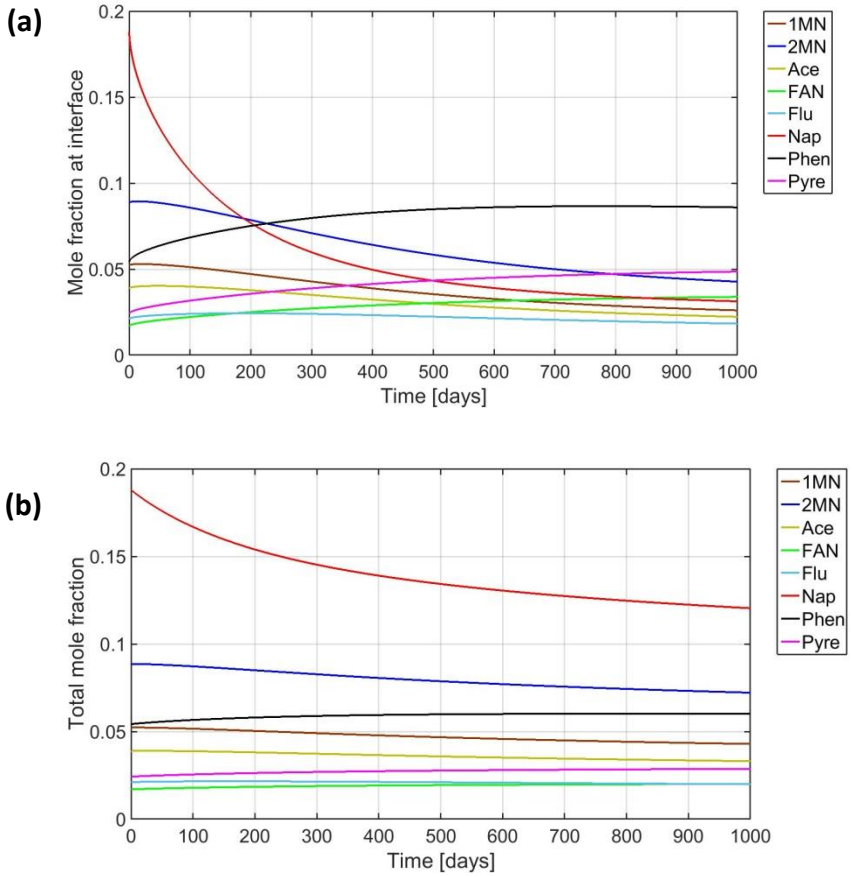


**Figure 3.9:** Temporal variation of the mole fractions for the very-high viscous NAPL ($\eta_{initial}$ = 200 g/(cm s)) at the (a) interface, and (b) within the entire NAPL body.

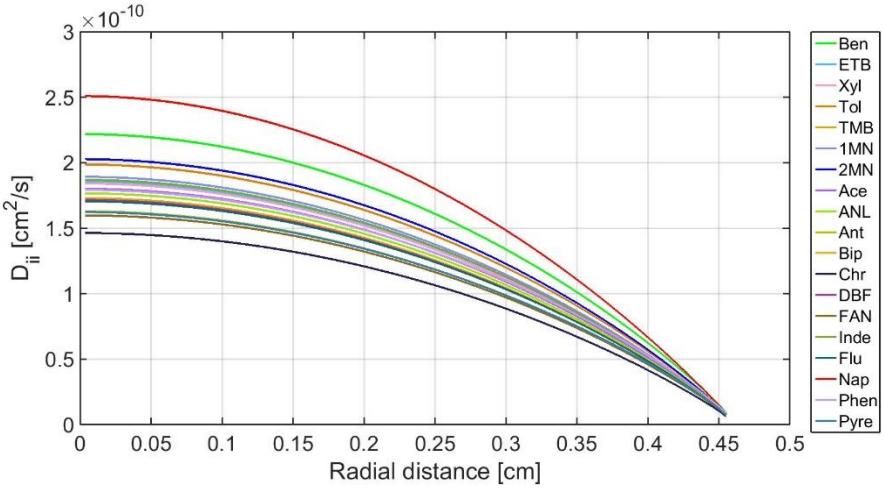


**Figure 3.10:** The radial distribution of the main intra-NAPL diffusion coefficients for the very-high viscous NAPL ($\eta_{initial}$ = 200 g/(cm s)) after 1000 days.

**Table 3.1:** Suite of organic components detected in the former MGP NAPL used in this study along with associated properties.

| Component | Identifier | NAPL Concentration [g/L] | Mole Fraction [-] | MW [g/mol] | Solubility [mg/L] | $f^S/f^L$ [-] | density [g/mL] | Viscosity (Eq.14) [g/(cm s)] | $V_{boiling}$ (Eq.17) [$cm^3$/mol] | Initial Activity Coefficient | |
|---|---|---|---|---|---|---|---|---|---|---|---|
| | | | | | | | | | | Experimental | UNIFAC |
| Benzene | Ben | 2.84E+00 | 6.89E-03 | 78.1 | 1780 [1] | 1 [1] | 0.88 | 6.49E-03 | 77 | 0.42 | 0.25 |
| Ethylbenzene | ETB | 5.97E+00 | 1.07E-02 | 106.2 | 161.2 [1] | 1 [1] | 0.87 | 6.78E-03 | 119 | 0.49 | 0.38 |
| Xylene(s) | Xyl | 3.50E+00 | 6.27E-03 | 106 | 373 [1] | 1 [1] | 0.87 | 6.97E-03 | 119 | 0.41 | 0.40 |
| Toluene | Tol | 1.13E+00 | 2.34E-03 | 92.1 | 534.8 [1] | 1 [1] | 0.86 | 6.00E-03 | 98 | 0.04 | 0.33 |
| Trimethylbenzene(s) | TMB | 5.78E+00 | 9.13E-03 | 120.2 | 57.4 [1] | 1 [1] | 0.88 | 8.75E-03 | 140 | 0.45 | 0.47 |
| 1-Methylnaphthalene | 1MN | 3.92E+01 | 5.23E-02 | 142.2 | 28.5 [1] | 1 [1] | 1.02 | 1.63E-02 | 140 | 0.38 | 0.49 |
| 2-Methylnaphthalene | 2MN | 6.63E+01 | 8.85E-02 | 142.2 | 25.4 [1] | 0.86 [1] | 1.01 | 1.63E-02 | 140 | 0.21 | 0.49 |
| Acenaphthene | Ace | 3.16E+01 | 3.89E-02 | 154.2 | 3.9 [1] | 0.2 [1] | 1.22 | 3.02E-02 | 147 | 0.22 | 0.64 |
| Acenaphthylene | ANL | 7.89E+00 | 9.83E-03 | 154 | 9.8 [1] | 0.22 [1] | 0.90 | 2.05E-02 | 133 | - | 0.57 |
| Anthracene | Ant | 8.19E+00 | 8.72E-03 | 178.2 | 0.05 [1] | 0.01 [1] | 1.28 | 4.10E-02 | 161 | - | 0.60 |
| Biphenyl | Bip | 1.10E+01 | 1.35E-02 | 154.2 | 7.5 [2] | 1 [3] | 1.04 | 2.08E-02 | 147 | - | 0.45 |
| Chrysene | Chr | 6.90E+00 | 5.74E-03 | 228.2 | 0.002 [1] | 0.0097 [1] | 1.27 | 9.32E-02 | 203 | - | 0.86 |
| Dibenzofuran | DBF | 4.82E+00 | 5.44E-03 | 168.2 | 10 [2] | 0.25 [4] | 1.09 | 3.23E-02 | 140 | - | 0.55 |
| Fluoranthene | FAN | 1.81E+01 | 1.70E-02 | 202.3 | 0.26 [1] | 0.21 [1] | 1.25 | 7.24E-02 | 175 | - | 0.86 |
| Indene | Inde | 2.42E-01 | 3.95E-04 | 116.16 | 390 [1] | 1 [3] | 1.00 | 1.10E-02 | 112 | - | 0.42 |
| Fluorene | Flu | 1.85E+01 | 2.11E-02 | 166.2 | 2 [1] | 0.16 [1] | 1.20 | 3.64E-02 | 154 | - | 0.63 |
| Naphthalene | Nap | 1.27E+02 | 1.88E-01 | 128.2 | 31.7 [1] | 0.3 [1] | 1.03 | 1.32E-02 | 119 | 0.35 | 0.40 |
| Phenanthrene | Phen | 5.09E+01 | 5.42E-02 | 178.2 | 1.3 [1] | 0.28 [1] | 0.98 | 3.14E-02 | 161 | - | 0.60 |
| Pyrene | Pyre | 2.59E+01 | 2.43E-02 | 202.3 | 0.13 [1] | 0.11 [1] | 1.27 | 6.39E-02 | 175 | - | 0.86 |
| Bulk | Bulk | 6.45E+02 | 4.37E-01 | 280 [5] | 2.00E-06 [5] | 1.00 | 1.14 | 2.37E+02 | 119 [6] | - | 0.73 |

1) From Eberhardt & Grathwohl (2002).
2) From Thomson et al. (2008).
3) Not available, assumed equal 1.
4) Mackay et al. (2006).
5) Assumed.
6) Assumed similar to naphthalene.

**Table 3.2:** Aqueous equilibrium concentration, and experimental lumped mass transfer rate coefficient ($k_w$) for the nine detected components present in the aqueous phase.

| | Aqueous Equilibrium Concentration | | | |
|---|---|---|---|---|
| | Experimental | Ideal | $k_w$ | |
| Component | [µg/L] | | [1/day] | $r^2$ |
| Benzene | 5200 | 12300 | 0.080 | 0.83 |
| Ethylbenzene | 850 [1] | 1720 | 0.042 | 0.98 |
| Xylene(s) | 450 [1] | 1090 | 0.036 | 0.98 |
| Toluene | 50 | 1250 | 0.061 | 0.98 |
| Trimethylbenzene(s) | 235 | 524 | 0.062 | 0.94 |
| 1-Methylnaphthalene | 570 | 1490 | 0.093 | 0.91 |
| 2-Methylnaphthalene | 560 | 2620 | 0.104 | 0.91 |
| Acenaphthene | 170 | 758 | 0.055 | 0.83 |
| Naphthalene | 7000 [1] | 19800 | 0.036 | 0.94 |

1) Calibrated with a least-squares analyses framework.

# Chapter 4

# Intra-NAPL Diffusion and Dissolution of Multi-Component NAPLs Subjected to Persulfate

## OUTLINE

Intra-NAPL diffusion is a critical process that can influence NAPL/water mass transfer. A series of physical model experiments was performed to investigate the role of intra-NAPL diffusion on the transient dissolution of complex multi-component NAPLs subjected to persulfate. A diffusion-based numerical model was developed and calibrated using the experimental data. The findings showed that a combination of NAPL composition and geometry, and interphase mass transfer rate results in intra-NAPL diffusion limitations. Rate-limited intra-NAPL diffusion within complex multi-component NAPLs can restrict mass transfer and hence impact treatment efficiency. The experimental results indicated that while persulfate was able to completely degrade dissolved phase components, mass loss after ~410 pore volumes (PVs) of persulfate injection was less than a no treatment scenario. A comparison of experimental and simulated results indicated that processes related to persulfate/NAPL interactions restricted mass transfer, and hence the multi-component mass transfer rate coefficients were ~70 % less than those estimated during an equivalent water flushing period.

## 4.1 INTRODUCTION

Mass transfer between water and complex multi-component non-aqueous phase liquids (NAPL) such as crude oil, creosote, and coal tars from former manufactured gas plants (MGPs) is a critical process that can affect the performance of remediation technologies (Luthy et al., 1994). Field and laboratory data indicate that NAPL/water mass transfer is usually limited by NAPL architecture, preferential flow, low residual saturation (Powers et al., 1998; Soga et al., 2004), and intra-NAPL diffusion (Luthy et al., 1993; Ortiz et al., 1999; Lekmine et al., 2014).

Intra-NAPL diffusion within a multi-component NAPL is influenced by the concentration gradients of all components present in the system (Cussler, 1997). The molecular size of constituent

components, presence of structurally dissimilar molecules, and heterogeneity within the organic mixture can limit intra-NAPL diffusion (Banerjee, 1984; Miller et al., 1985; Mukherji et al., 1997). When complex multi-component NAPLs are exposed to groundwater, the more soluble components will be depleted at the NAPL/water interface (Peters et al., 2000; Wehrer et al., 2013). This phenomenon is called weathering or ageing and affects dissolution. Weathering effects have been reported for coal tar (Luthy et al., 1993; Nelson et al., 1996), crude oil (Jada & Salou, 2002; Ghoshal et al., 2004; Varadaraj & Brons, 2012) and creosote (Alshafie & Ghoshal, 2004), and have been attributed to NAPL composition or inter-molecular interactions between water and organic compounds.

The low solubility of complex multi-component NAPLs due to compositional complexity and weathering effects can restrict the efficiency of water-based remediation methods. Hence, most remediation efforts have been limited to isolation and removal of these source materials (Luthy et al., 1994; Peters et al., 2000). Since chemical oxidants (i.e., permanganate and persulfate) have been able to oxidize most of the environmentally significant organic compounds (Krembs et al., 2010), it should be theoretically possible to use chemical oxidants to treat these complex multi-component NAPLs. When oxidants are added to these systems, in addition to the compositional complexities of multi-component NAPLs, other factors may also be involved that can influence NAPL/water mass transfer and treatment efficiency (Siegrist et al., 2011). For example, side reactions can result in the generation of by-products and/or precipitates which may hinder mass transfer (Thomson et al., 2008). Surfactant-like compounds that are temporally produced in reactions involving persulfate can enhance solubilization and potentially mobilize NAPL by decreasing interface tension (Conrad et al., 2002; Corbin et al., 2007; Gryzenia et al., 2009). Ndjou'ou and Cassidy (Ndjou'ou & Cassidy, 2006) reported that produced organic surfactants decreased surface tension, emulsified hydrocarbons, and eventually were degraded. Blanchard (Blanchard, 2010) reported that oxidants (i.e., hydrogen peroxide and ozone) increased MGP tar viscosity by degrading volatile components and naphthalene; and thus, indirectly influenced intra-NAPL diffusion and mass transfer (Ortiz et al., 1999).

Surprisingly, only a few studies have considered the role of intra-NAPL diffusion on NAPL/water mass transfer (Holman & Javandel, 1996; Brahma & Harmon, 2003). While a number of studies have investigated multi-component mass transfer processes (Peters & Luthy, 1993; Wehrer et al., 2013) and chemical oxidation of complex multi-component NAPLs (Hauswirth & Miller, 2014; Peng et al., 2016; Wang et al., 2015), to the best of our knowledge, no study has investigated intra-NAPL diffusion, film formation, and compositional changes of multi-component NAPLs in the

presence of a chemical oxidant. Hence the objective of this study was to explore the role of intra-NAPL diffusion on transient dissolution of multi-component NAPLs subjected to a chemical oxidant, and to identify some of the controlling processes which can restrict mass transfer. For the purpose of this evaluation, a numerical dissolution model was developed to simulate intra-NAPL diffusion within a multi-component NAPL exposed to water or oxidant solution. In addition, a series of physical model experiments without sediments was performed to investigate the direct interaction between a NAPL and persulfate or water under dynamic conditions. Changes in the NAPL and aqueous phase were monitored over the time and used to determine realistic model parameters (i.e., mass transfer rate coefficients, equilibrium concentration of NAPL constituents, activity coefficients, and NAPL characteristics).

# 4.2 EXPERIMENTAL INVESTIGATION

## 4.2.1 Materials and Methods

The MGP residuals used in this study were collected from the West Florida Natural Gas Company site located in Ocala, Florida. For the purpose of this experiment, our focus was on the dense portion (DNAPL) of the NAPL which was separated from the sample (see the Appendix C for more information). Table 4.1 lists the most abundant and soluble components within the DNAPL portion along some associated properties. The identified components account for ~33% of the total DNAPL by mass (19 compounds) and the remainder was unidentified.

The physical model experiments were designed to simulate an isolated rectangular NAPL body with only the top available for mass transfer (Figure 4.1). The physical model was a ~7 cm long cylindrical flow-through chamber made of glass with a pore volume (PV) of 9.7 mL. A Teflon sleeve was inserted snuggly into the bottom of the chamber and contained a DNAPL reservoir with surface area of 0.5 x 2.0 $cm^2$ and depth of ~0.22 cm (Figure C.1 in Appendix C). DNAPL in the reservoir was directly exposed to flowing water or persulfate solution while the NAPL surface area remained essentially constant. An in-line sampling system was used to collect aqueous samples from the effluent as required. The temporal mass loss and compositional changes of the NAPL was quantified in each system. Ten physical model experiments were performed.

Initially, each physical model was flushed by Milli-Q water at a nominal rate of 0.043 mL/min using a peristaltic pump. To ensure hydraulic consistency, a tracer test was performed on each model system by injecting 4 PVs of 100 mg/L NaBr solution. Following the tracer test, three (3) PVs of

Milli-Q water were injected to remove remnant NaBr from the physical model, and then 0.2 mL of the DNAPL was injected from the end of the physical model through the water using a 200 µL glass syringe (Hamilton, Sigma Aldrich) to completely fill the DNAPL reservoir. The surface of the NAPL within the Teflon reservoir was concave downward. During the filling process, one sub-sample was collected from the remnant NAPL in the glass syringe to establish the initial NAPL composition for each model.

Five (5) physical models were subsequently flushed with a 20 g/L persulfate solution (identified as OX) and five (5) systems were flushed with Milli-Q water as experimental controls (identified as CO) at a nominal rate of 0.043 mL/min (velocity of ~51 cm/day). The physical models were covered by aluminum foil and operated at ambient temperature (~20 $^{o}$C). Aqueous samples were collected daily and analyzed for a suite of organic components (Table 4.1), and persulfate concentration. The solution pH was determined and random effluent samples from each physical system were also collected for ion analysis. One oxidant and one control physical model was sacrificed on Day 7, 14, 30, 45, and 64. The NAPL from each physical model was homogenized and analyzed for the concentration for the suite of organic components (Table 4.1). Approximately ~410 PVs were flushed through the physical models sacrificed on Day 64.

The initial viscosity of the DNAPL was 1.22 g/(cm s) using a dilution viscometer (Cannon-Ubbelhode), and the initial density was 1.08 g/mL. Details of all reagents and analytical methods used in this study are presented in Appendix C.

## 4.2.2 Results and Discussion

The organic concentrations in the effluent samples collected from the persulfate systems indicated that all quantifiable dissolved phase components were < the method detection limit (MDL) and thus completely oxidized. However, for the control reactors a total of nine components were detected in the effluent including benzene, toluene, ethylbenzene, xylene (BTEX), trimethylbenzene(s), and four polycyclic aromatic hydrocarbons (PAHs) (naphthalene, 1-methylnaphthalene, 2-methylnaphthalene, and acenaphthene). The aqueous concentrations of the other quantifiable components were < MDL. The final NAPL concentrations (after flushing with 410 PVs) for BTEX was < 30% of the initial values, for naphthalene was ~60%, for trimethylbenzene, 1-mthlnaphthalene, 2-methylnaphthalene, and acenaphthene was ≤ 80%, and for the rest of components which were not detected in the aqueous phase were ~90% of the initial NAPL concentrations. The effluent pH steadily decreased from 5.5 to 4 for the control systems,

and from 3.5 to 2.5 for the persulfate systems likely due to the dissolution of organic acids. The effluent concentration of persulfate fluctuated around 20 g/L in the persulfate systems. Aside from sulfate and sodium present in the effluent from the persulfate systems, no other ions were detected.

No physical changes (i.e., color, temperature, precipitation) were observed in the control systems over the 64-day experimental period. In all the persulfate systems, the DNAPL was mobilized and spread out of the reservoir in the Teflon sleeve. After one week of flushing with the persulfate solution the NAPL/water surface area had increased by ~50% (Figure C.2 in Appendix C). This mobilization is likely related to changes in wettability and interfacial tension that did not occur in the control systems. Surfactants have been reported to be produced during chemical oxidation of hydrocarbons (Ndjou'ou & Cassidy, 2006; Gryzenia et al., 2009) and thus impact interfacial tension. In addition, the acidic condition in the persulfate physical models can have altered the wettability of the MGP NAPL (Barranco & Dawson, 1999; Zheng & Powers, 1999). Also the higher density of the persulfate solution compared to water in the control systems can have enhanced DNAPL mobilization. Thus, the observed NAPL mobilization in the persulfate systems is related to a lower interfacial tension, acidic condition and wettability of the system, and a higher density of the flushing solution.

Except for benzene and toluene, the effluent concentrations of the other seven (7) detectable components from control systems remained > MDL but steadily decreased (Figure 4.2). Naphthalene had the highest initial effluent concentration of ~1000 µg/L and decreased to ~600 µg/L after flushing with ~410 PVs of water. The effluent concentrations of other the PAHs (i.e., 2-methylnaphthalene and 1-methylnaphthalene) were relatively constant but significantly lower than naphthalene. While BTEX and trimethylbenzene have higher solubility's compared to PAHs, their effluent concentrations were lower due to their lower mole fractions and higher fugacity ratios. Benzene and toluene, which are the most soluble components, initially had a high effluent concentration but decreased to < MDL after flushing ~160 and ~100 PVs of water, respectfully.

The concentrations of organic components in the NAPL (Figure 4.3) decreased over the experimental period and were proportional to the decreasing trend of dissolved phase concentrations. The toluene NAPL concentration in the control systems remained > 1 g/kg after flushing ~300 PVs of water. However, toluene aqueous concentration decreased < MDL after flushing 100 PVs of water. Hence, while toluene has been present in the NAPL after flushing 100 PVs of water, the aqueous concentration of toluene was < MDL. This can be attributed to the

potential depletion of toluene at the interface that prevented toluene dissolution. In addition, benzene concentration in the NAPL fluctuated around 0.1 mg/g (close to MDL) after flushing 50 PVs of water, however, its aqueous concentration reached < MDL after flushing 160 PVs of water. Consequently, after 410 PVs of water flushing the two most soluble components were depleted. The xylene and ethylbenzene concentrations within NAPL also reached to ~1 g/kg and were close to be depleted.

The concentrations of organic components within the NAPL from the oxidant systems were higher than those values from control systems except for benzene and toluene which were depleted (Figure 4.3). The component concentrations within the NAPL from each physical model were divided by the associated initial values to determine normalized NAPL concentrations. The results indicated that after 410 PVs of flushing, the average normalized NAPL concentrations from the oxidant systems were ~5% higher than the associated values from the control systems. Hence, the NAPL/water mass transfer rate was larger in the control systems compared to the oxidant systems. Based on theoretical considerations, including the increased NAPL/water surface area due to NAPL mobilization, enhanced mass transfer and lower NAPL concentrations were expected in the oxidant systems. For this reduced mass transfer to occur when persulfate was present, some physical or chemical processes (e.g., interfacial interactions (Nelson et al., 1996), NAPL compositional changes (Peters et al., 2000), skin layer formation (Ghoshal et al., 2004), and precipitation (Thomson et al., 2008)) connected to the interaction between persulfate and MGP residuals restricted mass transfer in the oxidant systems compared to the control systems.

Toluene was the only component that had a lower NAPL concentration in the oxidant systems compared to the control systems (Figure 4.3). This difference was more pronounced after the first 50 PVs, and hence toluene dissolution appears to have been enhanced during the persulfate flush. However, due to restricted mass transfer, toluene concentration fluctuated around 1.2 g/kg within the persulfate systems until the end of experimental period. Since there was no limiting process in the control systems, the toluene concentration gradually decreased and eventually was less than the toluene concentration in the oxidant systems (Figure 4.3).

Despite efforts to ensure a homogeneous DNAPL was used in all physicals models, some data variability is evident in the assembled experimental results especially for components which have lower NAPL concentrations (e.g., BTEX). However, for the purpose of this study, the accumulated experimental data set was sufficient to provide information about the direct interaction of multi-

component NAPLs with water or persulfate, and to generate the required input parameters for simulation purposes.

# 4.3 MULTI-COMPONENT INTRA-NAPL DIFFUSION MODEL

## 4.3.1 Model Description

To investigate the role of intra-NAPL diffusion on transient dissolution of multi-component NAPLs subjected to persulfate, a temporal-spatial numerical dissolution model was developed. For the purpose of this evaluation, an isolated rectangular NAPL body with uniform initial concentration and only one side available for mass transfer was considered (Figure 4.1). The mass balance for each component within the NAPL can be written as (Bird et al., 2002):

$$\frac{\partial \mathrm{C_i}}{\partial \mathrm{t}} = \frac{\partial}{\partial \mathrm{x}} \left( \sum_{j=1}^{n-1} \mathrm{D_{ij}} \frac{\partial \mathrm{C_j}}{\partial \mathrm{x}} \right) \tag{4.1}$$

where $n$ is the total number of species with component $n$ chosen as the bulk portion of the NAPL, $\frac{\partial C_j}{\partial \mathrm{x}}$ is concentration gradient within the NAPL, $t$ is time, and $D_{ij}$ are intra-NAPL diffusion coefficients which were estimated by employing Kett and Anderson method (Kett & Anderson, 1969a). The diagonal terms of multi-component diffusion coefficients or main coefficients ($D_{ii}$) can be represented as:

$$D_{ii} = \frac{RTC_i}{\eta} \left\{ \left( \frac{1 - V_i C_i}{\sigma_i} + \frac{V_n C_i}{\sigma_n} \right) \left[ \left( \frac{\partial ln \gamma_i}{\partial C_i} \right) + \frac{1}{C_i} - \frac{1}{C_T} \left( 1 - \frac{V_i}{V_n} \right) \right] + \sum_{k=1,(k \neq i)}^{n-1} C_k \left( \frac{V_n}{\sigma_n} - \frac{V_k}{\sigma_k} \right) \left[ \left( \frac{\partial ln \gamma_k}{\partial C_i} \right) - \frac{1}{C_T} \left( 1 - \frac{V_i}{V_n} \right) \right] \right\} \tag{4.2a}$$

and off-diagonal coefficients ($D_{ij,i \neq j}$) can be written as:

$$D_{ij} = \frac{RTC_i}{\eta} \left\{ \left( \frac{1 - V_i C_i}{\sigma_i} + \frac{V_n C_i}{\sigma_n} \right) \left[ \left( \frac{\partial ln \gamma_i}{\partial C_j} \right) - \frac{1}{C_T} \left( 1 - \frac{V_j}{V_n} \right) \right] + C_j \left( \frac{V_n}{\sigma_n} - \frac{V_j}{\sigma_j} \right) \left[ \left( \frac{\partial ln \gamma_j}{\partial C_j} \right) + \frac{1}{C_j} - \frac{1}{C_T} \left( 1 - \frac{V_j}{V_n} \right) \right] + \sum_{k=1,(k \neq i,j)}^{n-1} C_k \left( \frac{V_n}{\sigma_n} - \frac{V_k}{\sigma_k} \right) \left[ \left( \frac{\partial ln \gamma_k}{\partial C_j} \right) - \frac{1}{C_T} \left( 1 - \frac{V_j}{V_n} \right) \right] \right\} \tag{4.2b}$$

where $C_T$ is the sum of molar concentrations of constituent components present in the mixture, $\gamma$ is the activity coefficient, $R$ is the universal gas constant, $V$ is the molar volume, $\sigma_i$ is the friction factor, $T$ is the absolute temperature, and $\eta$ is mixture viscosity.

The rectangular NAPL body was subjected to impermeable boundary conditions at external boundaries except at NAPL/water interface (Figure 4.1) which was subjected to the first-order mass transfer flux ($J_i$) (Miller et al., 1990; Weber & DiGiano, 1995) as given by:

$$J_i = K(C_{eq,i}^w - C_i^w) \tag{4.3}$$

where $K$ is mass transfer rate coefficient (L/T), $C_{eq,i}^w$ is the aqueous equilibrium concentration of each component, and $C_i^w$is the aqueous concentration. The aqueous equilibrium concentration for each component ($C_{eq,i}^w$) was estimated by using a modified form of Raoult's law (Lee et al., 1992) as:

$$C_{eq,i}^w = X_i^N \gamma_i^N \frac{S_i}{(f_i^s/f_i^l)} \tag{4.4}$$

where $N$ and $w$ superscripts refer to NAPL and water phase respectively, $S_i$ is the aqueous solubility of each component, and $f_i^s$ and $f_i^l$ are fugacities in the pure solid and pure liquid states, respectively (Table 4.1). To account for the film transfer resistances and compositional changes at the NAPL/water interface, the mole fractions in Eq. 4.4 were calculated based on the component concentrations at the NAPL/water boundary of the rectangular NAPL body.

To simulate aqueous concentrations along the cylindrical chamber (Figure 4.1), Eq. 4.1 was linked to the following one-dimensional advection-dispersion-reactive expression (Weber & DiGiano, 1995):

$$\frac{\partial C_i^w}{\partial t} = -v\frac{\partial C_i^w}{\partial x} + D\frac{\partial^2 C_i^w}{\partial x^2} + \frac{K}{d}\left(C_{eq,i}^w - C_i^w\right) - k_{ox,i}C_{ox}C_i^w \tag{4.5}$$

where $v$ is the aqueous velocity, $d$ is the depth of each cell, $D$ is dispersion coefficient, $C_{ox}$ is the oxidant concentration, and $k_{ox,i}$ is the second-order oxidation rate coefficient with respect to the oxidant for the $i^{th}$ constituent. The third term on right-hand side of Eq. 4.5 is active when NAPL is present. The oxidant concentration ($C_{ox}$) was calculated by employing a mass balance equation as (Weber & DiGiano, 1995):

$$\frac{\partial C_{ox}}{\partial t} = -v\frac{\partial C_{ox}^w}{\partial x} + D\frac{\partial^2 C_{ox}^w}{\partial x^2} - \sum_1^n \beta_i\, k_{ox,i}C_{ox}C_i^w \tag{4.6}$$

where $\beta_i$ is the stoichiometric mass ratio defined as the mass of oxidant consumed per mass of constituent degraded. The numerical model was coded and implemented in MATLAB 2014b (see Appendix C for details).

## 4.3.2 Model Parameterization and Investigated Scenarios

For the initial condition, a 0.2 g well-mixed rectangular NAPL body was specified and the initial concentrations of constituent components were assigned to be identical to the former MGP NAPL employed in the physical model experiments (Table 4.1) along with associated solubility, fugacity, and $\beta_i$ values. Similar to the physical models (Figure 4.1), the rectangular NAPL body was assumed to be in the middle of a cylindrical chamber with a length of 8 cm and cross surface area of ~1.2 cm$^2$. The NAPL body was in contact with the aqueous phase only on the top. A flow rate of 0.043 mL/min was used. Three different scenarios were considered: (1) water flushing scenario (identified as *W*) which is similar to the control system, (2) oxidant flushing scenario (identified as *OX*) which is the persulfate system, and (3) mobilized NAPL scenario (identified as *Mob*) which is persulfate system with increased NAPL/water contact area. The NAPL/water contact area was assigned 2.0 x 0.5 cm$^2$ for the water and oxidant scenarios. For the mobilized NAPL scenario, the NAPL/water interface was increased by 50% (2.0 x 0.75 cm$^2$) to be consistent with the experimental observations. Unfortunately, only a few second-order oxidation rate coefficients are available for persulfate in the literature (Sra et al., 2013) and therefore a single constant $k_{ox}$ of 1 L/(g day) was assigned for all of the components. To reduce the concentration of all dissolved components to ~MDL to be in agreement with the experimental results. The inlet oxidant concentration was set as 20 g/L for OX and Mob scenarios for the initial 410 PVs (64 days). The dispersion coefficient was determined to be 0.03 cm$^2$/day by fitting the simulated effluent concentrations to the tracer test results.

To estimate intra-NAPL diffusion coefficients (Eq. 4.2), the mixture viscosity ($\eta$) was estimated by using the Yon and Toor relationship (Kett & Anderson, 1969b). Activity coefficients were estimated using the universal Quasi-chemical functional group activity coefficient (UNIFAC) method (Poling et al., 2001) by assuming that the bulk portion of the NAPL is composed of an equal numbers (9) of individual functional groups within the identified components (Table 4.1) similar to Chapter 2. Kett and Anderson (1969a) suggested that if the self-diffusion ($D_i$) and infinite dilution diffusion coefficients ($D_{ij}^o$) for each component are available, the local friction factor can be estimated as:

$$\sigma_i = RT\left(\frac{X_i}{D_i\eta_i} + \sum_{j=1,j\neq i}^{n}\frac{X_j}{D_{ij}^o\eta_j}\right) \quad (4.7)$$

where $X_i$ is the mole fraction of each component within mixture, and $\eta_j$ is the viscosity of each pure component. For the purpose of this investigation, the viscosity of each component ($\eta_i$) was obtained from the literature (Lide, 1999) or estimated by using Orrick and Erbar method (Poling et al., 2001). Table 4.1 lists the molecular weight, viscosity, and density for each component. To estimate the friction factors (Eq. 4.7), the self and infinite dilution diffusion coefficients are required. Since most of the organic components are liquid in their pure state at ambient temperature their self and infinite dilution diffusion coefficients can be estimated with proposed relationships in the literature. PAHs with a fugacity ratio less than unity are solid at ambient temperature and estimation of their self and infinite diffusion coefficients requires consideration. In this modeling effort two different approaches were employed to estimate the self-diffusion coefficients for PAHs with a fugacity ratio less than unity as well as the infinite dilution diffusion coefficients of the remaining components within these PAHs.

In the first approach, identified as regular diffusion (RD) approach, the self and infinite dilution diffusion coefficients for PAHs with a fugacity ratio less than unity were estimated similar to the other components which are liquid at ambient temperature. This approach is plausible since PAHs with a fugacity ratio less than unity can exist as liquid due to melting point depression within multi-component mixtures (Peters et al., 1997). In the RD approach, self and infinite dilution diffusion coefficients were determined using estimation methods for organic liquids. The infinite dilution diffusion coefficients ($D_{ij}^{o}$) were estimated by a modified form of Tyn and Calus relationship (Poling et al., 2001), and self-diffusion data ($D_i$) were calculated using Houghton's Cubic Cell model (Houghton, 1964). The self and infinite dilution diffusion coefficients (range between $10^{-5}$ to $10^{-6}$ $cm^2/s$) used in this study are presented in Table C.1 in Appendix C.

To address the pure state of PAHs with a fugacity ratio less than unity that are solid at ambient temperature, the second approach, identified as modified diffusion approach (MD), was employed. In the MD approach the self and infinite dilution diffusion coefficients (Table C.1 in Appendix C) were modified for PAHs with a fugacity ratio less than unity so they are in the range as the self-diffusion coefficients in the crystal form. Unfortunately, there are only a few self-diffusion coefficients available for the crystal forms of PAHs and they are in the range of $10^{-10}$ to $10^{-13}$ $cm^2/s$ (Burns & Sherwood, 1972a, 1972b; Sherwood & Thomson, 1960; Sherwood & White, 1967). Thus, to investigate the complete range of self-diffusion coefficients for the crystal forms of PAHs with a fugacity ratio < 1, their self and infinite diffusion coefficients (which are in the same order for each component (Table C.1 in Appendix C)) were multiplied by $10^{-2}$, $10^{-3}$, and $10^{-6}$ $cm^2/s$ and identified as MD2, MD3, and MD6, respectively. This modification will decrease all of the

intra-NAPL diffusion coefficients by affecting the associated friction factors (Eq. 4.7). Hence, in this study four (4) different approaches (RD, MD2, MD3, and MD6) were employed and calibrated using the experimental NAPL and effluent concentrations from the physical model experiments.

NAPL viscosity can control mass transfer process and intra-NAPL diffusion (Ortiz et al., 1999). Birak and Miller (Birak & Miller, 2009) reported that the viscosity of MGP tars comprised of coal, water-gas, and oil gas tars can range from 0.091 to 6600 g/(cm s). To investigate the effect of viscosity on intra-NAPL diffusion within complex NAPLs subjected to chemical oxidation, a high viscous NAPL (viscosity of 200 g/(cm s)) was also simulated in addition to the NAPL used in the physical model experiments (viscosity of 1.2 g/(cm s)).

## 4.3.3 Results and Discussion

### 4.3.3.1 Water Flushing Scenario Calibration

Since the focus of this study was on the intra-NAPL conditions and diffusion resistance, a single constant mass transfer rate coefficient (Eq. 4.3) for each approach (RD, MD2, MD3, and MD6) for the water flushing scenario was determined. A least-squares analysis framework was used in conjunction with the experimental effluent concentrations from the control systems (Figure 4.2) for all detectable components except benzene and toluene. Benzene and toluene were excluded from the least-squares analysis since their aqueous concentrations where < MDL during the experimental period and this would influence the calibration results. The mass transfer rate coefficients for benzene ($K_{Ben}$) and toluene ($K_{Tol}$) were determined separately.

The comparison of the experimental and simulation results (Figure 4.2) for the water flushing scenario indicates that while the MD6 approach was in agreement with the effluent concentration for toluene which had low aqueous and NAPL concentrations, the RD approach captured the effluent concentration of the other components better. The results from the MD2 to MD6 approaches gradually deviate from the experimental results. Hence the RD approach which assumes that all the organic components are liquid within the MGP NAPL better represents intra-NAPL diffusion. As expected, the calibration framework employed was controlled with the most dominant components. For example, the naphthalene aqueous concentration is 5 times higher compared to the rest of the components. Thus, while the simulated results match the observed naphthalene concentration profile, they are slightly dissimilar for the other components (Figure 4.2).

The RD approach matched the experimental aqueous concentrations the best and was chosen for the long-term simulations. The best-fit mass transfer rate coefficient was 9.6 cm/day for all components expect for benzene ($K_{Ben}$ = 24.5 cm/day) and toluene ($K_{Tol}$ = 0.6 cm/day). These calibrated mass transfer rate coefficients for the water flushing scenario using RD approach were identified by $K_w$.

4.3.3.2 Calibration of Oxidant Flushing and Mobilized NAPL Scenarios

The experimental results indicated that in the physical models that were flushed with persulfate the NAPL was mobilized and the overall mass transfer was less than the control systems. To address these issues, the mass transfer rate coefficients during persulfate flushing using the RD approach (identified as $K_{ox}$) were estimated so that the simulated NAPL concentrations for the Mob scenario (equivalent to the experimental persulfate systems) were higher than those for the W scenario (equivalent to the experimental control systems) to be consistent with the experimental observations (Figure 4.3).

The experimental NAPL concentrations from both the persulfate and control systems after 410 PVs of flushing (final concentrations) were divided by the associated initial concentrations to determine the final experimental normalized NAPL concentrations (identified as $C_{ox\text{-}N}$ for the persulfate systems and $C_{co\text{-}N}$ for the control systems). Then, the ratio of $C_{ox\text{-}N}$ to $C_{co\text{-}N}$ were calculated and identified as $R_{exp}$. In addition, the ratio of the simulated NAPL concentrations from the Mob scenario after 410 PVs to those from the W scenario were also determined (identified as $R_{sim}$). A least-squares analysis framework was used to determine the best-fit $K_{ox}$ values so that $R_{sim}$ matched $R_{exp}$. Only the most dominant components (naphthalene, 1-methylnaphthalene, 2-methylnaphthalene) were used in this calibration procedure. The results from this calibration exercise indicate that the best-fit $K_{ox}$ values are 70% smaller than the $K_w$ values (Figure 4.3) which is consistent with the experimental observations that persulfate/NAPL interactions inhibited interphase mass transfer.

4.3.3.3 Long-term Simulations

To investigate treatment expectations and compare temporal compositional changes within the complex NAPLs following persulfate or water flushing, a series of long-term simulations were performed. The long-term simulations were run arbitrarily for 6400 PVs (1000 days) which was deemed sufficient to observe changes in intra-NAPL diffusional flux and composition. Because it is possible that at the end of an oxidant flushing episode $K_{ox}$ values might increase to the $K_w$

values the long-term simulations of the oxidant and mobilized NAPL scenarios were performed using two different methods. Hence, a total of five scenarios were simulated:

i. Water flushing scenario with NAPL/water contact area of 2.0 x 0.5 $cm^2$ using $K_w$ values during the 6400 PV flushing period, identified as *W*, representative of the experimental control systems.
ii. Mobilized NAPL scenario with NAPL/water contact area of 2.0 x 0.75 $cm^2$ using $K_{ox}$ values during the 6400 PV flushing period, identified as $Mob_{ox}$.
iii. Mobilized NAPL scenario with NAPL/water contact area of 2.0 x 0.75 $cm^2$ using $K_{ox}$ values during the persulfate flushing period (initial 410 PVs) and then $K_{ox}$ values were replaced with $K_w$ values, identified as $Mob_{ox\text{-}w}$.
iv. Oxidant flushing scenario with NAPL/water contact area of 2.0 x 0. 5 $cm^2$ using $K_{ox}$ values during the 6400 PV flushing period, identified as $OX_{ox}$.
v. Oxidant flushing scenario with NAPL/water contact area of 2.0 x 0. 5 $cm^2$ using $K_{ox}$ values during the persulfate flushing period (initial 410 PVs) and then $K_{ox}$ values were replaced with $K_w$ values, identified as $OX_{ox\text{-}w}$.

Similar to the experimental aqueous results (Figure 4.2), naphthalene had the highest initial simulated aqueous concentration in the effluent. The long-term temporal expectations for naphthalene effluent concentrations are presented in Figure 4.4 for all the five scenarios. The initial naphthalene aqueous concentration for the W scenario was ~0.85 mg/L and gradually decreased to < 0.1 mg/L. Following 410 PVs of persulfate flushing the aqueous concentrations rebounded for both the Mob and OX scenarios. The highest naphthalene aqueous concentration following persulfate injection as well as the lowest value after 6400 PVs was produced from the $Mob_{ox\text{-}w}$ scenario. This is attributed to the larger NAPL/water contact area as well as the large mass transfer rate coefficients ($K_w$). The aqueous concentration of naphthalene for the $OX_{ox\text{-}w}$ scenario following persulfate flushing was similar to that from the W scenario due to similar contact area and mass transfer rate coefficient. The lowest naphthalene aqueous concentrations after persulfate flushing was produced from the $Mob_{ox}$ and $OX_{ox}$ scenarios due to smaller mass transfer rate coefficient. Hence, if the persulfate/NAPL interactions which restricted interphase mass transfer remain after persulfate flushing, the dissolved phase concentrations after treatment period will be initially lower than those from the no-treatment (W) scenario. However, in the long-term, aqueous concentrations from the treatment scenarios will be higher than those from the no-

treatment scenario. If the mass transfer rate coefficients increase following persulfate flushing, no significant difference can be expected between treatment and no-treatment scenarios.

The final NAPL concentrations after 6400 PVs of flushing for the W scenario (Figure C.3 in Appendix C) indicate that naphthalene and 2-methylnaphthalene concentrations decreased considerably while phenanthrene concentration increased. However, no concentration gradient was established and the NAPL body was homogeneous. The initial estimated main intra-NAPL diffusion coefficients were in the range of $1x10^{-7}$ $cm^2/s$, and internal diffusion did not restrict mass transfer at the NAPL/water boundary. A sensitivity analyses was performed to explore potential conditions when intra-NAPL diffusion limitations would arise. The findings indicated that when the mass transfer rate coefficient (Eq. 4.3) was increased to > 30 cm/day, or the NAPL depth increased to > 1 cm (mass of >1 g and surface area of ~1 $cm^2$), intra-NAPL concentration gradients were established. Thus, a combination of NAPL composition, NAPL geometry, and interphase mass transfer rate can result in intra-NAPL diffusion limitations. Numerous flushing-based remediation technologies that rely on an elevated system flow rate to increase mass transfer rate will therefore restrict internal diffusion and enhance mass transfer limitations.

Due to larger NAPL/water contact area and hence larger mass transfer rate, the NAPL concentrations from the $Mob_{ox\text{-}w}$ after 6400 PVs of flushing are lower than those from the W scenario (Figure 4.5). However, the NAPL concentrations from the $Mob_{ox}$ scenario after 6400 PVs of flushing are higher than those from the W scenario and can be attributed to the smaller mass transfer rate coefficients ($K_{ox}$) used for the $Mob_{ox}$ scenario compared to those ($K_w$) used for the W scenario. This impact is significant for the more soluble components (i.e., naphthalene, ethylbenzene, and xylene) except for benzene and toluene. Benzene was depleted due to higher solubility and mass transfer rate coefficient. The toluene mass transfer rate coefficient was significantly smaller than for other organic components. After 6400 PVs of flushing for the W, $Mob_{ox\text{-}w}$, and $Mob_{ox}$ scenarios, 60%, 65%, and 40% of the initial mass quantified was removed, respectively. The final NAPL concentrations from the $OX_{ox\text{-}w}$ scenario (Figure C.4 in Appendix C) are the same (within 1%) as the results from the W scenario indicating that persulfate flushing did not enhance mass transfer. The final NAPL concentrations from the $OX_{ox}$ scenario (Figure C.4 in Appendix C) are significantly higher than those from the $Mob_{ox}$ scenario (Figure 4.5). After 6400 PVs of flushing 60% and 40% of the initial mass quantified was removed for the $OX_{ox\text{-}w}$ and $OX_{ox}$ scenarios, respectively. If the persulfate/NAPL interactions which restricted interphase mass transfer remain following persulfate flushing, the water flushing (no-treatment) scenario would be more efficient compared to 410 PVs (64 days) persulfate flushing. Even if the mass transfer rate

coefficients increase following persulfate flushing, chemical oxidation without mobilization effects would be similar to the no-treatment scenario. However, if NAPL mobilization occurs, it can enhance mass removal.

#### 4.3.3.4 High Viscous NAPL

The initial naphthalene aqueous concentration for the high viscous NAPL (Figure C.5 in Appendix C) is similar to that for the low viscous NAPL; however, naphthalene aqueous concentration for the high viscous NAPL for all five scenarios decreased faster than that for the low viscous NAPL. The simulated NAPL concentrations indicate that due to the high viscosity, concentration gradients are established even for the thin NAPL body simulated (Figure 4.6 and C.6 in Appendix C). After 6400 PVs of water flushing using W scenario, the interfacial naphthalene concentration within the high viscous NAPL is similar to that for the low viscous NAPL (Figure C.3 in Appendix C). However, naphthalene has the highest concentration at the bottom of the high viscous NAPL indicating the effects of rate-limited intra-NAPL diffusion. After 6400 PVs of flushing, 40 and 60% of the initial mass quantified was removed from the high viscous and low viscous NAPLs; respectively, for the W scenario indicating restricted mass transfer for the high viscous NAPL. The initial main intra-NAPL diffusion coefficients for the high viscous NAPL were ~$5x10^{-10}$ $cm^2/s$ which result in internal diffusion limitations for this system.

While the NAPL concentrations after 6400 PVs of flushing for the $OX_{ox-w}$ scenario are similar to the W scenario (Figure 4.6(a)), the results from the $OX_{ox}$ scenario indicate that more soluble components have higher concentrations (Figure 4.6(b)) and can be attributed to the lower mass transfer rate coefficients. It was demonstrated that 40% and 25% of the initial mass quantified was removed with the $OX_{ox-w}$ and $OX_{ox}$, respectively. In addition, 50 and 35% of the initial mass quantified was removed in the $Mob_{ox-w}$ and $Mob_{ox}$ scenarios, respectively. Hence, if the mass transfer rate coefficients do not increase following persulfate flushing even the larger contact area cannot compensate for mass transfer limitations.

#### 4.3.3.5 Environmental Implications

The experimental and computational effort described here is the first effort to provide information regarding the role of intra-NAPL diffusion on the dissolution of MGP NAPLs subjected to persulfate. The diffusion-based model developed provides an appropriate platform to capture the temporal and spatial mass flux and compositional changes within complex NAPLs. It was demonstrated that a combination of NAPL composition, NAPL geometry, and interphase mass

transfer can result in intra-NAPL diffusion limitations; hence, increasing mass transfer by remediation activities or the presence of thick NAPL pools may result in internal concentration gradients and film formation. Therefore, methods to overcome mass transfer limitations and intra-NAPL resistance are required for the effective remediation of complex multi-component NAPLs.

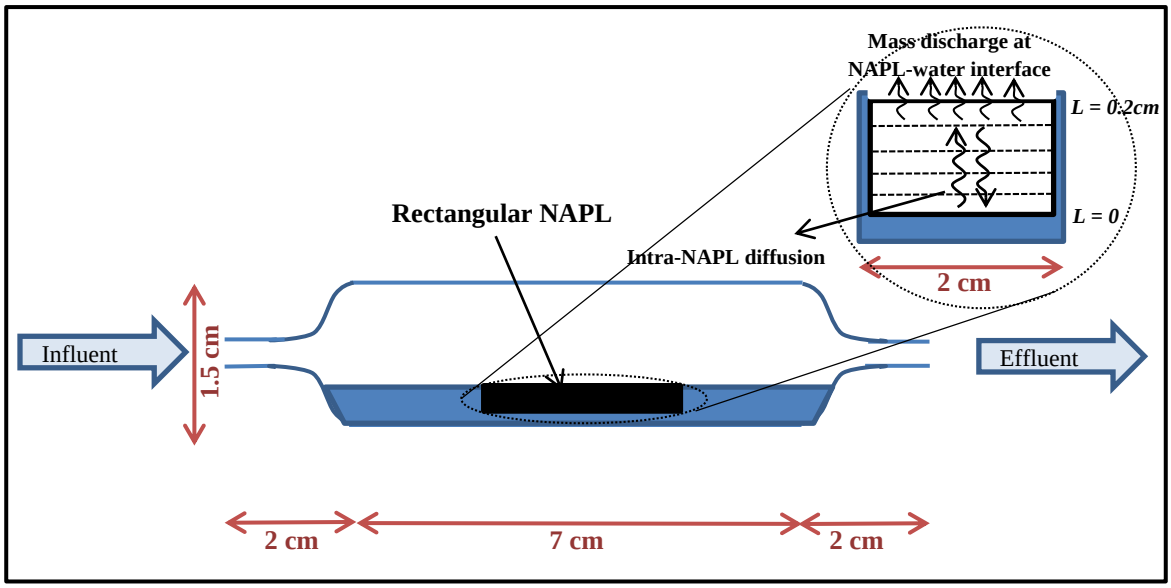


**Figure 4.1:** Schematic of the physical model system. The outer glass chamber is cylindrical and a sleeve which contains a DNAPL reservoir is inserted into the bottom of the chamber. The insert shows the numerical representation associated with Eq. 4.1.

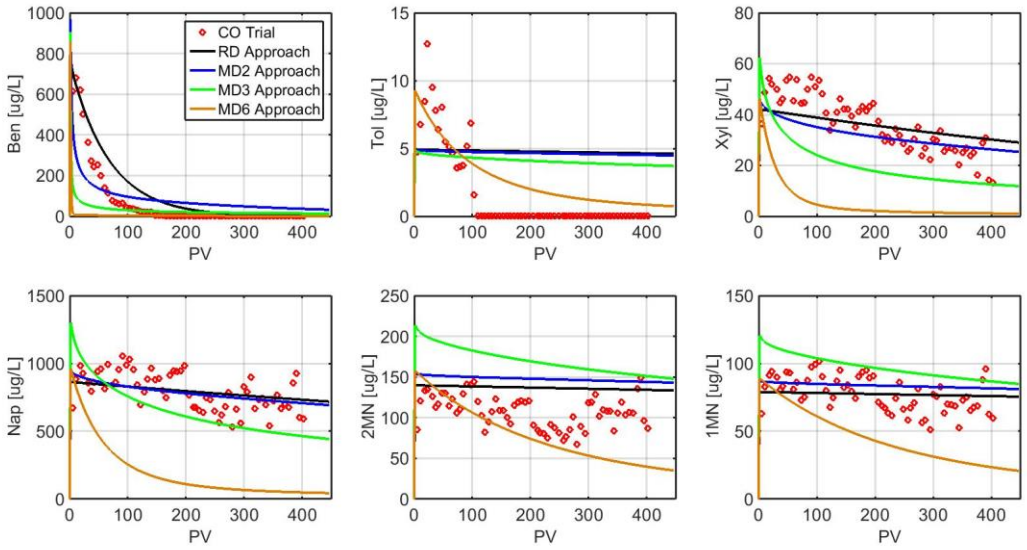


**Figure 4.2:** Effluent aqueous concentrations from the control systems and simulated results under the water flushing scenario using different approaches.

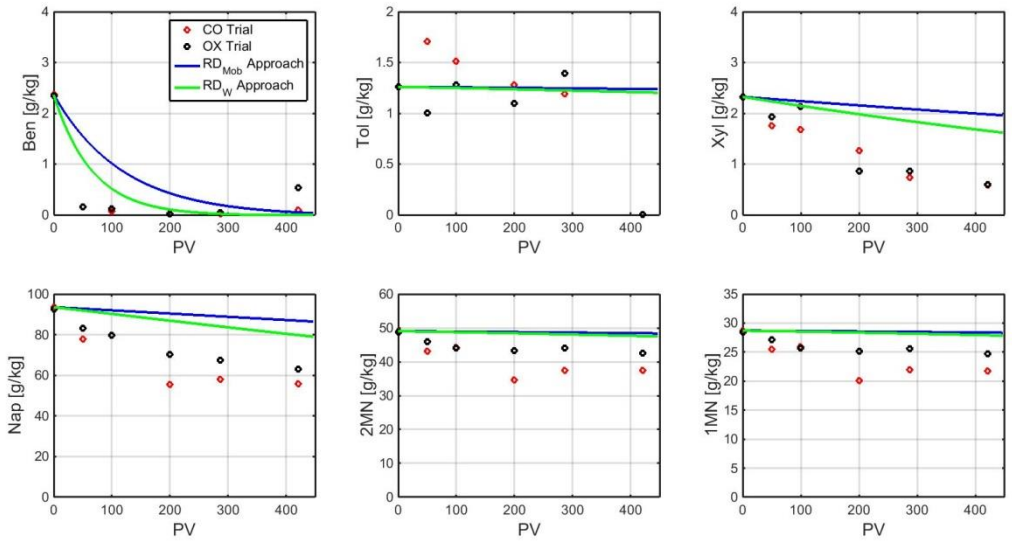


**Figure 4.3:** NAPL concentrations from the control (red symbols) and persulfate (black symbols) physical models, and simulated results (lines) for the water flushing and mobilized NAPL scenarios using the RD approach.

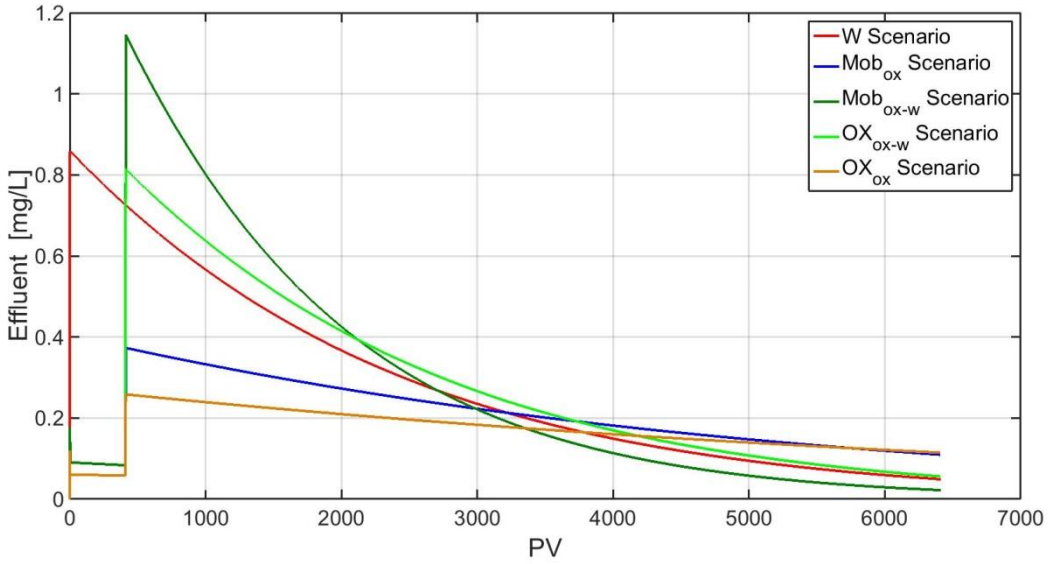


**Figure 4.4:** Naphthalene effluent concentration for the low viscous NAPL for the water flushing (W), mobilized NAPL (Mob), and oxidant flushing (OX) scenarios.

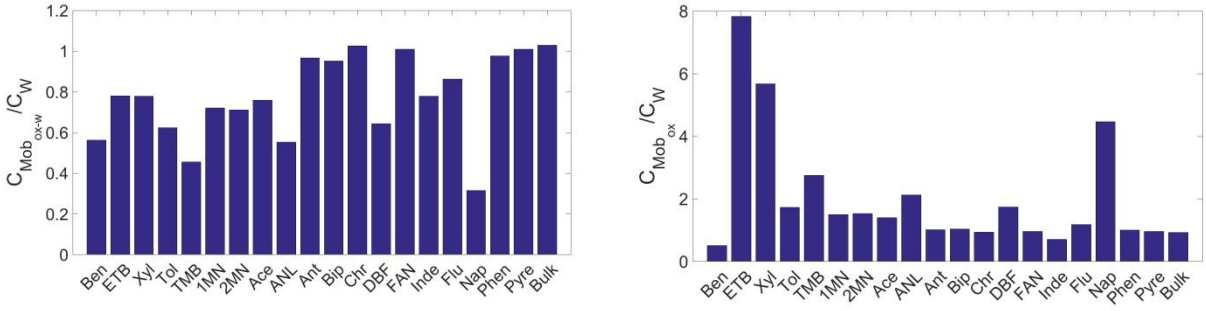


**Figure 4.5:** Ratios of the NAPL concentrations from the mobilized NAPL scenario ($C_{Mob}$) to the water flushing scenario ($C_w$) after 6400 PVs.

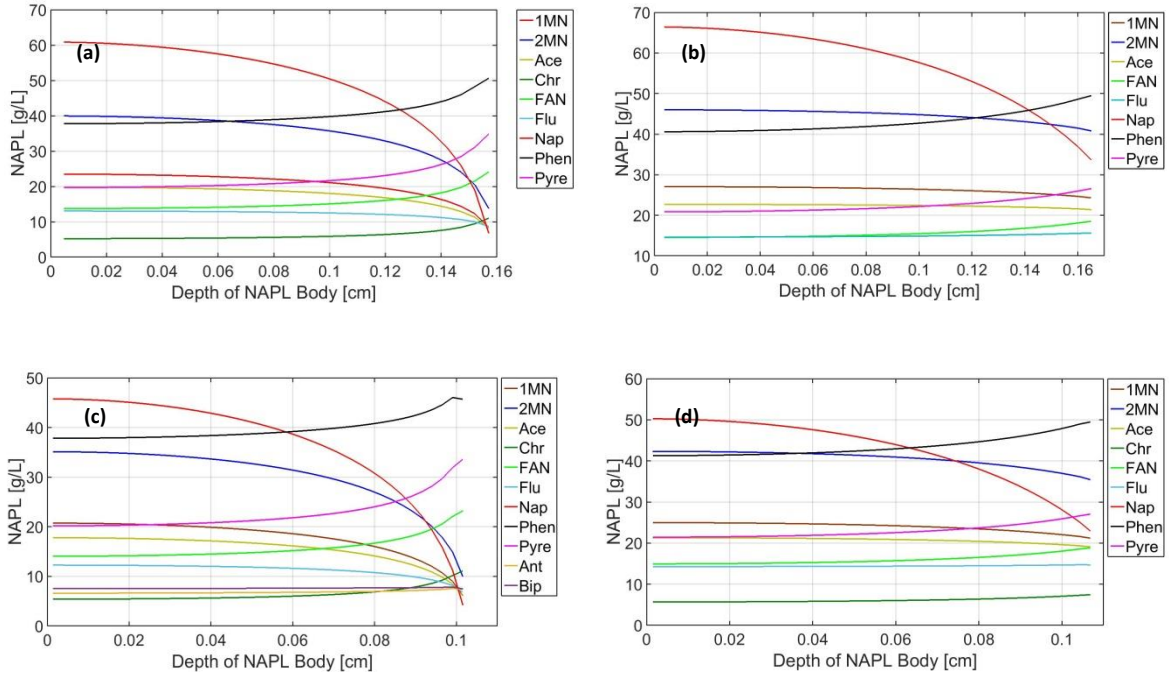


**Figure 4.6:** High viscous NAPL concentrations of the most predominant components after 6400 PVs of flushing: a) water and $OX_{ox}$ scenarios, b) $OX_{ox}$ scenario, c) $Mob_{ox-w}$ scenario, d) $Mob_{ox}$ scenario.

**Table 4.1:** Suite of organic components detected in the NAPL along with associated properties.

| Compound | Identifier | NAPL Concentration [g/L] | Mole Fraction [-] | MW [g/mol] | Solubility [mg/L] | $f^S/f^L$ [-] | Density [g/mL] | Viscosity [g/(cm.sec)] | Beta [g/g] |
|---|---|---|---|---|---|---|---|---|---|
| Benzene | Ben | 2.57E+00 | 6.57E-03 | 78.1 | 1780 [1] | 1 [1] | 0.88 | 6.49E-03 | 45.74 |
| Ethylbenzene | ETB | 4.72E+00 | 8.86E-03 | 106.2 | 161.2 [1] | 1 [1] | 0.87 | 6.78E-03 | 47.12 |
| Xylene(s) | Xyl | 2.52E+00 | 4.74E-03 | 106 | 173 [1] | 1 [1] | 0.87 | 6.97E-03 | 47.12 |
| Toluene | Tol | 1.51E+00 | 3.27E-03 | 92.1 | 534.8 [1] | 1 [1] | 0.86 | 6.00E-03 | 46.53 |
| Trimethylbenzene(s) | TMB | 4.40E+00 | 7.30E-03 | 120.2 | 57.4 [1] | 1 [1] | 0.88 | 8.75E-03 | 47.56 |
| 1-Methylnaphthalene | 1MN | 3.11E+01 | 4.37E-02 | 142.2 | 28.5 [1] | 1 [1] | 1.02 | 1.63E-02 | 45.23 |
| 2-Methylnaphthalene | 2MN | 5.32E+01 | 7.46E-02 | 142.2 | 25.4 [1] | 0.86 [1] | 1.01 | 1.63E-02 | 45.23 |
| Acenaphthene | Ace | 2.55E+01 | 3.30E-02 | 154.2 | 3.9 [1] | 0.2 [1] | 1.22 | 3.02E-02 | 44.79 |
| Acenaphthylene | ANL | 6.25E+00 | 8.19E-03 | 154 | 9.8 [1] | 0.22 [1] | 0.90 | 2.05E-02 | 43.82 |
| Anthracene | Ant | 7.25E+00 | 8.13E-03 | 178.2 | 0.05 [1] | 0.01 [1] | 1.28 | 4.10E-02 | 44.1 |
| Biphenyl | Bip | 8.45E+00 | 1.09E-02 | 154.2 | 7.5 [2] | 1 [3] | 1.04 | 2.08E-02 | 44.79 |
| Chrysene | Chr | 5.42E+00 | 4.74E-03 | 228.2 | 0.002 [1] | 0.0097 [1] | 1.27 | 9.32E-02 | 43.83 |
| Dibenzofuran | DBF | 4.14E+00 | 4.91E-03 | 168.2 | 10 [2] | 0.25 [4] | 1.09 | 3.23E-02 | 38.24 |
| Fluoranthene | FAN | 1.44E+01 | 1.42E-02 | 202.3 | 0.26 [1] | 0.21 [1] | 1.25 | 7.24E-02 | 43.57 |
| Indene | Inde | 4.03E-01 | 6.92E-04 | 116.16 | 390 [1] | 1 [3] | 1.00 | 1.10E-02 | 45.11 |
| Fluorene | Flu | 1.56E+01 | 1.87E-02 | 166.2 | 2 [1] | 0.16 [1] | 1.20 | 3.64E-02 | 44.42 |
| Naphthalene | Nap | 1.01E+02 | 1.58E-01 | 128.2 | 31.7 [1] | 0.3 [1] | 1.03 | 1.32E-02 | 44.6 |
| Phenanthrene | Phen | 4.08E+01 | 4.57E-02 | 178.2 | 1.3 [1] | 0.28 [1] | 0.98 | 3.14E-02 | 44.1 |
| Pyrene | Pyre | 2.06E+01 | 2.04E-02 | 202.3 | 0.13 [1] | 0.11 [1] | 1.27 | 6.39E-02 | 43.58 |
| Bulk | Bulk | 7.34E+02 | 5.23E-01 | 280 [5] | 2.00E-06 [5] | 1.00 | 1.14 | 5.25E+01 | 0 |

1) From Eberhardt & Grathwohl (2002).
2) From Thomson et al. (2008).
3) Not available, assumed equal 1.
4) Mackay et al. (2006).
5) Assumed.

# Chapter 5

# Closure

## 5.1 CONCLUSION AND CONTRIBUTIONS

The primary goal of this research was to provide an understanding of mass transfer from multi-component NAPLs subjected to chemical oxidants. A series of static and physical model experiments were performed to investigate the performance of two chemical oxidants to degrade MGP residuals, assess the diffusion-limited multi-component mass transfer behavior, and determine the effects of chemical oxidation on multi-component mass transfer processes. In addition, numerical simulations were employed to assess the long-term behavior of dissolved phase concentrations following chemical oxidation of MGP residuals and capture some of the controlling situations where multi-component mass transfer processes can be restricted by intra-NAPL diffusion.

The significant contributions of this research are:

- The experimental study described in Chapter 2 is the first investigation to compare the feasibility and performance of two important chemical oxidants under both static and dynamic conditions to degrade MGP residuals. The developed screening model is the first study that investigates the long-term behaviour of 22 dissolved components following ISCO treatment. The results provide a data set that can be used to define end-point expectations of chemical oxidation of MGP residuals and distinguish the most important parameters which can influence treatment efficiency.
- The modeling study described in Chapter 3 is the first effort to simulate the temporal and spatial compositional changes within complex NAPLs. The role of multi-component intra-NAPL diffusion on NAPL-water mass transfer processes was investigated to identify some of the controlling conditions where this process needs to be considered. The model provides an appropriate platform in which the complex processes involved in NAPL-water mass transfer and internal diffusional fluxes are captured.
- The experimental and computational study described in Chapter 4 is the first effort that provides comprehensive information about the role of intra-NAPL diffusion on dissolution

of a MGP NAPL which is directly in contact with persulfate under controlled conditions. The lessons learned have applicable aspects for remediation of complex NAPLs.

The major conclusions of this research are:

- Dissolved phase organic components were readily degraded with persulfate or permanganate (except for benzene) in well-mixed aqueous systems. In well-mixed slurry systems, permanganate, unactivated persulfate, and alkaline activated persulfate were able to degrade >95%, 45% and 30% of the initial mass quantified, respectively. The results demonstrate that when constituent components are dissolved, chemical oxidants were powerful enough to degrade MGP mass. Due to the well-mixed conditions in the batch experiments, the oxidant/NAPL contact was optimal and hence, the findings provide an optimistic view of the end point expectations of chemical oxidation of MGP residuals.
- There was no net benefit of flushing 6 PVs of permanganate or persulfate at a concentration of 30 g/L through MGP impacted soil under the physical model operating conditions. The results provided a more realistic picture of the potential for ISCO treatment of MGP residuals. The comparison of the initial and final bulk soil concentration data indicated that both persulfate and permanganate had lower efficiency in the physical model experiments compared to the well-mixed slurry batch experiments. Permanganate outperformed persulfate in terms of impacting a change to the system effluent concentration and bulk soil concentration; albeit this change was minor.
- Long-term simulation results that involved a NAPL saturation of between 4% and 8% indicated that the effluent profiles were reduced temporality as a result of the injection of 6 PVs of oxidant and then rebounded to a profile that was coincident with a no-treatment/natural dissolution scenario. Oxidant treatment (6 PVs at 30 g/L) was only effective at low NAPL saturations (<1%) and factors such as oxidant concentration and water velocity were unable to significantly alter the long-term effluent profiles, however, increasing the mass transfer rate coefficient from 0.09 to 1.8 /day significantly affected the long-term dissolved phase concentrations.
- Experimental results indicated that under diffusion-controlled mass transfer conditions, the estimated mass transfer rate coefficients were lower than typical mass transfer rate coefficients determined under continuous stirring conditions. No overall trend was observed between the mass transfer rate coefficients for the various organic compounds identified, however, an inverse dependency between the mass transfer rate coefficient and molecular weight was clear but different for BTEX and some PAHs compounds

suggesting that the intra-NAPL diffusion behavior of these two organic compound classes are different.

- It was demonstrated that a combination of NAPL composition, NAPL geometry, and interphase mass transfer rate can result in intra-NAPL diffusion limitations. Diffusion-limited mass transfer can result in an interfacial depletion of the more soluble compounds which restricts dissolution. When the main intra-NAPL diffusion coefficients were in the range of the self-diffusion coefficients ($10^{-5}$ to $10^{-6}$ $cm^2/s$), intra-NAPL diffusion was not limiting since NAPL concentration gradients could not be established except when high mass transfer rates were present. The threshold of the mass transfer rate coefficient which could result in intra-NAPL diffusion limitations was 15 and 180 cm/day for the medium ($\eta = 1.2$ g/(cm s)), and low viscous ($\eta = 0.12$ g/(cm s)) NAPLs, respectively. In the case of complex and highly viscous NAPLs, smaller intra-NAPL diffusion coefficients are expected and even the low range of mass transfer rates can result in the diffusion-limited dissolution.
- Two different approaches were employed to estimate intra-NAPL diffusion coefficients: 1) regular diffusion (RD) approach, and 2) modified diffusion approach. It was indicated that the RD approach which assumed all the organic components exist as liquid, better match the experimental results. It was demonstrated that the intra-NAPL diffusion coefficient of each NAPL component is proportional to its NAPL concentration and has an inverse dependency on its molecular weight.
- Rate-limited intra-NAPL diffusion within complex multi-component NAPLs can result in interfacial depletion of the more soluble compounds which restricts mass transfer processes and hence impacts chemical oxidation. The experimental results indicated that while chemical oxidation was able to completely degrade dissolved phase components and mobilize the NAPL, mass loss after ~410 PVs of persulfate injection was slightly less than a no-treatment scenario. The comparison of experimental and simulated results indicated that some limiting processes related to persulfate-NAPL interactions can restrict NAPL-water mass transfer. It was determined that during 410 PVs of persulfate flushing the multi-component mass transfer rate coefficients were ~70 % smaller than those estimated during an equivalent water injection period.

## 5.2 RECOMMENDATIONS FOR FUTURE WORK

While important conclusions were drawn and significant contributions were made at the end of this study, some questions remained unanswered and some interesting research topics raised during the course of this endeavor. The opportunities for further research are summarized as follows:

- To better assess multi-component NAPL-water mass transfer processes, it is recommended to experimentally investigate the role of the most important parameters (i.e. NAPL composition, NAPL geometry, and interphase mass transfer) which could result in intra-NAPL diffusion limitations. Designing an experimental apparatus which allows multi-level NAPL sampling is required to distinguish internal concentration gradients, NAPL viscosity, and interfacial compositional changes.

- While in the present study the direct interaction of MGP residuals with unactivated persulfate was demonstrated, investigating the impact of using different oxidants as well as different persulfate activation methods (i.e. permanganate, hydrogen peroxide, alkaline activation, and heat activation) on the mass transfer process under both static and dynamic conditions is recommended to compare the interactions of different oxidants with complex multi-component NAPLs.

- Development/application of experimental methods is recommended to determine intra-NAPL diffusion coefficients within synthetic and field collected complex multi-component NAPLs. Therefore, the role of the most important parameters which could influence intra-NAPL diffusion coefficients (i.e. molecular weight and NAPL component concentrations) can be investigated experimentally. The experimental results can be used to confirm the developed model for the estimation of intra-NAPL diffusion coefficients.

- There is no clear understanding of the root cause of the MGP NAPL-persulfate interactions observed and hence, the physical/chemical processes which restricted mass transfer during persulfate injection compared to the equivalent water injection are unknown. Therefore, further research is recommended to conduct controlled experiments to identify the interactions of persulfate with MGP NAPLs and determine the limiting processes.

- In the present study it was demonstrated that while chemical oxidation is able to degrade MGP residuals in well-mixed conditions, rate-limited NAPL-water mass transfer restricts

treatment in systems more representative of *in situ* conditions. It is also possible that under some conditions implementation of remediation strategies results in the interfacial film formation and thus restrict the mass transfer and dissolution process. Therefore, methods to overcome the mass transfer limitations are required for the remediation of complex multi-component NAPLs.

- In the present study some of the parameters (i.e. NAPL composition, NAPL geometry, and interphase mass transfer) which could result in intra-NAPL diffusion limitations were identified. To better assess the interactions of these parameter, it is recommended to conduct a comprehensive series of sensitivity analysis to determine critical conditions resulting from the combination of these parameters.

- In this study we investigated the effect of just one phenomenon (intra-NAPL diffusion) which can result in mass transfer limitation at the NAPL-water boundary; however, other phenomena such as interfacial inter molecular interactions, biofilm formation, precipitation, and pH of the system can also influence film formation and mass transfer at NAPL-water interface that is required to be further investigated. Moreover, it is recommended to enhance the developed diffusion-based model to capture the effects of other phenomena which can result in film formation and mass transfer limitations.

# References

## CHAPTER 1


Abriola, L. M., & Pinder, G. F. (1985). A Multiphase Approach to the Modeling of Porous Media Contamination by Organic Compounds: 2. Numerical Simulation. Water Resources Research, 21(1), 19–26.

Brahma, P. P., & Harmon, T. C. (2003). The effect of multicomponent diffusion on NAPL dissolution from spherical ternary mixtures. Journal of Contaminant Hydrology, 67, 43–60. http://doi.org/10.1016/S0169-7722(03)00087-1

Brown, D. G., Knightes, C. D., & Peters, C. A. (1999). Risk Assessment for Polycyclic Aromatic Hydrocarbon NAPLs Using Component Fractions. Environ. Sci. Technol., 33(24), 4357–4363.

Ghoshal, S., Pasion, C., & Alshafie, M. (2004). Reduction of Benzene and Naphthalene Mass Transfer from Crude Oils by Aging-Induced Interfacial Films. Environmental Science and Technology, 38(7), 2102–2110. http://doi.org/10.1021/es034832j

Hauswirth, S. C., & Miller, C. T. (2014). A comparison of physicochemical methods for the remediation of porous medium systems contaminated with tar. Journal of Contaminant Hydrology, 167C, 44–60. http://doi.org/10.1016/j.jconhyd.2014.08.002

Holman, H.-Y. N., & Javandel, I. (1996). Evaluation of Transient Dissolution of Slightly Water-Soluble Compounds From a Light Nonaqueous Phase Liquid Pool. Water Resources Research, 32(4), 915–923. http://doi.org/10.1029/96WR00075

Huling, S. G., & Pivetz, B. E. (2006). In-Situ Chemical Oxidation. US Environmental Protection Agency. Retrieved from http://www.epa.gov/ada/gw/pdfs/insituchemicaloxidation_engineering_issue.pdf

Krembs, F. J., Siegrist, R. L., Crimi, M. L., Furrer, R. F., & Petri, B. G. (2010). ISCO for Groundwater Remediation : Analysis of Field Applications and Performance. Groundwater Monitoring & Remediation, 30(4), 42–53. http://doi.org/10.1111/j1745

Luthy, R. G., Ramaswaml, A., Ghoshal, S., & Merkelt, W. (1993). Interfacial Films in Coal Tar Nonaqueous-Phase Liquid-Water Systems. Environ. Sci. Technol., 27(13), 2914–2918.

Miller, C. T., Poirier-Mcneill, M. M., & Mayer, A. S. (1990). Dissolution of trapped nonaqueous phase liquids: mass transfer characteristics. Water Resources Research, 26, 2783–2796.

Peters, C. A., Knightes, C. D., & Brown, D. G. (1999). Long-Term Composition Dynamics of PAH-Containing NAPLs and Implications for Risk Assessment. Environ. Sci. Technol., (609), 4499–4507.

Powers, E., Abriola, M., & Weber, J. (1992). An Experimental Investigation of Nonaqueous Phase Liquid Dissolution in Saturated Subsurface Systems â€TM Steady State Mass Transfer Rates. Water Resources Research, 28(10), 2691–2705.

Powers, S. E., Loureiro, C. O., Abriola, L. M., & Weber, W. J. (1991). Theoretical study of the

significance of nonequilibrium dissolution of nonaqueous phase liquids in subsurface systems. Water Resources Research, 27(4), 463–477. http://doi.org/10.1029/91WR00074

Sleep, B. E., & Sykes, J. F. (1993). Compositional simulation of groundwater contamination by organic compounds: 2. Model applications. Water Resources Research, 29(6), 1709–1718.

Soga, K., Page, J. W. E., & Illangasekare, T. H. (2004). A review of NAPL source zone remediation efficiency and the mass flux approach. Journal of Hazardous Materials, 110(1–3), 13–27. http://doi.org/10.1016/j.jhazmat.2004.02.034

Tsitonaki, A., Petri, B., Crimi, M., Mosbaek, H., Siegrist, R. L., & Bjerg, P. L. (2010). In Situ Chemical Oxidation of Contaminated Soil and Groundwater Using Persulfate: A Review. Critical Review in Environmental Science and Technology, 40, 55–91.

# CHPATER 2

APHA (American Public Health Association and America Water Works Association, (1998). Standard Methods for the Examination of Water and Sewage, 20th ed., New York.

Birak, P. S., & Miller, C. T. (2009). Dense non-aqueous phase liquids at former manufactured gas plants: challenges to modeling and remediation. Journal of Contaminant Hydrology, 105(3–4), 81–98. http://doi.org/10.1016/j.jconhyd.2008.12.001

Brown's Directory of North American Gas Companies, 1964. Harcourt Brace Jovanovich Publications, Duluth, Minnesota.

Brown, D. G., Gupta, L., Kim, T. H., Keith Moo-Young, H., & Coleman, A. J. (2006). Comparative assessment of coal tars obtained from 10 former manufactured gas plant sites in the Eastern United States. Chemosphere, 65(9), 1562–1569. http://doi.org/10.1016/j.chemosphere.2006.03.068

Brown, G. S., Barton, L. L., & Thomson, B. M. (2003). Permanganate oxidation of sorbed polycyclic aromatic hydrocarbons. Waste Management, 23, 737–740.

Cassidy, D. P., Srivastava, V. J., Dombrowski, F. J., & Lingle, J. W. (2015). Combining In-Situ Chemical Oxidation, Stabilization and Anaerobic Bioremediation in a Single Application to Reduce Contaminant Mass and Leachability in Soil. Journal of Hazardous Materials. http://doi.org/10.1016/j.jhazmat.2015.05.030

Crimi, M., T.J. Simpkin, T. Palaia, B.G. Petri, R.L. Siegrist, 2011. Systematic approach for site specific engineering of ISCO. In Situ Chemical Oxidation for Groundwater Remediation, Eds. R.L. Siegrist, M. Crimi, T.J Simpkin, Springer, NY, Chapter 9, pp. 355-412, 2011.

Eberhardt, C., & Grathwohl, P. (2002). Time scales of organic contaminant dissolution from complex source zones: coal tar pools vs. blobs. Journal of Contaminant Hydrology, 59(1–2), 45–66. Retrieved from http://www.ncbi.nlm.nih.gov/pubmed/12683639

Ferrarese, E., Andreottola, G., & Oprea, I. A. (2008). Remediation of PAH-contaminated sediments by chemical oxidation. Journal of Hazardous Materials, 152(1), 128–39. http://doi.org/10.1016/j.jhazmat.2007.06.080

Forsey, S. P. (2004). In situ Chemical Oxidation of Creosote / Coal Tar Residuals: Experimental and Numerical Investigation. University of waterloo, ON.

Forsey, S. P., Thomson, N. R., & Barker, J. F. (2010). Oxidation kinetics of polycyclic aromatic hydrocarbons by permanganate. Chemosphere, 79(6), 628–36. http://doi.org/10.1016/j.chemosphere.2010.02.027

Gan, S., Lau, E. V, & Ng, H. K. (2009). Remediation of soils contaminated with polycyclic aromatic hydrocarbons (PAHs). Journal of Hazardous Materials, 172(2–3), 532–49. http://doi.org/10.1016/j.jhazmat.2009.07.118

Gates-anderson, B. D. D., Siegrist, R. L., & Cline, S. R. (2001). Comparison of Potassium Permanganate and Hydrogen Peroxide as Chemical Oxidants for Organically Contaminated Soils. J. Environ. Eng., 337–347.

Hatheway, A. W. (2012). Remediation of former manufactured gas plants and other coal-tar sites. CRC Press, Talor & Francis Group.

Hauswirth, S. C., Birak, P. S., Rylander, S. C., & Miller, C. T. (2012). Mobilization of Manufactured Gas Plant Tar with Alkaline Flushing Solutions. Environ. Sci. Technol., 46, 426–433.

Hauswirth, S. C., & Miller, C. T. (2014). A comparison of physicochemical methods for the remediation of porous medium systems contaminated with tar. Journal of Contaminant Hydrology, 167C, 44–60. http://doi.org/10.1016/j.jconhyd.2014.08.002

Huang, K., R.A. Couttenye, G.E. Hoag, (2002). Kinetics of heat-assisted persulfate oxidation of methyl tert-butyl ether (MTBE), Chemosphere, 49, 413-420.

Krembs, F. J., Siegrist, R. L., Crimi, M. L., Furrer, R. F., & Petri, B. G. (2010). ISCO for Groundwater Remediation : Analysis of Field Applications and Performance. Groundwater Monitoring & Remediation, 30(4), 42–53. http://doi.org/10.1111/j1745

Lee, L. S., Rao, P. S. C., & Okuda, I. (1992). Equilibrium partitioning of polycyclic aromatic hydrocarbon from coal tars into water. Environ. Sci. Technol., 26(11), 2110–2115.

Lemaire, J., Laurent, F., Leyval, C., Schwartz, C., Buès, M., & Simonnot, M.-O. (2013). PAH oxidation in aged and spiked soils investigated by column experiments. Chemosphere, 91(3), 406–14. http://doi.org/10.1016/j.chemosphere.2012.12.003

Liang, C., Huang, C.-F., Mohanty, N., & Kurakalva, R. M. (2008). A rapid spectrophotometric determination of persulfate anion in ISCO. Chemosphere, 73(9), 1540–3. http://doi.org/10.1016/j.chemosphere.2008.08.043

Lide, D. R. (1999). CRC handbook of physics and chemistry.

Luthy, R. G., Dzombak, D. A., Peters, C. A., Roy, S. B., Ramaswami, A., Nakles, D. V., & Nott, B. R. (1994). Remediating Tar-Contaminated Soils at Manufactured Gas Plant Sites: Technological Challenges. Environ. Sci. Technol., 28(6), 266A–276A.

Mueller, J. G., Chapman, P. J., & Pritchard, P. H. (1989). Creosote-contaminated sites. Their potential for bioremediation. Environmental Science & Technology, 23(10), 1197–1201. http://doi.org/10.1021/es00068a003

Nadim, F., Huang, K.-C., & Dahmani, A. M. (2005). Remediation of Soil and Ground Water Contaminated with PAH using Heat and Fe(II)-EDTA Catalyzed Persulfate Oxidation. Water, Air, & Soil Pollution: Focus, 6(1–2), 227–232. http://doi.org/10.1007/s11267-005-9008-z

Peng, L., Wang, L., Hu, X., Wu, P., Wang, X., Huang, C., … Deng, D. (2016). Ultrasound assisted, thermally activated persulfate oxidation of coal tar DNAPLs. Journal of Hazardous Materials, 318, 497–506. http://doi.org/10.1016/j.jhazmat.2016.07.014

Peters, C. A., Mukherji, S., Knightes, C. D., & Weber, W. (1997). Phase Stability of Multicomponent NAPLs Containing PAHs. Environ. Sci. Technol., 31(9), 2540–2546.

Petri, B.G, N.R. Thomson, M.A. Urynowicz, 2011a. Fundamentals of ISCO using permanganate, In Situ Chemical Oxidation for Groundwater Remediation, Eds. R.L.

Siegrist, M. Crimi, T.J Simpkin, Springer, NY, Chapter 3, pp. 89-146, 2011.

Petri, B.G, R.J. Watts, A. Tsitonaki, M. Crimi, N.R. Thomson, A.L. Teel, 2011b. Principles of ISCO related subsurface transport and modeling, In Situ Chemical Oxidation for Groundwater Remediation, Eds. R.L. Siegrist, M. Crimi, T.J Simpkin, Springer, NY, Chapter 4, pp. 147-191, 2011.

Powers, S. E., Abriola, L. M., Dunkin, J. S., & Weber, W. J. (1994). Phenomenological models for transient NAPL-water mass-transfer processes. Journal of Contaminant Hydrology, 16, 1–33.

Richardson, S. D., Lebron, B. L., Miller, C. T., & Aitken, M. D. (2011). Recovery of Phenanthrene-Degrading Bacteria after Simulated in Situ Persulfate Oxidation in Contaminated Soil. Environ. Sci. Technol., 45(2), 719–725.

Rivas, F. J. (2006). Polycyclic aromatic hydrocarbons sorbed on soils: a short review of chemical oxidation based treatments. Journal of Hazardous Materials, 138(2), 234–51. http://doi.org/10.1016/j.jhazmat.2006.07.048

Siegrist, R. L., Crimi, M., & Simpkin, T. J. (2011). In situ chemical oxidation for groundwater remediation. Springer Science +Business Media.

Soga, K., Page, J. W. E., & Illangasekare, T. H. (2004). A review of NAPL source zone remediation efficiency and the mass flux approach. Journal of Hazardous Materials, 110(1–3), 13–27. http://doi.org/10.1016/j.jhazmat.2004.02.034

Sra, K. S., Thomson, N. R., Asce, M., & Barker, J. F. (2013). Persulfate Treatment of Dissolved Gasoline Compounds. J. Hazardous, Toxic, and Radioactive Waste, 17, 9–15. http://doi.org/10.1061/(ASCE)HZ.2153-5515.0000143.

Sra, K. S., Thomson, N. R., & Barker, J. F. (2010). Persistence of Persulfate in Uncontaminated Aquifer Materials. Environ. Sci. Technol., 44(8), 3098–3104.

Thomson, N. R., Fraser, M. J., Lamarche, C., Barker, J. F., & Forsey, S. P. (2008). Rebound of a coal tar creosote plume following partial source zone treatment with permanganate. Journal of Contaminant Hydrology, 102(1–2), 154–71. http://doi.org/10.1016/j.jconhyd.2008.07.001

USEPA, (2006), Huling, S. G., Pivetz, B. E. Engineering Issue: In-Situ Chemical Oxidation. EPA/600/R- 06/072.U.S.Environmental Protection Agency, Office of Research and Development, National Risk Management Research Laboratory, Cincinnati, OH.

USEPA, (2013). *Superfund Remedy Selection Report, 14th Edition*.EPA 542-R-13-016, Solid Waste and Emergency Response.

Usman, M., Faure, P., Ruby, C., & Hanna, K. (2012). Application of magnetite-activated persulfate oxidation for the degradation of PAHs in contaminated soils. Chemosphere, 87(3), 234–40. http://doi.org/10.1016/j.chemosphere.2012.01.001

Wang, W., Liu, G., Shen, J., Chang, H., Li, R., Du, J., … Xu, Q. (2015). Reducing polycyclic aromatic hydrocarbons content in coal tar pitch by potassium permanganate oxidation and solvent extraction. Journal of Environmental Chemical Engineering.

http://doi.org/10.1016/j.jece.2015.05.024

Xu, X., & Thomson, N. R. (2009). A long-term bench-scale investigation of permanganate consumption by aquifer materials. Journal of Contaminant Hydrology, 110(3–4), 73–86. http://doi.org/10.1016/j.jconhyd.2009.09.001

Zhang, C., Werth, C. J., & Webb, A. G. (2007). Characterization of NAPL Source Zone Architecture and Dissolution Kinetics in Heterogeneous Porous Media Using Magnetic Resonance Imaging. Environmental Science & Technology, 41(10), 3672–3678.

Zhang, C., Yoon, H., Werth, C. J., Valocchi, A. J., Basu, N. B., & Jawitz, J. W. (2008). Evaluation of simplified mass transfer models to simulate the impacts of source zone architecture on nonaqueous phase liquid dissolution in heterogeneous porous media. Journal of Contaminant Hydrology, 102(1–2), 49–60. http://doi.org/10.1016/j.jconhyd.2008.05.007

# CHAPTER 3

Albright, J. G., & Mills, R. (1965). A Study of Diffusion in the Ternary System, Labeled Urea-Urea-Water at 25 °C by Measurements of the Intradiffusion Coefficients of Urea. The Journal of Physical Chemistry, 69(9), 3120–3126. http://doi.org/10.1021/j100893a052

Alshafie, M., & Ghoshal, S. (2004). The role of interfacial films in the mass transfer of naphthalene from creosotes to water. Journal of Contaminant Hydrology, 74(1–4), 283–298. http://doi.org/10.1016/j.jconhyd.2004.03.004

Banerjee, S. (1984). Solubility of organic mixtures in water. Environmental Science & Technology, 18(8), 587–91. http://doi.org/10.1021/es00126a004

Barranco, F. T., & Dawson, H. E. (1999). Influence of aqueous pH on the interfacial properties of coal tar. Environmental Science and Technology, 33(10), 1598–1603. http://doi.org/10.1021/es980196r

Birak, P. S., & Miller, C. T. (2009). Dense non-aqueous phase liquids at former manufactured gas plants: challenges to modeling and remediation. Journal of Contaminant Hydrology, 105(3–4), 81–98. http://doi.org/10.1016/j.jconhyd.2008.12.001

Bird, R. B., Stewart, W. E., & Lightfoot, E. N. (2002). Transport Phenomena. New York: John Wiley & Sons, Inc.

Brahma, P. P., & Harmon, T. C. (2003). The effect of multicomponent diffusion on NAPL dissolution from spherical ternary mixtures. Journal of Contaminant Hydrology, 67, 43–60. http://doi.org/10.1016/S0169-7722(03)00087-1

Brown, C. E., & Neustadter, E. L. (1980). The wettability of oil/water/silica systems with reference to oil recovery. Journal of Canadian Petroleum Technology, 19(3), 100–109. http://doi.org/10.2118/80-03-06

Brown, D. G., Knightes, C. D., & Peters, C. A. (1999). Risk Assessment for Polycyclic Aromatic Hydrocarbon NAPLs Using Component Fractions. Environ. Sci. Technol., 33(24), 4357–4363.

Crank, J. (1975). The mathematics of diffusion. Annals of Nuclear Energy. Oxford university Press. http://doi.org/10.1016/0306-4549(77)90072-X

Crank, J. (1984). Free and moving boundary problems. Oxford university Press.

Crank, J., & Gupta, R. S. (1972). A method for solving moving boundary problems in heat flow using cubic splines or polynomials. IMA Journal of Applied Mathematics, 10(3), 296–304. Retrieved from http://hdl.handle.net/2438/2288

Cussler, E. L. (1997). Diffusion Mass Transfer in Fluid Systems (Second edi). Cambridge University Press.

Ghoshal, S., Pasion, C., & Alshafie, M. (2004). Reduction of Benzene and Naphthalene Mass Transfer from Crude Oils by Aging-Induced Interfacial Films. Environmental Science and Technology, 38(7), 2102–2110. http://doi.org/10.1021/es034832j

Ghoshal, S., Ramaswami, A., & Luthy, R. G. (1996). Biodegradation of naphthalene from coal

tar and heptamethylnonane in mixed batch systems. Environmental Science and Technology, 30(4), 1282–1291. http://doi.org/10.1021/es950494d

Hartley, G. S., & Crank, J. (1949). Some fundamental definitions and concepts in diffusion processes. Transactions of the Faraday Society, 45, 801–818. http://doi.org/10.1039/TF9494500801

Heyse, E., Augustijn, D., Rao, P. S. C., & Delfino, J. J. (2002). Nonaqueous Phase Liquid Dissolution and Soil Organic Matter Sorption in Porous Media: Review of System Similarities. Critical Reviews in Environmental Science and Technology, 32(4), 337–397. http://doi.org/10.1080/10643380290813471

Holman, H.-Y. N., & Javandel, I. (1996). Evaluation of Transient Dissolution of Slightly Water-Soluble Compounds From a Light Nonaqueous Phase Liquid Pool. Water Resources Research, 32(4), 915–923. http://doi.org/10.1029/96WR00075

Houghton, G. (1964). Cubic Cell Model for Self-Diffusion in Liquids. The Journal of Chemical Physics, 40(6), 1628. http://doi.org/10.1063/1.1725371

Hunt, J. R., Sitar, N., & Udell, K. S. (1988). Nonaqueous phase liquid transport and cleanup: 2. Experimental studies. Water Resour. Res., 24(8), 1259–1269. http://doi.org/10.1029/WR024i008p01259

Jada, A., & Salou, M. (2002). Effects of the asphaltene and resin contents of the bitumens on the water-bitumen interface properties. Journal of Petroleum Science and Engineering, 33(1–3), 185–193. http://doi.org/10.1016/S0920-4105(01)00185-1

Kett, T. K., & Anderson, D. K. (1969a). Multicomponent Diffusion in Nonassociating, Nonelectrolyte Solutions. J. Phys. Chem., 73, 1262–1267.

Kett, T. K., & Anderson, D. K. (1969b). Ternary isothermal diffusion and the validity of the Onsager reciprocal relations in nonassociating systems. J. Phys. Chem., 73(8), 1262–1267.

Khachikian, C., & Harmon, T. C. (2000). Nonaqueous Phase Liquid Dissolution in Porous Media : Current State of Knowledge and Research Needs. Transport in Porous Media, 38(5), 3–28.

Leahy-Dios, A., & Firoozabadi, A. (2007). Unified model for nonideal multicomponent molecular diffsuion coefficients. AIChE Journal, 53, 2932–2939. http://doi.org/10.1002/aic

Lee, L. S., Rao, P. S. C., & Okuda, I. (1992). Equilibrium partitioning of polycyclic aromatic hydrocarbon from coal tars into water. Environ. Sci. Technol., 26(11), 2110–2115.

Lekmine, G., Bastow, T. P., Johnston, C. D., & Davis, G. B. (2014). Dissolution of multi-component LNAPL gasolines: the effects of weathering and composition. Journal of Contaminant Hydrology, 160, 1–11. http://doi.org/10.1016/j.jconhyd.2014.02.003

Lide, D. R. (1999). CRC handbook of physics and chemistry.

Liu, L., Endo, S., Eberhardt, C., Grathwohl, P., & Schmidt, T. C. (2009). Partition Behavior of Polycyclic Aromatic Hydrocarbons Between Aged Coal Tar and Water. Environmental Toxicology and Chemistry, 28(8), 1578–1584.

Luthy, R. G., Dzombak, D. A., Peters, C. A., Roy, S. B., Ramaswami, A., Nakles, D. V., & Nott, B. R. (1994). Remediating Tar-Contaminated Soils at Manufactured Gas Plant Sites: Technological Challenges. Environ. Sci. Technol., 28(6), 266A–276A.

Luthy, R. G., Aiken, G. R., Brusseau, M. L., Cunningham, S. D., Gschwend, P. M., Pignatello, J. J., … Westall, J. C. (1997). Sequestration of hydrophobic organic contaminants by geosorbents. Environmental Science and Technology, 31(12), 3341–3347. http://doi.org/10.1021/es970512m

Luthy, R. G., Ramaswaml, A., Ghoshal, S., & Merkelt, W. (1993). Interfacial Films in Coal Tar Nonaqueous-Phase Liquid-Water Systems. Environ. Sci. Technol., 27(13), 2914–2918.

Mahjoub, B., Jayr, E., Bayard, R., & Gourdon, R. (2000). Phase partition of organic pollutants between coal tar and water under variable experimental conditions. Water Research, 34(14), 3551–3560. http://doi.org/10.1016/S0043-1354(00)00100-7

Mercer, J. W., & Cohen, R. M. (1990). A review of immiscible fluids in the subsurface: Properties, models, characterization and remediation. J. Contaminant Hydrology, 6, 107–163.

Miller, C. T., Poirier-Mcneill, M. M., & Mayer, A. S. (1990). Dissolution of trapped nonaqueous phase liquids: mass transfer characteristics. Water Resources Research, 26, 2783–2796.

Miller, M. M., Waslk, S. P., Huang, G.-L., Shiu, W.-Y., & Mackay, D. (1985). Relationships between Octanol-Water Partition Coefficient and Aqueous Solubility. Environ. Sci. Technol., 19(6), 522–529.

Mobile, M., Widdowson, M., Stewart, L., Nyman, J., Deeb, R., Kavanaugh, M., … Gallagher, D. (2016). In-situ determination of field-scale NAPL mass transfer coefficients : Performance , simulation and analysis. Journal of Contaminant Hydrology, 187, 31–46. http://doi.org/10.1016/j.jconhyd.2016.01.010

Mohammed, R. A., Bailey, A. I., Luckham, P. F., & Taylor, S. E. (1993). Dewatering of crude oil emulsions 1. Rheological behaviour of the crude oil-water interface. Colloids and Surfaces A: Physicochemical and Engineering Aspects, 80(2–3), 223–235. http://doi.org/10.1016/0927-7757(93)80202-P

Mukherji, S., Peters, C. a., & Weber, W. J. (1997). Mass Transfer of Polynuclear Aromatic Hydrocarbons from Complex DNAPL Mixtures. Environmental Science & Technology, 31(2), 416–423. http://doi.org/10.1021/es960227n

Mukherji, S., & Weber, W. J. (1998). Mass Transfer Effects on Microbial Uptake of Naphthalene from Complex NAPLs Mass Transfer Effects on Microbial Uptake of Naphthalene from Complex NAPLs. Biotechnol. Bioeng., 60, 750–760.

Nelson, E. C., Ghoshal, S., Edwards, J. C., Marsh, G. X., & Luthy, R. G. (1996). Chemical Characterization of Coal Tar - Water Interfacial Films. Environ. Sci. Technol., 30(3), 1014–1022.

Ortiz, E., Kraatz, M., & Luthy, R. G. (1999). Organic Phase Resistance to Dissolution of Polycyclic Aromatic Hydrocarbon Compounds. Environ. Sci. Technol., 33(2), 235–242.

Peters, C. A., Knightes, C. D., & Brown, D. G. (1999). Long-Term Composition Dynamics of

PAH-Containing NAPLs and Implications for Risk Assessment. Environ. Sci. Technol., (609), 4499–4507.

Peters, C. A., Mukherji, S., Knightes, C. D., & Weber, W. (1997). Phase Stability of Multicomponent NAPLs Containing PAHs. Environ. Sci. Technol., 31(9), 2540–2546.

Peters, C. A., Wammer, K. H., & Knightes, Christopher, D. (2000). Multicomponent NAPL Solidification Thermodynamics. Transport in Porous Media, 38, 57–77.

Poling, B. E., Prausnitz, J. M., & O'Connell, J. P. (2001). Properties of Gases and Liquids, Fifth Edition. McGraw-Hill Education. Retrieved from http://accessengineeringlibrary.com/browse/properties-of-gases-and-liquids-fifth-edition#fullDetails

Powers, E., Abriola, M., & Weber, J. (1992). An Experimental Investigation of Nonaqueous Phase Liquid Dissolution in Saturated Subsurface Systems â€TM Steady State Mass Transfer Rates. Water Resources Research, 28(10), 2691–2705.

Powers, S. E., Anckner, W. H., & Seacord, T. F. (1996). Wettability of NAPL-Contaminated sands. J. Environ. Eng., 122(1), 889–896.

Powers, S. E., Nambi, I. M., & Curry Jr., G. W. (1998). Non-aqueous phase liquid dissolution in heterogeneous systems : Mechanisms and a local equilibrium modeling approach. Water Resources Research, 34(12), 3293–3302.

Seagren, E. a., Rittmann, B. E., & Valocchi, A. J. (1999). An experimental investigation of NAPL pool dissolution enhancement by flushing. Journal of Contaminant Hydrology, 37(1–2), 111–137. http://doi.org/10.1016/S0169-7722(98)00157-0

Seagren, E. a, Rittmann, B. E., & Valocchi, A. J. (1993). Quantitative evaluation of flushing and biodegradation for enhancing in situ dissolution of nonaqueous-phase liquids. Journal of Contaminant Hydrology, 12(1–2), 103–132. http://doi.org/10.1016/0169-7722(93)90017-M

Soga, K., Page, J. W. E., & Illangasekare, T. H. (2004). A review of NAPL source zone remediation efficiency and the mass flux approach. Journal of Hazardous Materials, 110(1–3), 13–27. http://doi.org/10.1016/j.jhazmat.2004.02.034

Strassner, J. E. (1968). Effect of pH on Interfacial Films and Stability of Crude Oil-Water Emulsions. Journal of Petroleum Technology, 20(3), 303–312. http://doi.org/10.2118/1939-PA

Varadaraj, R., & Brons, C. (2012). Molecular origins of crude oil interfacial activity. part 4: Oil-water interface elasticity and crude oil asphaltene films. Energy and Fuels, 26(12), 7164–7169. http://doi.org/10.1021/ef300830f

Weber, W. J., & DiGiano, J. F. A. (1995). process dynamic in environmental systems. John Wiley & Sons, Inc.

Wehrer, M., Rennert, T., & Totsche, K. U. (2013a). Kinetic control of contaminant release from NAPLs--experimental evidence. Environmental Pollution, 179, 315–25. http://doi.org/10.1016/j.envpol.2013.03.041

Wehrer, M., Mai, J., Attinger, S., & Totsche, K. U. (2013b). Kinetic control of contaminant release from NAPLs--information potential of concentration time profiles. Environmental

Pollution (Barking, Essex : 1987), 179, 301–14. http://doi.org/10.1016/j.envpol.2013.04.029

Zielinski, J. M., & Hanley, B. F. (1999). Practical friction-based approach to modeling multicomponent diffusion. AIChE Journal, 45(1), 1–12. http://doi.org/10.1002/aic.690450102

# CHAPTER 4

Alshafie, M., & Ghoshal, S. (2004). The role of interfacial films in the mass transfer of naphthalene from creosotes to water. Journal of Contaminant Hydrology, 74(1–4), 283–298. http://doi.org/10.1016/j.jconhyd.2004.03.004

Banerjee, S. (1984). Solubility of organic mixtures in water. Environmental Science & Technology, 18(8), 587–91. http://doi.org/10.1021/es00126a004

Barranco, F. T., & Dawson, H. E. (1999). Influence of aqueous pH on the interfacial properties of coal tar. Environmental Science and Technology, 33(10), 1598–1603. http://doi.org/10.1021/es980196r

Birak, P. S., & Miller, C. T. (2009). Dense non-aqueous phase liquids at former manufactured gas plants: challenges to modeling and remediation. Journal of Contaminant Hydrology, 105(3–4), 81–98. http://doi.org/10.1016/j.jconhyd.2008.12.001

Bird, R. B., Stewart, W. E., & Lightfoot, E. N. (2002). Transport Phenomena. New York: John Wiley & Sons, Inc.

Blanchard, C. (2010). Applying chemical oxidation technologies at NAPL-impacted sites to facilitate risk-based closure. Remediation Journal, 20(2), 77–91. http://doi.org/10.1002/rem.20241

Brahma, P. P., & Harmon, T. C. (2003). The effect of multicomponent diffusion on NAPL dissolution from spherical ternary mixtures. Journal of Contaminant Hydrology, 67, 43–60. http://doi.org/10.1016/S0169-7722(03)00087-1

Burns, G., & Sherwood, J. N. (1972a). Self- and Impurity Diffusion in γ-TiAl Single Crystals. J. Chem. Soc., Faraday Trans., 68, 1036–1040. http://doi.org/10.4028/www.scientific.net/DDF.258-260.259

Burns, G., & Sherwood, J. N. (1972b). Self-diffusion in Phenanthrene Single Crystals. Molecular Crystals and Liquid Crystals, 18(1), 91–94. http://doi.org/10.1080/15421407208083848

Conrad, S. H., Glass, R. J., & Peplinski, W. J. (2002). Bench-scale visualization of DNAPL remediation processes in analog heterogeneous aquifers : surfactant floods and in situ oxidation using permanganate. Journal of Contaminant Hydrology, 58, 13–49.

Corbin, J. F., Teel, A. L., Allen-King, R. M., & Watts, R. J. (2007). Reactive oxygen species responsible for the enhanced desorption of dodecane in modified Fenton's systems. Water Environment Research : A Research Publication of the Water Environment Federation, 79(1), 37–42. http://doi.org/10.2175/106143006X136793

Cussler, E. L. (1997). Diffusion Mass Transfer in Fluid Systems (Second edi). Cambridge University Press.

Ghoshal, S., Pasion, C., & Alshafie, M. (2004). Reduction of Benzene and Naphthalene Mass Transfer from Crude Oils by Aging-Induced Interfacial Films. Environmental Science and Technology, 38(7), 2102–2110. http://doi.org/10.1021/es034832j

Gryzenia, J., Cassidy, D., & Hampton, D. (2009). Production and accumulation of surfactants

during the chemical oxidation of PAH in soil. Chemosphere, 77(4), 540–545. http://doi.org/10.1016/j.chemosphere.2009.07.012

Hauswirth, S. C., & Miller, C. T. (2014). A comparison of physicochemical methods for the remediation of porous medium systems contaminated with tar. Journal of Contaminant Hydrology, 167C, 44–60. http://doi.org/10.1016/j.jconhyd.2014.08.002

Holman, H.-Y. N., & Javandel, I. (1996). Evaluation of Transient Dissolution of Slightly Water-Soluble Compounds From a Light Nonaqueous Phase Liquid Pool. Water Resources Research, 32(4), 915–923. http://doi.org/10.1029/96WR00075

Houghton, G. (1964). Cubic Cell Model for Self-Diffusion in Liquids. The Journal of Chemical Physics, 40(6), 1628. http://doi.org/10.1063/1.1725371

Jada, A., & Salou, M. (2002). Effects of the asphaltene and resin contents of the bitumens on the water-bitumen interface properties. Journal of Petroleum Science and Engineering, 33(1–3), 185–193. http://doi.org/10.1016/S0920-4105(01)00185-1

Kett, T. K., & Anderson, D. K. (1969a). Multicomponent Diffusion in Nonassociating, Nonelectrolyte Solutions. J. Phys. Chem., 73, 1262–1267.

Kett, T. K., & Anderson, D. K. (1969b). Ternary isothermal diffusion and the validity of the Onsager reciprocal relations in nonassociating systems. J. Phys. Chem., 73(8), 1262–1267.

Krembs, F. J., Siegrist, R. L., Crimi, M. L., Furrer, R. F., & Petri, B. G. (2010). ISCO for Groundwater Remediation : Analysis of Field Applications and Performance. Groundwater Monitoring & Remediation, 30(4), 42–53. http://doi.org/10.1111/j1745

Lee, L. S., Rao, P. S. C., & Okuda, I. (1992). Equilibrium partitioning of polycyclic aromatic hydrocarbon from coal tars into water. Environ. Sci. Technol., 26(11), 2110–2115.

Lekmine, G., Bastow, T. P., Johnston, C. D., & Davis, G. B. (2014). Dissolution of multi-component LNAPL gasolines: the effects of weathering and composition. Journal of Contaminant Hydrology, 160, 1–11. http://doi.org/10.1016/j.jconhyd.2014.02.003

Lide, D. R. (1999). CRC handbook of physics and chemistry.

Luthy, R. G., Dzombak, D. A., Peters, C. A., Roy, S. B., Ramaswami, A., Nakles, D. V., & Nott, B. R. (1994). Remediating Tar-Contaminated Soils at Manufactured Gas Plant Sites: Technological Challenges. Environ. Sci. Technol., 28(6), 266A–276A.

Luthy, R. G., Ramaswaml, A., Ghoshal, S., & Merkelt, W. (1993). Interfacial Films in Coal Tar Nonaqueous-Phase Liquid-Water Systems. Environ. Sci. Technol., 27(13), 2914–2918.

Miller, C. T., Poirier-Mcneill, M. M., & Mayer, A. S. (1990). Dissolution of trapped nonaqueous phase liquids: mass transfer characteristics. Water Resources Research, 26, 2783–2796.

Miller, M. M., Waslk, S. P., Huang, G.-L., Shiu, W.-Y., & Mackay, D. (1985). Relationships between Octanol-Water Partition Coefficient and Aqueous Solubility. Environ. Sci. Technol., 19(6), 522–529.

Mukherji, S., Peters, C. a., & Weber, W. J. (1997). Mass Transfer of Polynuclear Aromatic Hydrocarbons from Complex DNAPL Mixtures. Environmental Science & Technology,

31(2), 416–423. http://doi.org/10.1021/es960227n

Ndjou'ou, A.-C., & Cassidy, D. (2006). Surfactant production accompanying the modified Fenton oxidation of hydrocarbons in soil. Chemosphere, 65(9), 1610–5. http://doi.org/10.1016/j.chemosphere.2006.03.036

Nelson, E. C., Ghoshal, S., Edwards, J. C., Marsh, G. X., & Luthy, R. G. (1996). Chemical Characterization of Coal Tar - Water Interfacial Films. Environ. Sci. Technol., 30(3), 1014–1022.

Ortiz, E., Kraatz, M., & Luthy, R. G. (1999). Organic Phase Resistance to Dissolution of Polycyclic Aromatic Hydrocarbon Compounds. Environ. Sci. Technol., 33(2), 235–242.

Peng, L., Wang, L., Hu, X., Wu, P., Wang, X., Huang, C., … Deng, D. (2016). Ultrasound assisted, thermally activated persulfate oxidation of coal tar DNAPLs. Journal of Hazardous Materials, 318, 497–506. http://doi.org/10.1016/j.jhazmat.2016.07.014

Peters, C. a., & Luthy, R. G. (1993). Coal tar dissolution in water-miscible solvents: experimental evaluation. Environmental Science & Technology, 27(13), 2831–2843. http://doi.org/10.1021/es00049a025

Peters, C. A., Mukherji, S., Knightes, C. D., & Weber, W. (1997). Phase Stability of Multicomponent NAPLs Containing PAHs. Environ. Sci. Technol., 31(9), 2540–2546.

Peters, C. A., Wammer, K. H., & Knightes, Christopher, D. (2000). Multicomponent NAPL Solidification Thermodynamics. Transport in Porous Media, 38, 57–77.

Poling, B. E., Prausnitz, J. M., & O'Connell, J. P. (2001). Properties of Gases and Liquids, Fifth Edition. McGraw-Hill Education. Retrieved from http://accessengineeringlibrary.com/browse/properties-of-gases-and-liquids-fifth-edition#fullDetails

Powers, S. E., Nambi, I. M., & Curry Jr., G. W. (1998). Non-aqueous phase liquid dissolution in heterogeneous systems : Mechanisms and a local equilibrium modeling approach. Water Resources Research, 34(12), 3293–3302.

Sherwood, J. N., & Thomson, S. J. (1960). THE DIFFUSION OF ANTHRACENE-9-C-14 IN SlNGLE CRYSTALS OF ANTHRACENE. J. N. Sherwood and S. J. Thomson Trans. Faraday Soc., 56, 1443–1451.

Sherwood, J., & White, D. (1967). Self-diffusion in naphthalene single crystals. Philosophical Magazine, 8086(February). http://doi.org/10.1080/14786436708220922

Siegrist, R. L., Crimi, M., & Simpkin, T. J. (2011). In situ chemical oxidation for groundwater remediation. Springer Science +Business Media.

Soga, K., Page, J. W. E., & Illangasekare, T. H. (2004). A review of NAPL source zone remediation efficiency and the mass flux approach. Journal of Hazardous Materials, 110(1–3), 13–27. http://doi.org/10.1016/j.jhazmat.2004.02.034

Sra, K. S., Thomson, N. R., Asce, M., & Barker, J. F. (2013). Persulfate Treatment of Dissolved Gasoline Compounds. J. Hazardous, Toxic, and Radioactive Waste, 17, 9–15. http://doi.org/10.1061/(ASCE)HZ.2153-5515.0000143.

Thomson, N. R., Fraser, M. J., Lamarche, C., Barker, J. F., & Forsey, S. P. (2008). Rebound of a coal tar creosote plume following partial source zone treatment with permanganate. Journal of Contaminant Hydrology, 102(1–2), 154–71. http://doi.org/10.1016/j.jconhyd.2008.07.001

Varadaraj, R., & Brons, C. (2012). Molecular origins of crude oil interfacial activity. part 4: Oil-water interface elasticity and crude oil asphaltene films. Energy and Fuels, 26(12), 7164–7169. http://doi.org/10.1021/ef300830f

Wang, W., Liu, G., Shen, J., Chang, H., Li, R., Du, J., … Xu, Q. (2015). Reducing polycyclic aromatic hydrocarbons content in coal tar pitch by potassium permanganate oxidation and solvent extraction. Journal of Environmental Chemical Engineering. http://doi.org/10.1016/j.jece.2015.05.024

Weber, W. J., & DiGiano, J. F. A. (1995). process dynamic in environmental systems. John Wiley & Sons, Inc.

Wehrer, M., Rennert, T., & Totsche, K. U. (2013). Kinetic control of contaminant release from NAPLs--experimental evidence. Environmental Pollution, 179, 315–25. http://doi.org/10.1016/j.envpol.2013.03.041

Zheng, J., & Powers, S. E. (1999). Organic bases in NAPLs and their impact on wettability. Journal of Contaminant Hydrology, 39(1–2), 161–181. http://doi.org/10.1016/S0169-7722(99)00023-6

# Appendix A:
# Supplementary Material for Chapter 2

## Natural Oxidant Interaction – Experimental Procedures

### Material Handling

Aquifer material each location as completely air-dried at 80 $^{o}$C in an incubator oven (Gallenkamp, 1H-100) to constant weight, and then allowed to cool to room temperature. Dried materials were separated into three size fractions (< 250 µm, between 250 µm and 2 mm, and > 2 mm) using No. 10 and No. 60 U.S. Standard mesh size sieves. The fine fraction (< 250 µm) was not used in these experiments since it interfered with the spectrophotometric analytical methods used. Composite samples blended from the > 250 µm and the < 2 mm, and from the > 2 mm mass fractions were used in these NOI tests pro-rated by the respective mass fractions observed. Following the sieving procedure, the aquifer material for each of the selected locations was homogenized for each mass fraction in large sterilized tubs by gently mixing by hand. Care was taken to avoid excess abrasion that might lead to grinding or pulverizing of sediment particles. After mixing, the material was transferred to high density polyethylene (HDPE) bags (Cole-Parmer, 60104), sealed and stored at 4 $^{o}$C. As required, sub-samples were selected at random from the re-mixed stored material and air dried at 80 $^{o}$C to a constant mass again prior to use.

### Permanganate NOI Procedure

A series of six (6) tests were performed on the composite aquifer material samples from each location (see Table SM-2) using well-mixed 125 mL wide-mouth batch reactors. The NOI for an oxidant mass to solids ratio of 5, 20, 30 and 40 g/kg (nominal) using an initial permanganate concentration of 5, 20, 30 and 40 g-$KMnO_4$/L respectively were investigated (denoted as Series 1 to 4). For the remaining two series of tests (Series 5 and 6) the initial permanganate concentration was held constant at 30 g-$KMnO_4$/L and the mass of solids was varied to achieve a nominal oxidant mass to solids ratio of 20 and 50 g/kg. To each batch reactor the required mass of solids was added followed by the required volume of the reagent stock solution. Reactors were shaken gently by hand and left in the dark at an ambient temperature of ~20 $^{o}$C. All reactors were constructed in triplicate including controls (no solids added). Aliquots of the supernatant were sampled after a reaction period of 1, 4, 8, 15 and 30 days. Following sampling, each reactor was shaken gently by hand. Reagent stock solutions were prepared by adding analytical grade $KMnO_4$ (EM Science) to Milli-Q water and boiling for ~1 hour. The cooled solution was filtered

(0.75 µm glass fibre, Pall Corporation) and standardized by titration into a sulphuric acid and sodium oxalate solution (APHA, 1998). At the specified times each reactor was sampled by removing an aliquot (2.3 mL) of the solution and determining the $KMnO_4$ concentration (500 times dilution factor) by spectrophotometry (Milton Roy Company, Spectronic 20D) at 525 nm (method detection limit (MDL) of 1.3 mg/L). The spectrophotometer was calibrated prior to each sampling episode and a permanganate calibration curve (1 to 100 mg/L) using a standardized solution was prepared. The decrease in permanganate concentration and the initial mass of aquifer material was used to estimate the NOI (NOD) following Xu and Thomson (2009).

**Persulfate NOI Procedure**

NOI tests were conducted for three persulfate systems: (1) unactivated persulfate, (2) chelated ferrous iron activated persulfate and (3) alkaline activated persulfate. The general experimental design was identical for each of these persulfate systems except that for the latter two an activator stock solution was added. Well-mixed 125 mL wide-mouth batch reactors were used. A series of six (6) tests were performed for the unactivated persulfate system (see Table SM-3). The NOI for an oxidant mass to solids ratio of 5, 20, 30 and 40 g/kg (nominal) using an initial persulfate concentration of 5, 20, 30 and 40 g-$Na_2S_2O_8$/L, respectively, were investigated (denoted as Series 1 to 4). For the remaining two series of tests (Series 5 and 6) the initial persulfate concentration was held constant at 30 g-$Na_2S_2O_8$/L and the mass of solids was varied to achieve a nominal oxidant mass to solids ratio of 20 and 50 g/kg. To each batch reactor the required mass of solids was added followed by the required volume of the persulfate stock solution. A specified volume of the activator stock solution was then added to the reactors (if required). Reactors were shaken gently by hand and left in the dark at an ambient temperature of ~20 $^oC$. All reactors were constructed in triplicate including controls (no solids added). Aliquots of the supernatant (2.3 mL) were sampled after a reaction period of 1, 4, 8, 15 and 30 days. Following sampling, each reactor was shaken gently by hand.

For the chelated ferrous iron activated persulfate tests, the initial reactor conditions were: 50 g of solids and 50 mL of solution with a concentration of 30 g-$Na_2S_2O_8$/L, 300 mg/L Fe(II) and 0.5 moles of citric acid/mole Fe(II). Two series of controls were included: (Ctrl-1) 50 mL of solution with a concentration of 30 g-$Na_2S_2O_8$/L, 300 mg/L Fe(II) and 0.5 moles of citric acid/mole Fe(II) without solids, and (Ctrl-2) 50 mL of a 30 g-$NaS_2O_8$/L persulfate solution without solids.

For the alkaline activated persulfate tests, the initial reactor conditions were: 50 mL of 30 g-$Na_2S_2O_8$/L, 50 g of solids, and pH of 11. The mass of sodium hydroxide (NaOH) added to achieve an initial reactor solution pH of 11 was based on the results from the alkaline buffering capacity

tests (data not shown). Two series of controls were included: (Ctrl-1) 50 mL of a 30 g-$Na_2S_2O_8$/L persulfate solution at a pH of 11 without solids, and (Ctrl-2) 50 mL of a 30 g-$Na_2S_2O_8$/L persulfate solution without solids.

Reagent stock solutions were prepared by adding sufficient analytical grade $Na_2S_2O_8$ (purity >98%, Aldrich Chem. Co., Milwaukee) to Milli-Q water to reach the required concentrations. Activator solutions for ferrous sulfate heptahydrate ($FeSO_4$•$7H_2O$) (J.T.Baker, Phillipsbourg, NJ) and citric acid ($C_6H_8O_7$, Fischer, Fair Lawns, NJ), or sodium hydroxide (NaOH, Fischer, Fair Lawns, NJ) were prepared to the required concentrations using Milli-Q water. Persulfate analytical reagents were prepared using ACS grade ferrous ammonium sulfate (FAS) ($Fe(NH_4)_2(SO_4)_2 \cdot 6H_2O$) (EMD, Gibbstown, NJ), ammonium thiocyanate ($NH_4SCN$) (J.T. Baker, Phillipsbourg, NJ) and sulfuric acid ($H_2SO_4$) (EMD, Gibbstown, NJ) in Milli-Q water. Persulfate analysis was performed following Huang et al. (2002). For the ferrous iron activated persulfate tests, some modifications to this persulfate analysis method were employed to capture interference by Fe(III) that is produced in the citric acid/Fe(II) activation systems. In this case, two samples were taken during each sampling episode. The first one was measured following Huang et al. (2002), and the second one was measured in a similar manner but without addition of the FAS solution. This second measurement represents the Fe(III) concentration remaining from the citric acid/Fe(II) activation system. The final concentration of persulfate was taken as the difference between those two measurements.

## Supplementary Material Figures

**Figure A-1(a).** Image of impacted core materials from the weathered limestone unit stored on site in freezer.

**Figure A-1(b).** Image of some of the selected un-impacted core material.


**Figure A-2.** Impacted aquifer material samples used for (a) slurry experiments and the “bleb” architecture physical model experiments, and (b) the “saturated lense” architecture physical model experiments.

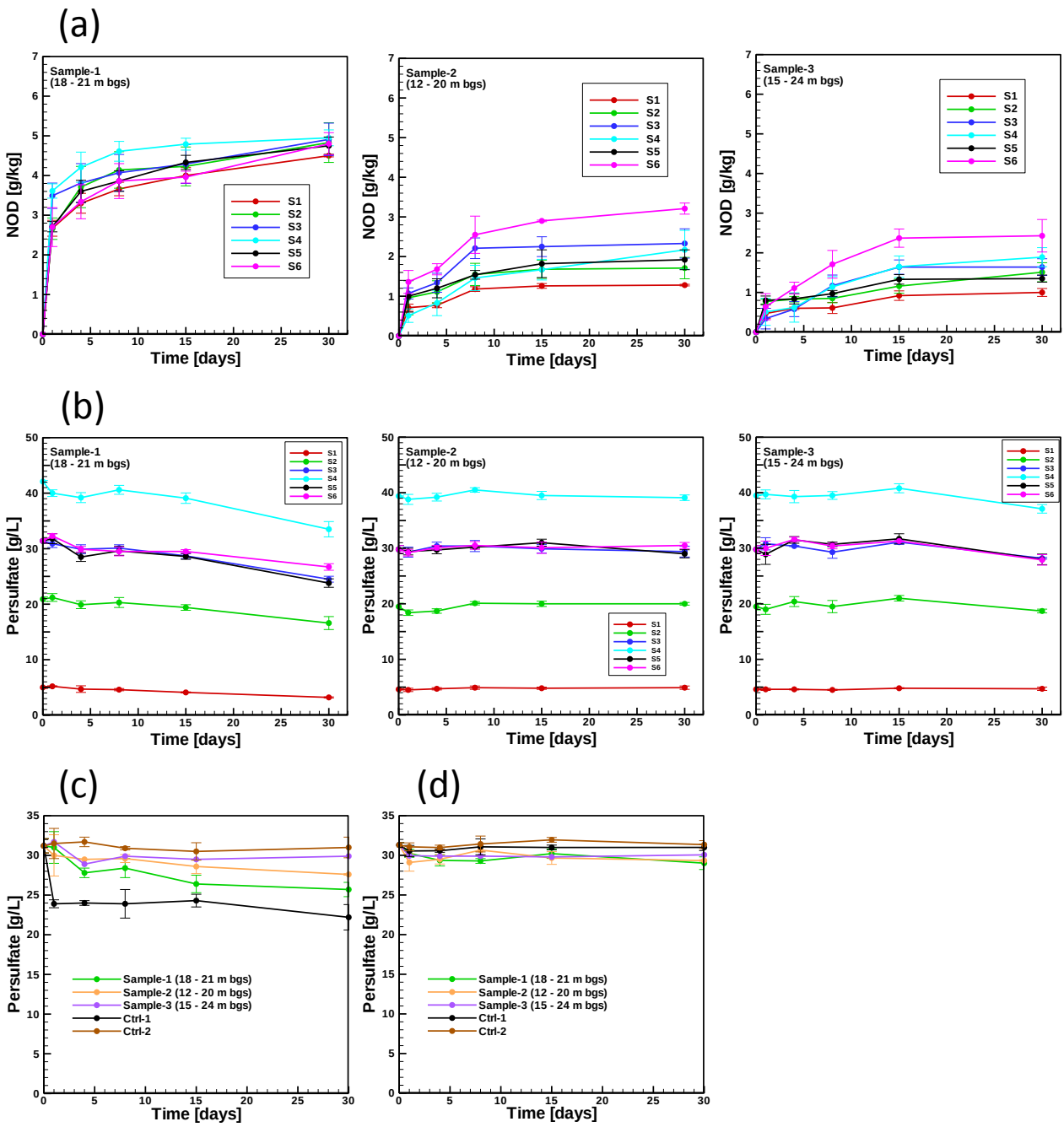


**Figure A-3.** (a) Permanganate NOI profiles expressed as NOD (g/kg) for the 3 samples examined (see Table A-2 for experimental details); (b) Unactivated persulfate NOI profiles for the 3 samples examined (see Table A-3 for experimental details); (c) Persulfate profiles from the Fe(II) activated persulfate NOI tests (see text in Appendix section for details); and (d) Persulfate profiles from the alkaline activated persulfate NOI tests (see text in Appendix section for details). The depth interval that the samples were collected from is also indicated.

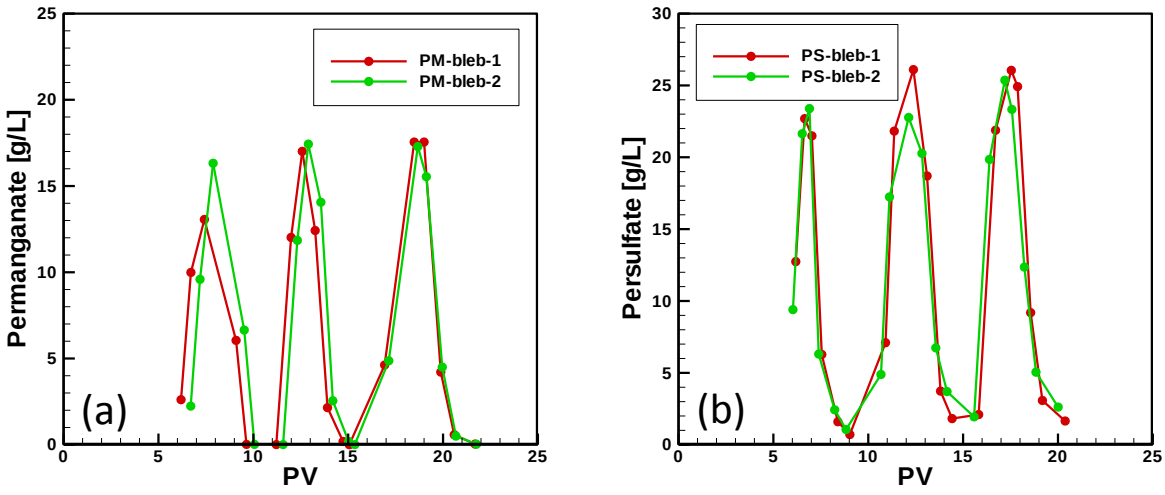


**Figure A-4.** Effluent concentration of (a) permanganate from the PM-bleb physical models and (b) persulfate from the PS-bleb physical models.

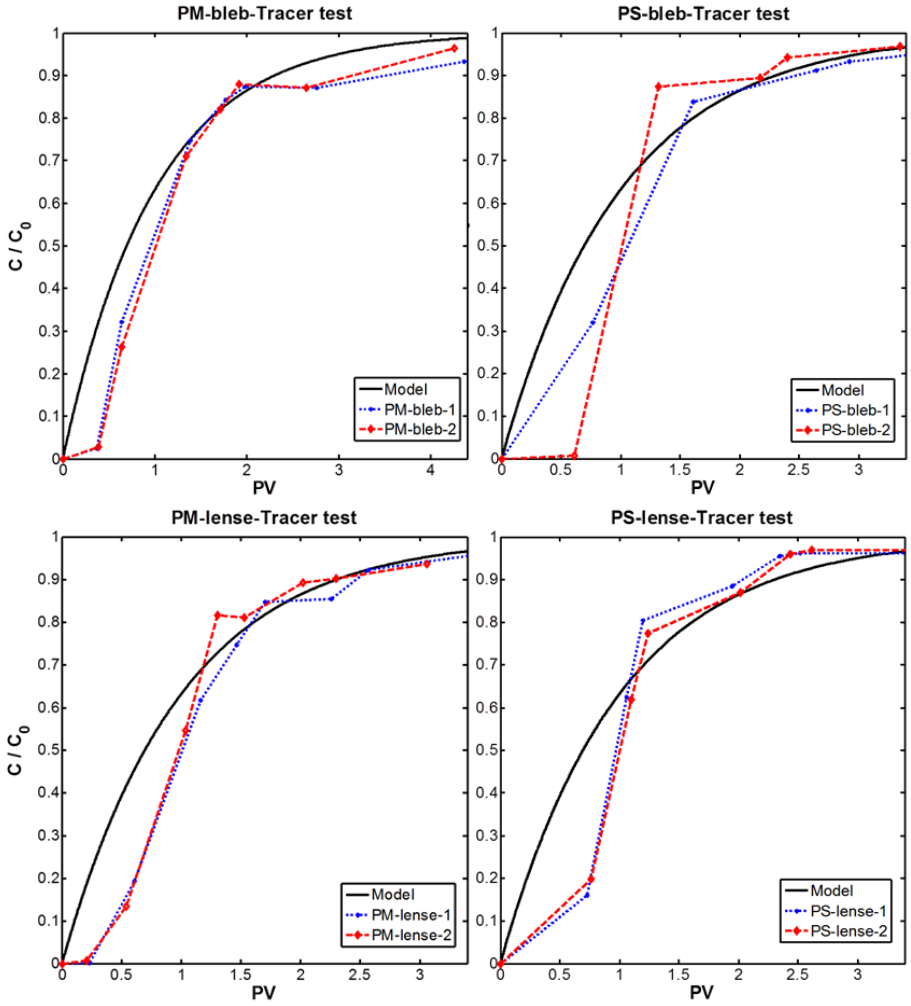


**Figure A-5.** Tracer test results: calibrated model BTC and observed BTCs for (a) bleb reactors upper panels, and (b) lense reactors lower panels.

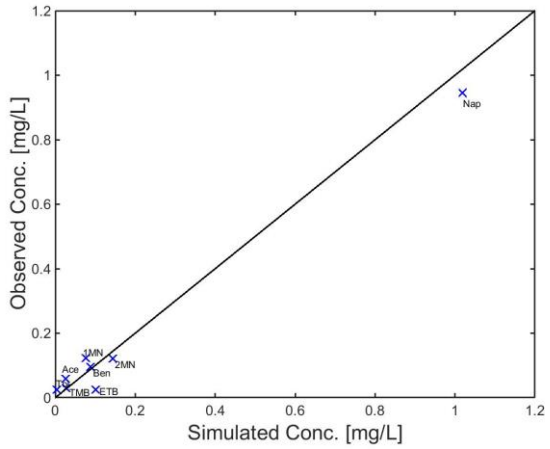


**Figure A-6.** Scatter plot from PS-bleb-1 of the simulated and observed concentrations for benzene, toluene, trimethylbenzene, acenaphthene, 1-methylnaphthalene, 2-methylnaphthalene, ethylbenzene, and naphthalene). The solid line has a slope of 1:1.

# Supplementary Material Tables

**Table A-1.** NAPL composition of sample obtained from 24 to 27 m bgs within the weathered limestone unit (data from Alpha Analytical Laboratories Westborough, MA).

| Organic Compound | Concentration mg/kg | MDL mg/kg | Percent of Identified |
|---|---|---|---|
| **BTEX** | | | |
| Benzene | 2640 | 11.40 | 0.77 |
| Ethylbenzene | 4480 | 8.09 | 1.32 |
| m-Xylene & p-Xylene | 1880 | 8.09 | 0.55 |
| o-Xylene | 738 | 7.83 | 0.22 |
| Toluene | 32.3 | 10.10 | 0.01 |
| **Trimethylbenzenes** | | | |
| 1,2,3-Trimethylbenzene | 734 | 8.35 | 0.22 |
| 1,2,4-Trimethylbenzene | 2260 | 7.75 | 0.66 |
| 1,3,5-Trimethylbenzene | 756 | 8.61 | 0.22 |
| **Methylethylbenzene** | | | |
| 1-Methyl-2-ethylbenzene | 395 | 6.37 | 0.12 |
| 1-Methyl-3-ethylbenzene | 2200 | 11.8 | 0.65 |
| 1-Methyl-4-ethylbenzene | 1660 | 10.6 | 0.49 |
| **Hydrocarbons** | | | |
| Dodecane | 880 | 41.7 | 0.26 |
| Hexadecane | 11200 | 28.8 | 3.29 |
| Nonacosane | 1610 | 128 | 0.47 |
| Octadecane | 1940 | 38.4 | 0.57 |
| Pentacosane | 3060 | 101 | 0.90 |
| Pentadecane | 16400 | 22.8 | 4.81 |
| Tetradecane | 1740 | 28.8 | 0.51 |
| Tridecane | 560 | 52.2 | 0.16 |
| Undecane | 1360 | 57.2 | 0.40 |
| **PAHs** | | | |
| 1-Methylnaphthalene | 25500 | 1100 | 7.49 |
| 2-Methylnaphthalene | 46700 | 990 | 13.71 |
| 2,6-Dimethylnaphthalene | 11500 | 3 | 3.38 |
| 2,3,5-Trimethylnaphthalene | 1000 | 2.35 | 0.29 |
| Acenaphthene | 13300 | 2.53 | 3.90 |
| Acenaphthylene | 4050 | 2.74 | 1.19 |
| Anthracene | 6280 | 2.96 | 1.84 |
| Benz (a) anthracene | 3180 | 2.93 | 0.93 |
| Benzo(a)fluoranthene | 702 | 2.85 | 0.21 |
| Benzo (a) pyrene | 3160 | 4.10 | 0.93 |
| Benz (b, k) fluoranthene | 2890 | 2.85 | 0.85 |
| Benzo(b)fluorene | 1450 | 4.16 | 0.43 |
| Benzo (g,h,i) perylene | 1230 | 3.82 | 0.36 |
| Benzothiophene | 883 | 4.50 | 0.26 |
| Biphenyl | 4990 | 4.44 | 1.46 |
| Carbazole | 61 | 4.70 | 0.02 |
| Chrysene | 2810 | 2.90 | 0.82 |
| Dibenzofuran | 1500 | 4.52 | 0.44 |
| Fluoranthene | 7930 | 4.56 | 2.33 |
| Indane | 11200 | 92.1 | 3.29 |
| Indene | 1700 | 4.34 | 0.50 |
| Fluorene | 7720 | 3.83 | 2.27 |
| Indeno[1,2,3-c,d] pyrene + Dibenz [a,h] anthracene | 1309 | 3.90 | 0.38 |
| Naphthalene | 83800 | 625 | 24.60 |
| Phenanthrene | 26400 | 23.8 | 7.75 |
| Pyrene | 12900 | 3.78 | 3.79 |
| Total (identified) | 340670 | | |

**Table A-2.** Design details for the permanganate NOI tests.

| Series | $C_{ox}$ [g-$KMnO_4$/L] | $V_{sol}$ [mL] | $M_{ox}$ [g-$KMnO_4$] | $M_{solids}$ [g-solids] | $V_{solids}$ [mL] | $M_{ox/s}$ [g-$KMnO_4$/kg-solids] | $V_{total}$ [mL] | $C_{solids}$ [kg/L] | Porosity [ - ] | $V_{headspace}$ [mL] |
|---|---|---|---|---|---|---|---|---|---|---|
| 1 | 5 | 50 | 0.25 | 50 | 18.9 | 5 | 68.9 | 0.73 | 0.73 | 56.1 |
| 2 | 20 | 50 | 1 | 50 | 18.9 | 20 | 68.9 | 0.73 | 0.73 | 56.1 |
| 3 | 30 | 50 | 1.5 | 50 | 18.9 | 30 | 68.9 | 0.73 | 0.73 | 56.1 |
| 4 | 40 | 50 | 2 | 50 | 18.9 | 40 | 68.9 | 0.73 | 0.73 | 56.1 |
| 5 | 30 | 50 | 1.5 | 75 | 28.3 | 20 | 78.3 | 0.96 | 0.64 | 46.7 |
| 6 | 30 | 67 | 2.01 | 40 | 15.1 | 50 | 82.1 | 0.49 | 0.82 | 42.9 |

$C_{ox}$ - permanagnate concentration
$V_{sol}$ - volume of oxidant solution
$M_{ox}$ - mass of oxdiant
$M_{solids}$ - mass of solids
$V_{solids}$ - estimated volume of solids
$M_{ox/s}$ - mass of oxdiant to solids ratio
$V_{total}$ - estimated total volume
$C_{solids}$ - estimated solids concentration
Porosity - estimated porosity
$V_{headspace}$ - estimated headspace in 125 mL reactor

**Table A-3.** Design details for the unactivated persulfate NOI tests.

| Series | $C_{ox}$ [g-$Na_2S_2O_8$/L] | $V_{sol}$ [mL] | $M_{ox}$ [g-$Na_2S_2O_8$] | $M_{solids}$ [g-solids] | $V_{solids}$ [mL] | $M_{ox/s}$ [g-$Na_2S_2O_8$/kg-solids] | $V_{total}$ [mL] | $C_{solids}$ [kg/L] | Porosity [ - ] | $V_{headspace}$ [mL] |
|---|---|---|---|---|---|---|---|---|---|---|
| 1 | 5 | 50 | 0.25 | 50 | 18.9 | 5 | 68.9 | 0.73 | 0.73 | 56.1 |
| 2 | 20 | 50 | 1 | 50 | 18.9 | 20 | 68.9 | 0.73 | 0.73 | 56.1 |
| 3 | 30 | 50 | 1.5 | 50 | 18.9 | 30 | 68.9 | 0.73 | 0.73 | 56.1 |
| 4 | 40 | 50 | 2 | 50 | 18.9 | 40 | 68.9 | 0.73 | 0.73 | 56.1 |
| 5 | 30 | 50 | 1.5 | 75 | 28.3 | 20 | 78.3 | 0.96 | 0.64 | 46.7 |
| 6 | 30 | 67 | 2.01 | 40 | 15.1 | 50 | 82.1 | 0.49 | 0.82 | 42.9 |

$C_{ox}$ - persulfate concentration
$V_{sol}$ - volume of oxidant solution
$M_{ox}$ - mass of oxdiant
$M_{solids}$ - mass of solids
$V_{solids}$ - estimated volume of solids
$M_{ox/s}$ - mass of oxdiant to solids ratio
$V_{total}$ - estimated total volume
$C_{solids}$ - estimated solids concentration
Porosity - estimated porosity
$V_{headspace}$ - estimated headspace in 125 mL reactor

**Table A-4.** Suite of organic compounds determined in this investigation and associated method detection limits (MDLs). The bulk soil concentration MDL is based on 8 g of soil and 10 mL of solvent.

| **Organic Compound** | Aqueous µg/L | Soil mg/kg |
|---|---|---|
| **BTEX** | | |
| Benzene | 1.11 | 0.0264 |
| Ethylbenzene | 0.77 | 0.0183 |
| m-Xylene & p-Xylene | 1.46 | 0.0347 |
| o-Xylene | 0.37 | 0.0088 |
| Toluene | 0.83 | 0.0197 |
| **Trimethylbenzenes** | | |
| 1,2,3-Trimethylbenzene | 0.76 | 0.0181 |
| 1,2,4-Trimethylbenzene | 0.82 | 0.0195 |
| 1,3,5-Trimethylbenzene | 0.74 | 0.0176 |
| **PAHs** | | |
| 1-Methylnaphthalene | 1.31 | 0.0311 |
| 2-Methylnaphthalene | 4.27 | 0.101 |
| Acenaphthene | 1.83 | 0.0435 |
| Acenaphthylene | 1.53 | 0.0363 |
| Anthracene | 5.53 | 0.131 |
| Benz [a] anthracene | 4.77 | 0.113 |
| Benzo [a] pyrene | 13.3 | 0.317 |
| Benz [b, k] fluoranthene | 5.62 | 0.133 |
| Benzo [g,h,i] perylene | 11.5 | 0.273 |
| Biphenyl | 1.09 | 0.0258 |
| Carbazole | 2.39 | 0.0568 |
| Chrysene | 5.75 | 0.137 |
| Dibenzofuran | 1.10 | 0.0262 |
| Fluoranthene | 1.80 | 0.0428 |
| Fluorene | 1.88 | 0.0447 |
| Indole | 2.12 | 0.0504 |
| Indeno[1,2,3-c,d] pyrene + Dibenz [a,h] anthracene | 18.7 | 0.444 |
| Naphthalene | 2.20 | 0.0523 |
| Phenanthrene | 3.78 | 0.0898 |
| Pyrene | 1.60 | 0.0381 |

# Appendix B:
# Supplementary Material for Chapter 3

## Supplementary Material Figures

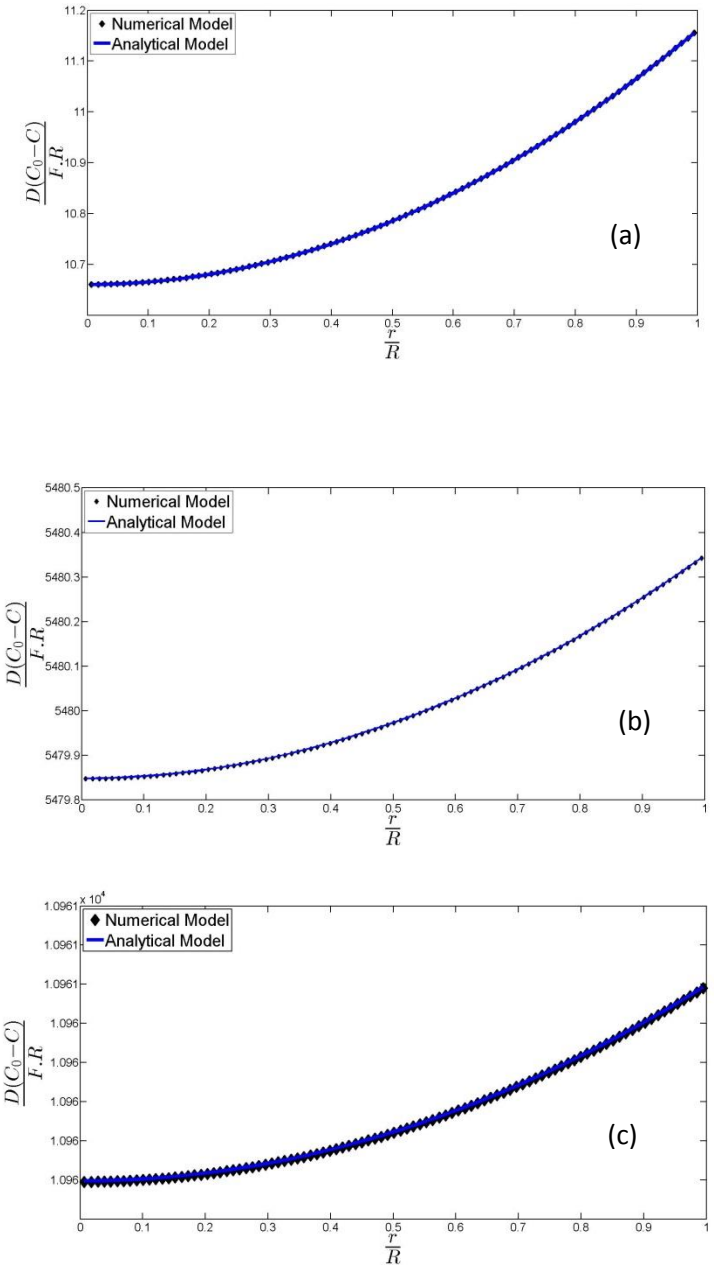


**Figure B-1:** Comparison of numerical and analytical model results for an initial concentration ($C_0$) of 3.5 mol/L, flux ($F$) of 1.9x10$^{-4}$ mmol/(cm$^2$ day), radius ($R$) of 0.49 cm, mesh size = 0.005 cm, Δt = 0.1 day, and diffusion coefficient ($D$) of 10$^{-5}$ cm$^2$/s, at: (a) 1 day; (b) 500 days, and (c) 1000 days.

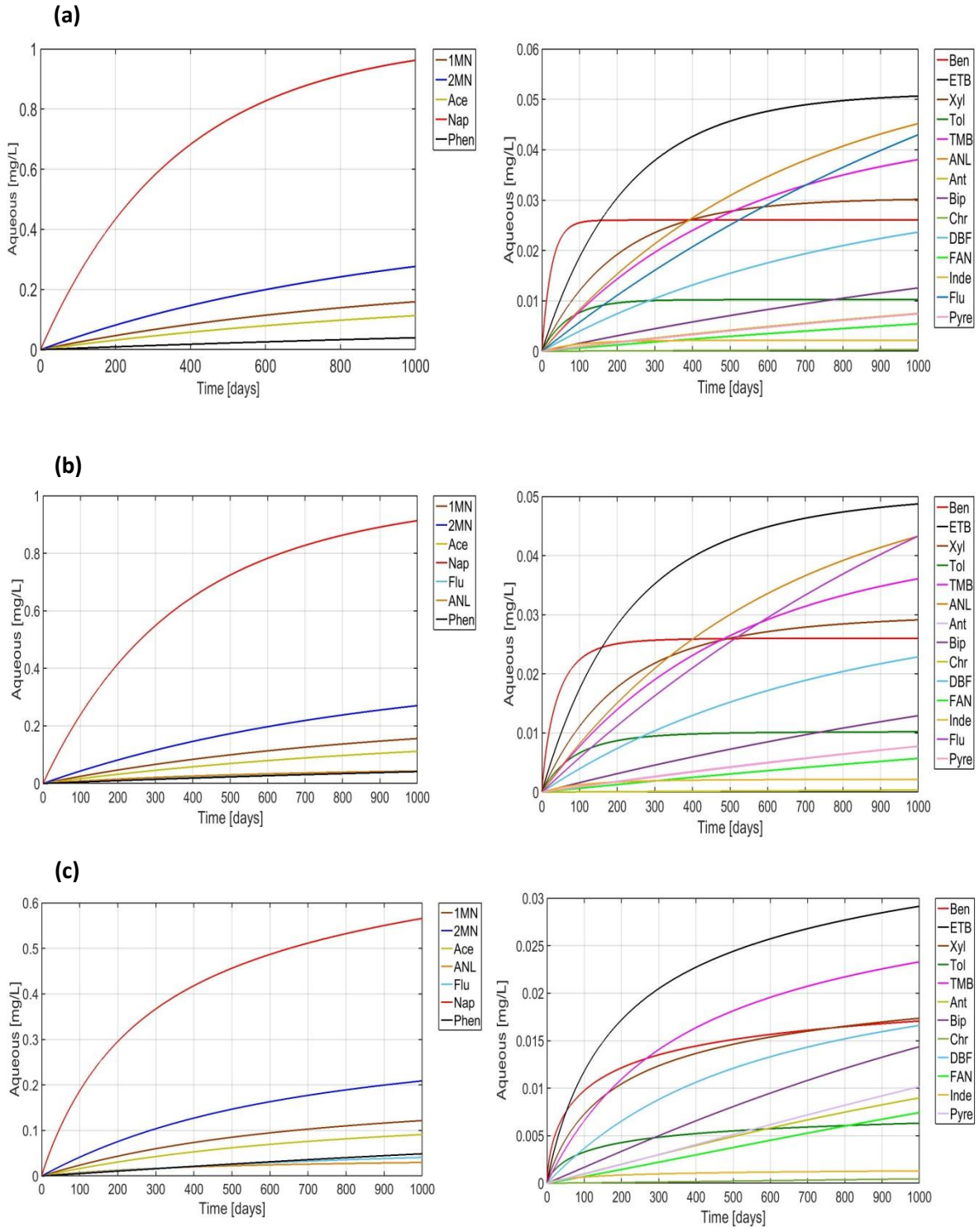


**Figure B-2:** Temporal aqueous concentrations from the (a) low and medium viscous NAPLs, (b) high viscous NAPL, and (c) very high viscous NAPL. (Note: left figures are the most predominant compounds and right figures are less predominant compounds)

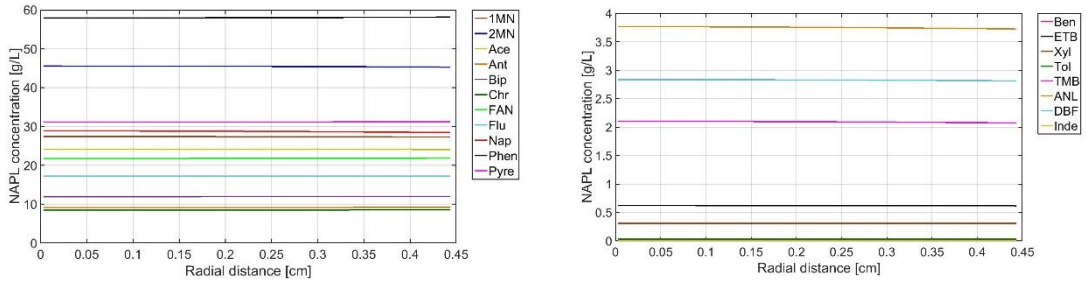


**Figure B-3:** Radial component concentration in the low and medium viscous NAPLs at 1000 days. (left: most predominant compounds, Right: less predominant compounds).

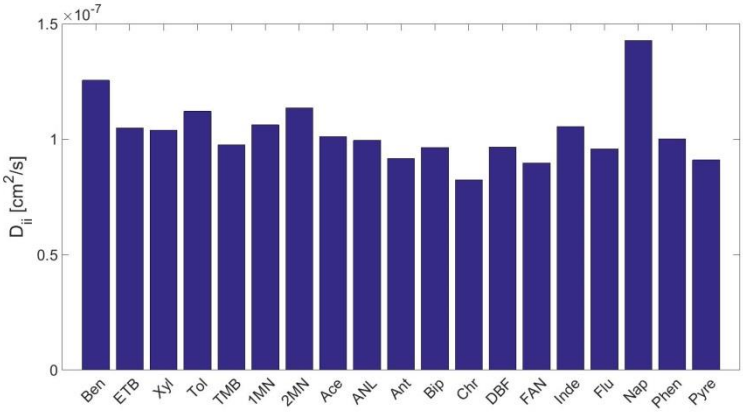


**Figure B.4:** Initial main intra-NAPL diffusion coefficients for the medium viscous NAPL.

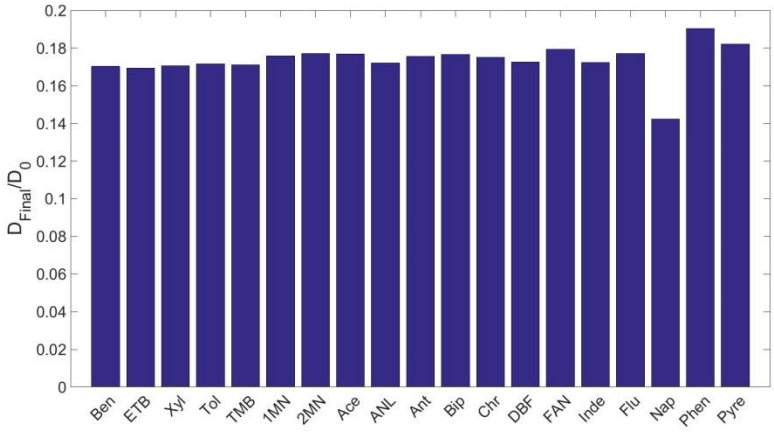


**Figure B.5:** Ratio of final to initial main intra-NAPL diffusion coefficients for the medium viscous NAPL.

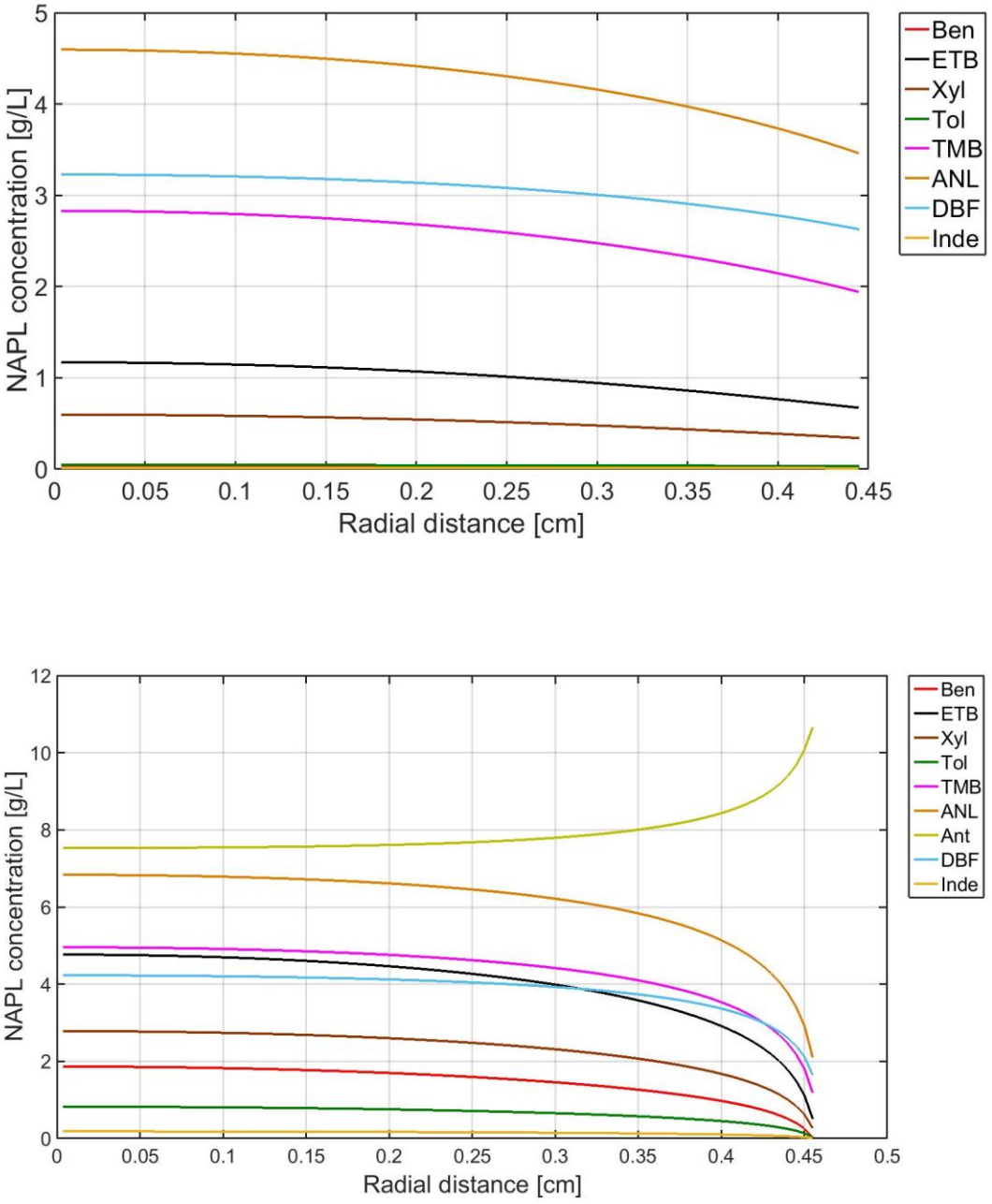


**Figure B.6:** Simulated NAPL radial composition at 1000 days for the less predominant components for a) the high viscous NAPL, and b) the very-high viscous NAPL.

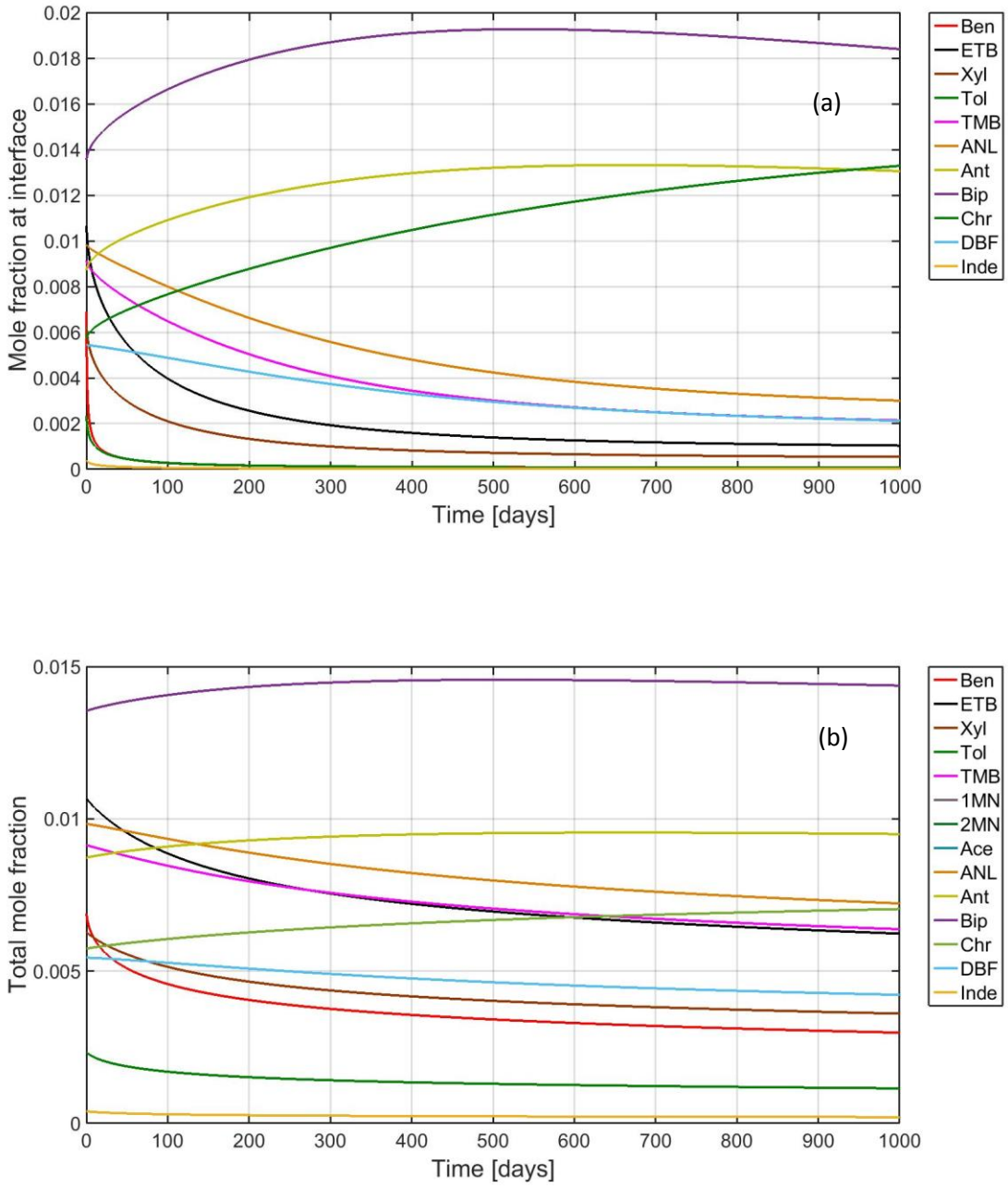


**Figure B.7:** Temporal a) interfacial, and b) total mole fractions for the less predominant components for the very-high viscous NAPL.

## Supplementary Material Tables

**Table B-1:** Comparison of intra-NAPL diffusion coefficients from this study with experimental and modeling results (Kett & Anderson, 1969b) for a ternary mixture composed of 1) dodecane, 2) hexadecane, and 3) hexane.

| | Experiment | Modeling by Kett & Anderson (1969b) | | Modeling in this study | |
|---|---|---|---|---|---|
| $D_{ij}$ | $[cm^2/s] \times 10^5$ | $[cm^2/s] \times 10^{-5}$ | Error (%) | $[cm^2/s] \times 10^{-5}$ | Error (%) |
| $D_{11}$ | 0.968 | 1.099 | 13.5 | 1.006 | 3.9 |
| $D_{12}$ | 0.266 | 0.366 | 37.5 | 0.211 | 20.7 |
| $D_{21}$ | 0.225 | 0.187 | 16.9 | 0.085 | 62 |
| $D_{22}$ | 1.031 | 1.007 | 2.3 | 0.955 | 7.4 |

**Table B-2:** Estimated self and infinite dilution diffusion coefficients ($cm^2/s$) using Eqs (15) and (16)

| Organic Component (i) | $D_i$ Eq. 13 $[cm^2/s]$ | Infinite-dilution diffusion coef. (Eq.12) j | | | | | | | | | | | | | | | | | | | |
|---|---|---|---|---|---|---|---|---|---|---|---|---|---|---|---|---|---|---|---|---|---|
| | | Ben | ETB | Xyl | Tol | TMB | 1MN | 2MN | Ace | ANL | Ant | Bip | Chr | DBF | FAN | Inde | Flu | Nap | Phen | Pyre | Bulk |
| Benzene | 1.97E-05 | - | 2.11E-05 | 2.05E-05 | 2.26E-05 | 1.71E-05 | 9.18E-06 | 9.18E-06 | 5.01E-06 | 7.18E-06 | 3.78E-06 | 7.26E-06 | 1.77E-06 | 4.62E-06 | 2.19E-06 | 1.27E-05 | 4.21E-06 | 1.08E-05 | 4.94E-06 | 2.48E-06 | 1.17E-07 |
| Ethylbenzene | 1.69E-05 | 1.62E-05 | - | 1.70E-05 | 1.87E-05 | 1.41E-05 | 7.60E-06 | 7.60E-06 | 4.15E-06 | 5.95E-06 | 3.13E-06 | 6.01E-06 | 1.47E-06 | 3.82E-06 | 1.81E-06 | 1.06E-05 | 3.49E-06 | 8.95E-06 | 4.09E-06 | 2.06E-06 | 9.71E-08 |
| Xylene(s) | 1.65E-05 | 1.62E-05 | 1.75E-05 | - | 1.87E-05 | 1.41E-05 | 7.60E-06 | 7.60E-06 | 4.15E-06 | 5.95E-06 | 3.13E-06 | 6.01E-06 | 1.47E-06 | 3.82E-06 | 1.81E-06 | 1.06E-05 | 3.49E-06 | 8.95E-06 | 4.09E-06 | 2.06E-06 | 9.71E-08 |
| Toluene | 2.00E-05 | 1.77E-05 | 1.90E-05 | 1.85E-05 | - | 1.54E-05 | 8.27E-06 | 8.27E-06 | 4.51E-06 | 6.47E-06 | 3.41E-06 | 6.54E-06 | 1.59E-06 | 4.16E-06 | 1.97E-06 | 1.15E-05 | 3.79E-06 | 9.74E-06 | 4.45E-06 | 2.24E-06 | 1.06E-07 |
| Trimethylbenzene(s) | 1.26E-05 | 1.51E-05 | 1.63E-05 | 1.58E-05 | 1.75E-05 | - | 7.08E-06 | 7.08E-06 | 3.87E-06 | 5.55E-06 | 2.92E-06 | 5.60E-06 | 1.37E-06 | 3.56E-06 | 1.69E-06 | 9.84E-06 | 3.25E-06 | 8.34E-06 | 3.81E-06 | 1.92E-06 | 9.05E-08 |
| 1-Methylnaphthalene | 6.75E-06 | 1.51E-05 | 1.63E-05 | 1.58E-05 | 1.75E-05 | 1.32E-05 | - | 7.08E-06 | 3.87E-06 | 5.55E-06 | 2.92E-06 | 5.60E-06 | 1.37E-06 | 3.56E-06 | 1.69E-06 | 9.84E-06 | 3.25E-06 | 8.34E-06 | 3.81E-06 | 1.92E-06 | 9.05E-08 |
| 2-Methylnaphthalene | 6.72E-06 | 1.51E-05 | 1.63E-05 | 1.58E-05 | 1.75E-05 | 1.32E-05 | 7.08E-06 | - | 3.87E-06 | 5.55E-06 | 2.92E-06 | 5.60E-06 | 1.37E-06 | 3.56E-06 | 1.69E-06 | 9.84E-06 | 3.25E-06 | 8.34E-06 | 3.81E-06 | 1.92E-06 | 9.05E-08 |
| Acenaphthene | 3.76E-06 | 1.48E-05 | 1.59E-05 | 1.55E-05 | 1.71E-05 | 1.29E-05 | 6.94E-06 | 6.94E-06 | - | 5.43E-06 | 2.86E-06 | 5.48E-06 | 1.34E-06 | 3.49E-06 | 1.65E-06 | 9.63E-06 | 3.18E-06 | 8.17E-06 | 3.73E-06 | 1.88E-06 | 8.86E-08 |
| Acenaphthylene | 5.02E-06 | 1.55E-05 | 1.66E-05 | 1.62E-05 | 1.79E-05 | 1.35E-05 | 7.24E-06 | 7.24E-06 | 3.95E-06 | - | 2.99E-06 | 5.73E-06 | 1.40E-06 | 3.64E-06 | 1.73E-06 | 1.01E-05 | 3.32E-06 | 8.53E-06 | 3.90E-06 | 1.96E-06 | 9.25E-08 |
| Anthracene | 2.68E-06 | 1.43E-05 | 1.53E-05 | 1.49E-05 | 1.64E-05 | 1.24E-05 | 6.67E-06 | 6.67E-06 | 3.64E-06 | 5.22E-06 | - | 5.27E-06 | 1.29E-06 | 3.35E-06 | 1.59E-06 | 9.26E-06 | 3.06E-06 | 7.85E-06 | 3.59E-06 | 1.80E-06 | 8.52E-08 |
| Biphenyl | 5.16E-06 | 1.48E-05 | 1.59E-05 | 1.55E-05 | 1.71E-05 | 1.29E-05 | 6.94E-06 | 6.94E-06 | 3.79E-06 | 5.43E-06 | 2.86E-06 | - | 1.34E-06 | 3.49E-06 | 1.65E-06 | 9.63E-06 | 3.18E-06 | 8.17E-06 | 3.73E-06 | 1.88E-06 | 8.86E-08 |
| Chrysene | 1.08E-06 | 1.29E-05 | 1.39E-05 | 1.35E-05 | 1.49E-05 | 1.12E-05 | 6.03E-06 | 6.03E-06 | 3.29E-06 | 4.72E-06 | 2.49E-06 | 4.77E-06 | - | 3.03E-06 | 1.44E-06 | 8.37E-06 | 2.77E-06 | 7.10E-06 | 3.25E-06 | 1.63E-06 | 7.70E-08 |
| Dibenzofuran | 3.28E-06 | 1.51E-05 | 1.63E-05 | 1.58E-05 | 1.75E-05 | 1.32E-05 | 7.08E-06 | 7.08E-06 | 3.87E-06 | 5.55E-06 | 2.92E-06 | 5.60E-06 | 1.37E-06 | - | 1.69E-06 | 9.84E-06 | 3.25E-06 | 8.34E-06 | 3.81E-06 | 1.92E-06 | 9.05E-08 |
| Fluoranthene | 1.44E-06 | 1.37E-05 | 1.48E-05 | 1.44E-05 | 1.59E-05 | 1.20E-05 | 6.43E-06 | 6.43E-06 | 3.51E-06 | 5.04E-06 | 2.65E-06 | 5.09E-06 | 1.24E-06 | 3.24E-06 | - | 8.93E-06 | 2.95E-06 | 7.57E-06 | 3.46E-06 | 1.74E-06 | 8.21E-08 |
| Indene | 1.06E-05 | 1.67E-05 | 1.79E-05 | 1.74E-05 | 1.92E-05 | 1.45E-05 | 7.80E-06 | 7.80E-06 | 4.26E-06 | 6.11E-06 | 3.22E-06 | 6.17E-06 | 1.50E-06 | 3.93E-06 | 1.86E-06 | - | 3.58E-06 | 9.19E-06 | 4.20E-06 | 2.11E-06 | 9.96E-08 |
| Fluorene | 3.03E-06 | 1.45E-05 | 1.56E-05 | 1.52E-05 | 1.68E-05 | 1.26E-05 | 6.80E-06 | 6.80E-06 | 3.71E-06 | 5.32E-06 | 2.80E-06 | 5.38E-06 | 1.31E-06 | 3.42E-06 | 1.62E-06 | 9.44E-06 | - | 8.00E-06 | 3.66E-06 | 1.84E-06 | 8.68E-08 |
| Naphthalene | 8.61E-06 | 1.62E-05 | 1.75E-05 | 1.70E-05 | 1.87E-05 | 1.41E-05 | 7.60E-06 | 7.60E-06 | 4.15E-06 | 5.95E-06 | 3.13E-06 | 6.01E-06 | 1.47E-06 | 3.82E-06 | 1.81E-06 | 1.06E-05 | 3.49E-06 | - | 4.09E-06 | 2.06E-06 | 9.71E-08 |
| Phenanthrene | 3.21E-06 | 1.43E-05 | 1.53E-05 | 1.49E-05 | 1.64E-05 | 1.24E-05 | 6.67E-06 | 6.67E-06 | 3.64E-06 | 5.22E-06 | 2.75E-06 | 5.27E-06 | 1.29E-06 | 3.35E-06 | 1.59E-06 | 9.26E-06 | 3.06E-06 | 7.85E-06 | - | 1.80E-06 | 8.52E-08 |
| Pyrene | 1.65E-06 | 1.37E-05 | 1.48E-05 | 1.44E-05 | 1.59E-05 | 1.20E-05 | 6.43E-06 | 6.43E-06 | 3.51E-06 | 5.04E-06 | 2.65E-06 | 5.09E-06 | 1.24E-06 | 3.24E-06 | 1.53E-06 | 8.93E-06 | 2.95E-06 | 7.57E-06 | 3.46E-06 | - | 8.21E-08 |
| Bulk | 8.61E-06 | 1.62E-05 | 1.75E-05 | 1.70E-05 | 1.87E-05 | 1.41E-05 | 7.60E-06 | 7.60E-06 | 4.15E-06 | 5.95E-06 | 3.13E-06 | 6.01E-06 | 1.47E-06 | 3.82E-06 | 1.81E-06 | 1.06E-05 | 3.49E-06 | 8.95E-06 | 4.09E-06 | 2.06E-06 | - |

**Table B-3:** Estimated initial main and off-diagonal intra-NAPL diffusion coefficients using the RD approach ($cm^2/s$) for the medium viscous NAPL

| | $D_{ij}$ [$cm^2/s$] | | | | | | | | | | | | | | | | | | |
|---|---|---|---|---|---|---|---|---|---|---|---|---|---|---|---|---|---|---|---|
| **Organic** | **j** | | | | | | | | | | | | | | | | | | |
| **Component (i)** | Ben | ETB | Xyl | Tol | TMB | 1MN | 2MN | Ace | ANL | Ant | Bip | Chr | DBF | FAN | Inde | Flu | Nap | Phen | Pyre |
| Benzene | 1.26E-07 | 1.62E-09 | 1.57E-09 | 1.61E-09 | 1.53E-09 | 1.57E-09 | 1.56E-09 | 1.51E-09 | 1.51E-09 | 1.56E-09 | 1.61E-09 | 1.52E-09 | 1.58E-09 | 1.51E-09 | 1.58E-09 | 1.54E-09 | 1.60E-09 | 1.57E-09 | 1.51E-09 |
| Ethylbenzene | 2.45E-09 | 1.05E-07 | 2.32E-09 | 2.38E-09 | 2.25E-09 | 2.30E-09 | 2.29E-09 | 2.23E-09 | 2.18E-09 | 2.29E-09 | 2.36E-09 | 2.21E-09 | 2.34E-09 | 2.20E-09 | 2.32E-09 | 2.25E-09 | 2.35E-09 | 2.26E-09 | 2.20E-09 |
| Xylene(s) | 1.42E-09 | 1.38E-09 | 1.04E-07 | 1.39E-09 | 1.33E-09 | 1.33E-09 | 1.33E-09 | 1.30E-09 | 1.24E-09 | 1.32E-09 | 1.36E-09 | 1.26E-09 | 1.36E-09 | 1.26E-09 | 1.35E-09 | 1.30E-09 | 1.36E-09 | 1.30E-09 | 1.26E-09 |
| Toluene | 5.43E-10 | 5.30E-10 | 5.19E-10 | 1.12E-07 | 5.07E-10 | 5.11E-10 | 5.11E-10 | 4.95E-10 | 4.83E-10 | 5.07E-10 | 5.23E-10 | 4.89E-10 | 5.18E-10 | 4.88E-10 | 5.16E-10 | 5.01E-10 | 5.21E-10 | 5.04E-10 | 4.88E-10 |
| Trimethylbenzene(s) | 2.03E-09 | 1.97E-09 | 1.95E-09 | 1.99E-09 | 9.75E-08 | 1.89E-09 | 1.89E-09 | 1.85E-09 | 1.73E-09 | 1.86E-09 | 1.91E-09 | 1.76E-09 | 1.94E-09 | 1.77E-09 | 1.91E-09 | 1.85E-09 | 1.92E-09 | 1.82E-09 | 1.77E-09 |
| 1-Methylnaphthalene | 1.17E-08 | 1.14E-08 | 1.11E-08 | 1.14E-08 | 1.08E-08 | 1.06E-07 | 1.08E-08 | 1.04E-08 | 1.02E-08 | 1.07E-08 | 1.12E-08 | 1.02E-08 | 1.11E-08 | 1.01E-08 | 1.10E-08 | 1.05E-08 | 1.11E-08 | 1.06E-08 | 1.02E-08 |
| 2-Methylnaphthalene | 1.97E-08 | 1.92E-08 | 1.87E-08 | 1.92E-08 | 1.83E-08 | 1.84E-08 | 1.14E-07 | 1.76E-08 | 1.73E-08 | 1.81E-08 | 1.89E-08 | 1.73E-08 | 1.88E-08 | 1.72E-08 | 1.85E-08 | 1.78E-08 | 1.87E-08 | 1.80E-08 | 1.72E-08 |
| Acenaphthene | 8.63E-09 | 8.38E-09 | 8.18E-09 | 8.40E-09 | 7.97E-09 | 7.89E-09 | 7.87E-09 | 1.01E-07 | 7.24E-09 | 7.67E-09 | 8.07E-09 | 7.15E-09 | 8.11E-09 | 7.16E-09 | 8.00E-09 | 7.57E-09 | 8.06E-09 | 7.54E-09 | 7.17E-09 |
| Acenaphthylene | 2.20E-09 | 2.12E-09 | 2.03E-09 | 2.12E-09 | 1.95E-09 | 2.00E-09 | 1.99E-09 | 1.88E-09 | 9.95E-08 | 1.98E-09 | 2.08E-09 | 1.86E-09 | 2.08E-09 | 1.85E-09 | 2.02E-09 | 1.93E-09 | 2.07E-09 | 1.95E-09 | 1.85E-09 |
| Anthracene | 1.95E-09 | 1.89E-09 | 1.82E-09 | 1.89E-09 | 1.76E-09 | 1.77E-09 | 1.77E-09 | 1.68E-09 | 1.66E-09 | 9.17E-08 | 1.84E-09 | 1.64E-09 | 1.81E-09 | 1.63E-09 | 1.81E-09 | 1.71E-09 | 1.83E-09 | 1.71E-09 | 1.63E-09 |
| Biphenyl | 3.07E-09 | 2.98E-09 | 2.88E-09 | 2.97E-09 | 2.78E-09 | 2.83E-09 | 2.83E-09 | 2.71E-09 | 2.68E-09 | 2.83E-09 | 9.65E-08 | 2.68E-09 | 2.87E-09 | 2.67E-09 | 2.87E-09 | 2.76E-09 | 2.91E-09 | 2.77E-09 | 2.67E-09 |
| Chrysene | 1.26E-09 | 1.21E-09 | 1.16E-09 | 1.21E-09 | 1.12E-09 | 1.12E-09 | 1.12E-09 | 1.06E-09 | 1.04E-09 | 1.10E-09 | 1.17E-09 | 8.24E-08 | 1.15E-09 | 1.01E-09 | 1.15E-09 | 1.08E-09 | 1.16E-09 | 1.07E-09 | 1.01E-09 |
| Dibenzofuran | 1.22E-09 | 1.20E-09 | 1.17E-09 | 1.19E-09 | 1.15E-09 | 1.14E-09 | 1.14E-09 | 1.11E-09 | 1.09E-09 | 1.13E-09 | 1.17E-09 | 1.08E-09 | 9.67E-08 | 1.08E-09 | 1.17E-09 | 1.12E-09 | 1.16E-09 | 1.11E-09 | 1.08E-09 |
| Fluoranthene | 3.75E-09 | 3.62E-09 | 3.49E-09 | 3.62E-09 | 3.37E-09 | 3.36E-09 | 3.36E-09 | 3.16E-09 | 3.10E-09 | 3.28E-09 | 3.49E-09 | 3.02E-09 | 3.45E-09 | 8.98E-08 | 3.43E-09 | 3.21E-09 | 3.47E-09 | 3.20E-09 | 3.02E-09 |
| Indene | 9.07E-11 | 8.80E-11 | 8.56E-11 | 8.81E-11 | 8.30E-11 | 8.38E-11 | 8.37E-11 | 8.04E-11 | 7.84E-11 | 8.28E-11 | 8.63E-11 | 7.86E-11 | 8.62E-11 | 7.86E-11 | 1.05E-07 | 8.15E-11 | 8.59E-11 | 8.18E-11 | 7.86E-11 |
| Fluorene | 4.71E-09 | 4.56E-09 | 4.43E-09 | 4.57E-09 | 4.29E-09 | 4.29E-09 | 4.28E-09 | 4.08E-09 | 3.97E-09 | 4.20E-09 | 4.42E-09 | 3.92E-09 | 4.39E-09 | 3.92E-09 | 4.36E-09 | 9.58E-08 | 4.41E-09 | 4.12E-09 | 3.92E-09 |
| Naphthalene | 4.24E-08 | 4.20E-08 | 4.06E-08 | 4.15E-08 | 3.98E-08 | 4.04E-08 | 4.04E-08 | 3.83E-08 | 3.90E-08 | 4.00E-08 | 4.19E-08 | 3.91E-08 | 4.12E-08 | 3.85E-08 | 4.04E-08 | 3.92E-08 | 1.43E-07 | 4.05E-08 | 3.85E-08 |
| Phenanthrene | 1.20E-08 | 1.16E-08 | 1.12E-08 | 1.16E-08 | 1.08E-08 | 1.10E-08 | 1.09E-08 | 1.04E-08 | 1.03E-08 | 1.08E-08 | 1.14E-08 | 1.01E-08 | 1.12E-08 | 1.01E-08 | 1.11E-08 | 1.06E-08 | 1.13E-08 | 1.00E-07 | 1.01E-08 |
| Pyrene | 5.34E-09 | 5.17E-09 | 4.98E-09 | 5.15E-09 | 4.80E-09 | 4.80E-09 | 4.79E-09 | 4.50E-09 | 4.43E-09 | 4.68E-09 | 4.97E-09 | 4.31E-09 | 4.92E-09 | 4.30E-09 | 4.89E-09 | 4.58E-09 | 4.95E-09 | 4.56E-09 | 9.10E-08 |

# Appendix C:
# Supplementary Material for Chapter 4

## MGP Site and NAPL Separation Method

The MGP residuals used in this study were obtained from the former West Florida Natural Gas Company Site located in Ocala, Florida. From the late 1890s until about 1953, water gas or carbureted water gas was manufactured at the Site by the "Lowe" carbonization process or destructive distillation of bituminous coal and coke. According to Brown's Directory, gas production was ~48 x $10^3$ $m^3$/yr in 1900 and steadily increased to 900 x $10^3$ $m^3$/yr by 1950. In 1952, manufacturing stopped at the plant and the facility converted to the sale of butane-propane-air. Residues from the MGP plant process, including tars and oily wastewaters, were deposited in the area of the former gas plant facilities during operations. There was an historic coal tar pit or area where residual tars were stored prior to sale for off-site use as roofing materials. The MGP residual received was obtained from a NAPL collection well screened from 24 to 27 m below ground surface in weathered limestone, and was a non-homogeneous mixture composed of a LNAPL and DNAPL component with minor sediment. For the purpose of this experiment, our focus was on the DNAPL component. Thus, 10 mL of the MGP residuals was mixed with 10 mL Milli-Q water in a 40 mL vial and centrifuged at 10,000 rpm for 15 min. The DNAPL portion was collected after centrifuging and again mixed with water and centrifuged. This process was repeated multiple times to separate a sufficient mass of DNAPL which was then used. The final DNAPL volume was assumed to be a homogeneous mixture.

## Reagents and Analytical Methods

Sodium persulfate ($Na_2S_2O_8$, Sigma-Aldrich Inc., St. Louis, MO), sodium bromide (NaBr, Sigma-Aldrich), and methylene chloride ($CH_2Cl_2$, EMD Millipore) were all reagent grade and used as received.

Due to large difference in the concentrations of organic component within NAPL and aqueous phase, different analytical methods were employed to analyze aqueous and NAPL samples. For organic analysis of aqueous phase, 19 mL sample was collected and mixed by 1.0 ml of methylene chloride (containing internal standards metafluoro-toluene and fluoro-biphenyl at 25 mg/L). The vial was quickly resealed and agitated on its side at 350 rpm on a platform shaker for

20 min. After shaking, the vial was inverted and the phases were allowed to separate for 30 min. Approximately 0.7 ml of the dichloromethane phase was removed from the inverted vial with a gas tight glass syringe, through the Teflon septum. The solvent was placed in a Teflon sealed autosampler vial for injection into the gas chromatograph.

In the case of NAPL organic analysis, samples were added directly to methylene chloride such that the concentration was within the calibration range and transferred to a 2 mL autosampler vial and crimp sealed with a Teflon cap. All NAPL and aqueous samples were analyzed using a HP 5890 capillary gas chromatograph (GC), a HP7673A autosampler, and a flame ionization detector. Three microliters of methylene chloride was injected in splitless mode (purge on 0.5 min, purge off 10 min) onto a 0.25mm x 30m length, DB5 capillary column with a stationary phase film thickness of 0.25µm. Helium column flow rate was 2 mL/min with a make-up gas flow rate of 30 mL/min. Injection temperature was 275$^{o}$C, detector temperature was 325$^{o}$C and initial column oven temperature was 35$^{o}$C held for 0.5 min, then ramped at 15$^{o}$C/min to a final temperature of 250$^{o}$C and held for 2 min. Chromatographic run time was 16 min. Data integration was completed with a SRI Model 302 Peak Simple chromatography data system. Method detection limit (MDL) for aqueous samples was 20 ug/L and for NAPL samples was 0.01 g/kg.

Anions/cations were analyzed using a Dionex® ICS2000 Ion Chromatograph equipped with an ioneluent generator and conductivity detector. For anions, a 25-µL sample was injected using a Dionex AS-40 Autosampler onto a Dionex® Ion Pac AS11-HC (4 × 250 mm) column. The mobile phase was 30 mM potassium hydroxide (KOH) at a flow rate of 1.0 mL/min. For cations, a 25 µL sample was injected using a Dionex IonPac® CS-12A column (4 × 250 mm). The mobile phase used was a 22.5 mM methanesulfonic Acid (MSA) at a flow rate of 1.0 mL/min. The chromatograph was obtained using Dionex Chromeleon software®. The MDL for anions was 0.5 mg/L, while for cations it ranged from 0.8 to 1.1 mg/L.

Persulfate analysis was performed following Liang et al. (Liang et al., 2008) with MDL of zero (0) M. An Orion pH meter (model 290A) was used to measure pH.

## Numerical Solution Method

Eq.1 and Eq.5 were solved decoupled using a fully-implicit finite volume scheme and linked by the mass transfer term (Eq.5) and the boundary condition (Eq.3). At each time step, equilibrium concentration (Eq.4), aqueous concentrations (Eq.5), and mass flux (Eq.3) of each component was determined. The shrinkage of the NAPL body due to mass loss was handled by assuming

the rectangular NAPL can shrink bottom-up. A modified grid system with uniform space interval (except for the control volume at $L = 0$) and a fixed time step was chosen. At each time step, mass loss and shrinkage length were determined using the estimated mass flux data at the interface (Eq.3), and then the length and constituent concentrations within the external boundary control volume were modified. Subsequently, by assuming an impermeable boundary condition ($J_i = 0$) at the interface the system of equations was solved by incorporating Eq.1 and Eq.2 to update concentration profiles within the NAPL. At the end of each time step, the whole grid system was modified by moving the mesh toward the bottom ($L = 0$) a distance equal to the shrinkage length and concentrations at the centroids of new control volumes were interpolated using cubic spline method (J Crank & Gupta, 1972). In addition, at the end of each time step oxidant concentration was updated using Eq.6.

Intra-NAPL diffusion mass balance algorithm (Eq.1) was verified by comparing it with an analytical solution for plane diffusion (John Crank, 1975). Multi-component diffusion coefficients estimation method was also verified by comparing the generated values to the experimental diffusion coefficients (T.K. Kett & Anderson, 1969) for a ternary mixture composed of dodecane, hexadecane, and hexane (Table C.2).

The rectangular NAPL depth in Eq.1 and aqueous phase (Eq.5) were discretized into control volumes with 0.005 cm and 0.025 cm length, respectively, and time step equal to 0.025 day. A mesh convergence test indicated that the concentrations for finer mesh increments and time steps varied by < 1%.

## Supplementary Material Figures

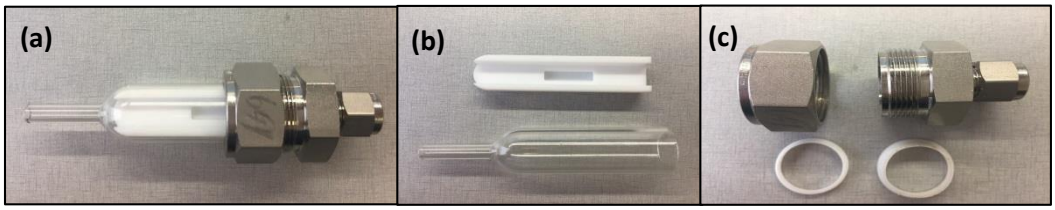


**Figure C.1:** a) Constructed physical model, b) Teflon sleeve and glass cylinder, c) Swagelok reducing union (¼" to ¾") (part# SS-1210-6-4) and ferrules front/back for ¾".

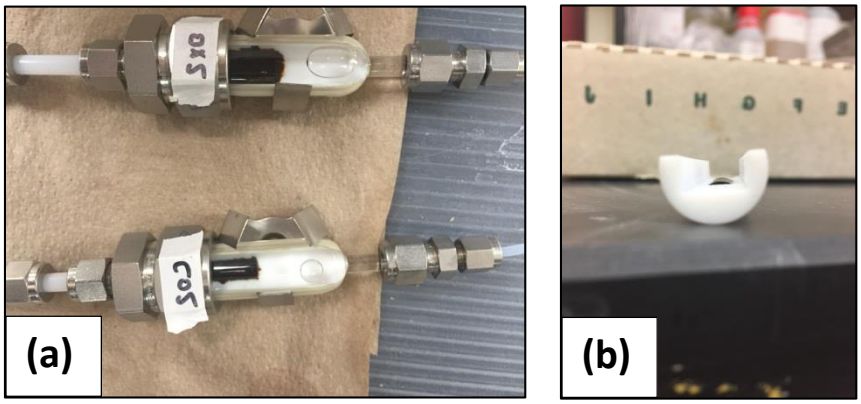


**Figure C.2:** a) control (CO) and persulfate (OX) physical models, b) Concave downward surface of MGP NAPL within Teflon sleeve.

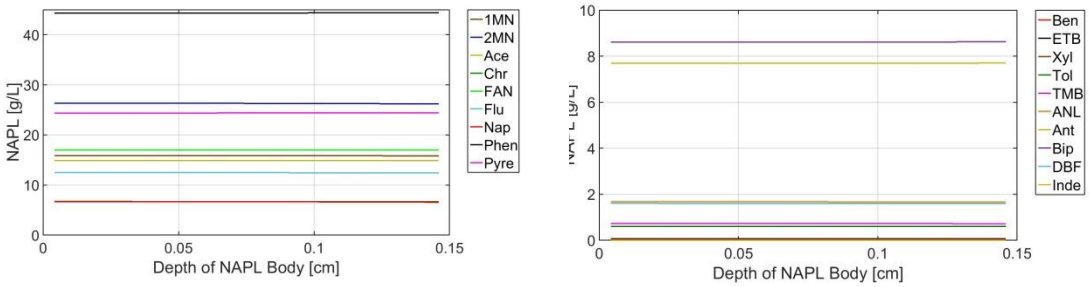


**Figure C.3:** Simulated NAPL concentrations for the water flushing scenario for the low viscous NAPL after 6400 PV.

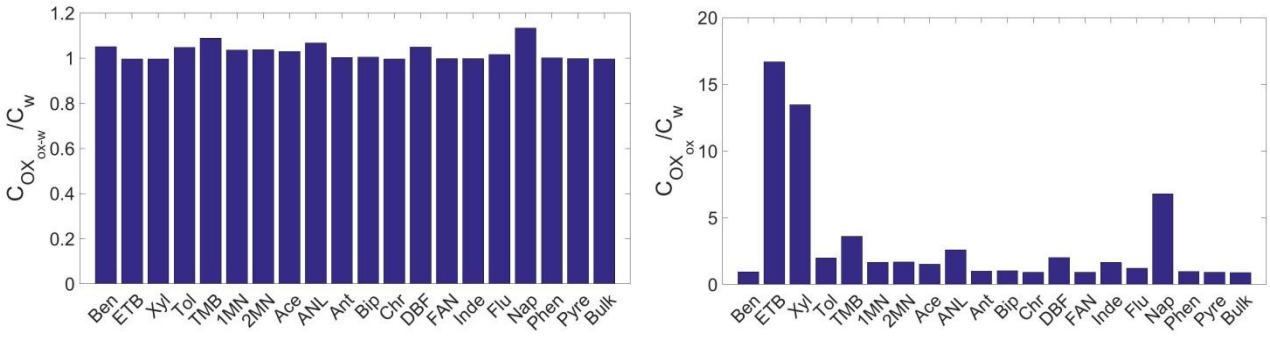


**Figure C.4:** Ratio of the NAPL concentrations for the oxidant flushing scenario ($C_{OX}$) to the water flushing scenario ($C_W$) after 6400 PVs.

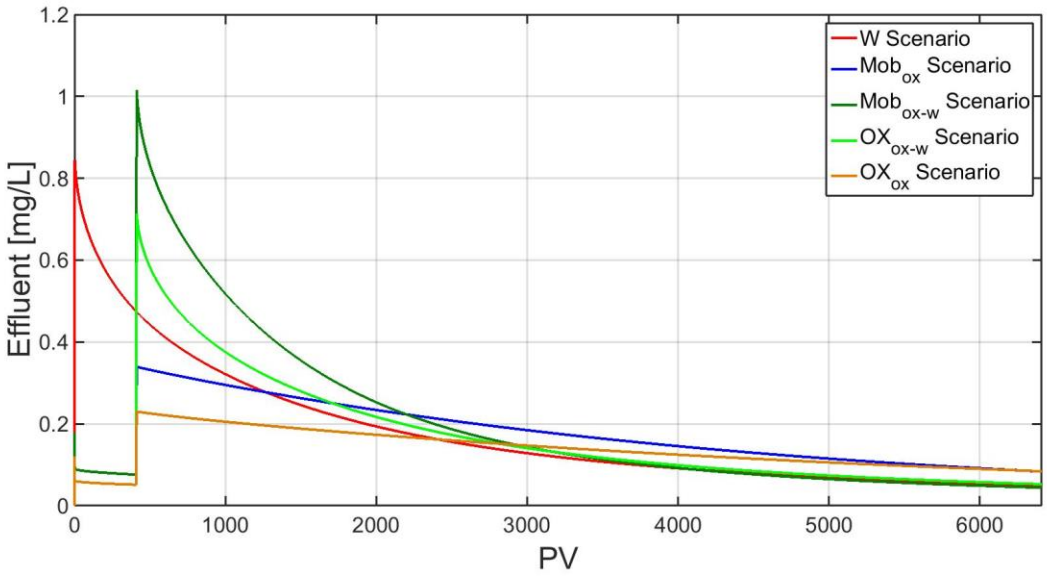


**Figure C.5:** Naphthalene effluent concentration for the high viscous NAPL for the water flushing (w), mobilized NAPL (Mob), and oxidant flushing (OX) scenarios.

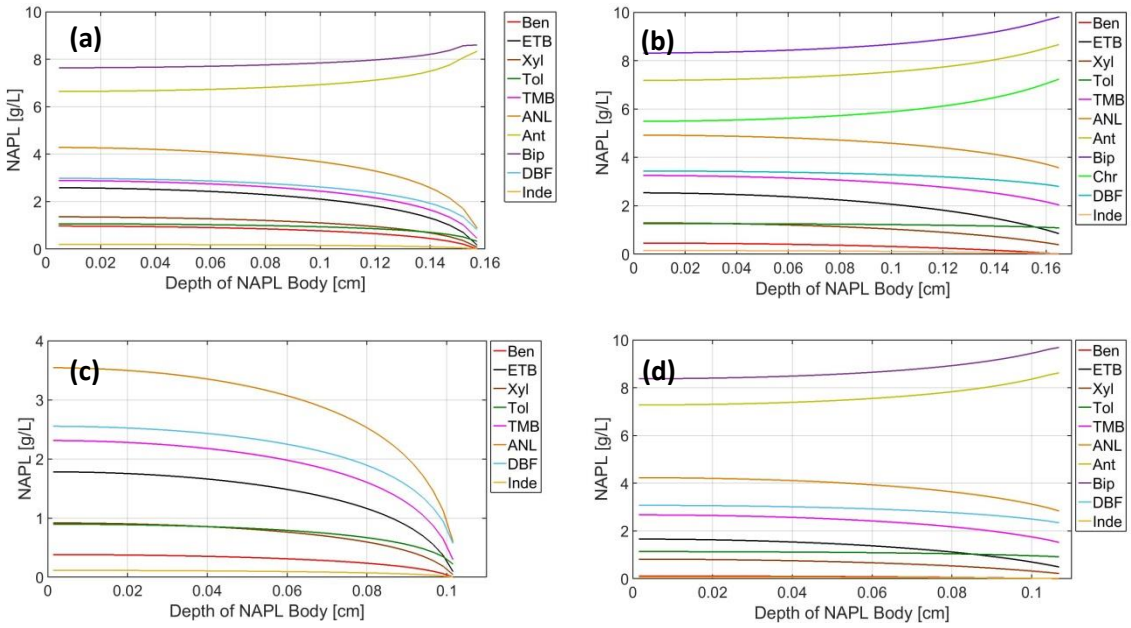


**Figure C.6:** High viscous NAPL concentrations for the less predominant components after 6400 PVs; a) water and $OX_{ox}$ scenarios, b) $OX_{ox}$ scenario, c) $Mob_{ox\text{-}w}$ scenario, d) $Mob_{ox}$ scenario.

# Supplementary Material Tables

**Table C-1:** Estimated self and infinite dilution diffusion coefficients ($cm^2/s$)

| Organic | $D_{self}$ | Infinite-dilution diffusion coef. j | | | | | | | | | | | | | | | | | | |
|---|---|---|---|---|---|---|---|---|---|---|---|---|---|---|---|---|---|---|---|---|
| **Component (i)** | [$cm^2/s$] | Ben | ETB | Xyl | Tol | TMB | 1MN | 2MN | Ace | ANL | Ant | Bip | Chr | DBF | FAN | Inde | Flu | Nap | Phen | Pyre | Bulk |
| Benzene | 1.97E-05 | - | 2.11E-05 | 2.05E-05 | 2.26E-05 | 1.71E-05 | 9.18E-06 | 9.18E-06 | 5.01E-06 | 7.18E-06 | 3.78E-06 | 7.26E-06 | 1.77E-06 | 4.62E-06 | 2.19E-06 | 1.27E-05 | 4.21E-06 | 1.08E-05 | 4.94E-06 | 2.48E-06 | 1.17E-07 |
| Ethylbenzene | 1.69E-05 | 1.62E-05 | - | 1.70E-05 | 1.87E-05 | 1.41E-05 | 7.60E-06 | 7.60E-06 | 4.15E-06 | 5.95E-06 | 3.13E-06 | 6.01E-06 | 1.47E-06 | 3.82E-06 | 1.81E-06 | 1.06E-05 | 3.49E-06 | 8.95E-06 | 4.09E-06 | 2.06E-06 | 9.71E-08 |
| Xylene(s) | 1.65E-05 | 1.62E-05 | 1.75E-05 | - | 1.87E-05 | 1.41E-05 | 7.60E-06 | 7.60E-06 | 4.15E-06 | 5.95E-06 | 3.13E-06 | 6.01E-06 | 1.47E-06 | 3.82E-06 | 1.81E-06 | 1.06E-05 | 3.49E-06 | 8.95E-06 | 4.09E-06 | 2.06E-06 | 9.71E-08 |
| Toluene | 2.00E-05 | 1.77E-05 | 1.90E-05 | 1.85E-05 | - | 1.54E-05 | 8.27E-06 | 8.27E-06 | 4.51E-06 | 6.47E-06 | 3.41E-06 | 6.54E-06 | 1.59E-06 | 4.16E-06 | 1.97E-06 | 1.15E-05 | 3.79E-06 | 9.74E-06 | 4.45E-06 | 2.24E-06 | 1.06E-07 |
| Trimethylbenzene(s) | 1.26E-05 | 1.51E-05 | 1.63E-05 | 1.58E-05 | 1.75E-05 | - | 7.08E-06 | 7.08E-06 | 3.87E-06 | 5.55E-06 | 2.92E-06 | 5.60E-06 | 1.37E-06 | 3.56E-06 | 1.69E-06 | 9.84E-06 | 3.25E-06 | 8.34E-06 | 3.81E-06 | 1.92E-06 | 9.05E-08 |
| 1-Methylnaphthalene | 6.75E-06 | 1.51E-05 | 1.63E-05 | 1.58E-05 | 1.75E-05 | 1.32E-05 | - | 7.08E-06 | 3.87E-06 | 5.55E-06 | 2.92E-06 | 5.60E-06 | 1.37E-06 | 3.56E-06 | 1.69E-06 | 9.84E-06 | 3.25E-06 | 8.34E-06 | 3.81E-06 | 1.92E-06 | 9.05E-08 |
| 2-Methylnaphthalene | 6.72E-06 | 1.51E-05 | 1.63E-05 | 1.58E-05 | 1.75E-05 | 1.32E-05 | 7.08E-06 | - | 3.87E-06 | 5.55E-06 | 2.92E-06 | 5.60E-06 | 1.37E-06 | 3.56E-06 | 1.69E-06 | 9.84E-06 | 3.25E-06 | 8.34E-06 | 3.81E-06 | 1.92E-06 | 9.05E-08 |
| Acenaphthene | 3.76E-06 | 1.48E-05 | 1.59E-05 | 1.55E-05 | 1.71E-05 | 1.29E-05 | 6.94E-06 | 6.94E-06 | - | 5.43E-06 | 2.86E-06 | 5.48E-06 | 1.34E-06 | 3.49E-06 | 1.65E-06 | 9.63E-06 | 3.18E-06 | 8.17E-06 | 3.73E-06 | 1.88E-06 | 8.86E-08 |
| Acenaphthylene | 5.02E-06 | 1.55E-05 | 1.66E-05 | 1.62E-05 | 1.79E-05 | 1.35E-05 | 7.24E-06 | 7.24E-06 | 3.95E-06 | - | 2.99E-06 | 5.73E-06 | 1.40E-06 | 3.64E-06 | 1.73E-06 | 1.01E-05 | 3.32E-06 | 8.53E-06 | 3.90E-06 | 1.96E-06 | 9.25E-08 |
| Anthracene | 2.68E-06 | 1.43E-05 | 1.53E-05 | 1.49E-05 | 1.64E-05 | 1.24E-05 | 6.67E-06 | 6.67E-06 | 3.64E-06 | 5.22E-06 | - | 5.27E-06 | 1.29E-06 | 3.35E-06 | 1.59E-06 | 9.26E-06 | 3.06E-06 | 7.85E-06 | 3.59E-06 | 1.80E-06 | 8.52E-08 |
| Biphenyl | 5.16E-06 | 1.48E-05 | 1.59E-05 | 1.55E-05 | 1.71E-05 | 1.29E-05 | 6.94E-06 | 6.94E-06 | 3.79E-06 | 5.43E-06 | 2.86E-06 | - | 1.34E-06 | 3.49E-06 | 1.65E-06 | 9.63E-06 | 3.18E-06 | 8.17E-06 | 3.73E-06 | 1.88E-06 | 8.86E-08 |
| Chrysene | 1.08E-06 | 1.29E-05 | 1.39E-05 | 1.35E-05 | 1.49E-05 | 1.12E-05 | 6.03E-06 | 6.03E-06 | 3.29E-06 | 4.72E-06 | 2.49E-06 | 4.77E-06 | - | 3.03E-06 | 1.44E-06 | 8.37E-06 | 2.77E-06 | 7.10E-06 | 3.25E-06 | 1.63E-06 | 7.70E-08 |
| Dibenzofuran | 3.28E-06 | 1.51E-05 | 1.63E-05 | 1.58E-05 | 1.75E-05 | 1.32E-05 | 7.08E-06 | 7.08E-06 | 3.87E-06 | 5.55E-06 | 2.92E-06 | 5.60E-06 | 1.37E-06 | - | 1.69E-06 | 9.84E-06 | 3.25E-06 | 8.34E-06 | 3.81E-06 | 1.92E-06 | 9.05E-08 |
| Fluoranthene | 1.44E-06 | 1.37E-05 | 1.48E-05 | 1.44E-05 | 1.59E-05 | 1.20E-05 | 6.43E-06 | 6.43E-06 | 3.51E-06 | 5.04E-06 | 2.65E-06 | 5.09E-06 | 1.24E-06 | 3.24E-06 | - | 8.93E-06 | 2.95E-06 | 7.57E-06 | 3.46E-06 | 1.74E-06 | 8.21E-08 |
| Indene | 1.06E-05 | 1.67E-05 | 1.79E-05 | 1.74E-05 | 1.92E-05 | 1.45E-05 | 7.80E-06 | 7.80E-06 | 4.26E-06 | 6.11E-06 | 3.22E-06 | 6.17E-06 | 1.50E-06 | 3.93E-06 | 1.86E-06 | - | 3.58E-06 | 9.19E-06 | 4.20E-06 | 2.11E-06 | 9.96E-08 |
| Fluorene | 3.03E-06 | 1.45E-05 | 1.56E-05 | 1.52E-05 | 1.68E-05 | 1.26E-05 | 6.80E-06 | 6.80E-06 | 3.71E-06 | 5.32E-06 | 2.80E-06 | 5.38E-06 | 1.31E-06 | 3.42E-06 | 1.62E-06 | 9.44E-06 | - | 8.00E-06 | 3.66E-06 | 1.84E-06 | 8.68E-08 |
| Naphthalene | 8.61E-06 | 1.62E-05 | 1.75E-05 | 1.70E-05 | 1.87E-05 | 1.41E-05 | 7.60E-06 | 7.60E-06 | 4.15E-06 | 5.95E-06 | 3.13E-06 | 6.01E-06 | 1.47E-06 | 3.82E-06 | 1.81E-06 | 1.06E-05 | 3.49E-06 | - | 4.09E-06 | 2.06E-06 | 9.71E-08 |
| Phenanthrene | 3.21E-06 | 1.43E-05 | 1.53E-05 | 1.49E-05 | 1.64E-05 | 1.24E-05 | 6.67E-06 | 6.67E-06 | 3.64E-06 | 5.22E-06 | 2.75E-06 | 5.27E-06 | 1.29E-06 | 3.35E-06 | 1.59E-06 | 9.26E-06 | 3.06E-06 | 7.85E-06 | - | 1.80E-06 | 8.52E-08 |
| Pyrene | 1.65E-06 | 1.37E-05 | 1.48E-05 | 1.44E-05 | 1.59E-05 | 1.20E-05 | 6.43E-06 | 6.43E-06 | 3.51E-06 | 5.04E-06 | 2.65E-06 | 5.09E-06 | 1.24E-06 | 3.24E-06 | 1.53E-06 | 8.93E-06 | 2.95E-06 | 7.57E-06 | 3.46E-06 | - | 8.21E-08 |
| Bulk | 8.61E-06 | 1.62E-05 | 1.75E-05 | 1.70E-05 | 1.87E-05 | 1.41E-05 | 7.60E-06 | 7.60E-06 | 4.15E-06 | 5.95E-06 | 3.13E-06 | 6.01E-06 | 1.47E-06 | 3.82E-06 | 1.81E-06 | 1.06E-05 | 3.49E-06 | 8.95E-06 | 4.09E-06 | 2.06E-06 | - |

**Table C-2:** Comparison of intra-NAPL diffusion coefficients from this study with experimental and modeling results (Kett & Anderson, 1969b) for a ternary mixture composed of 1) dodecane, 2) hexadecane, and 3) hexane.

| | Experiment | Modeling by Kett & Anderson (1969b) | | Modeling in this study | |
|---|---|---|---|---|---|
| $D_{ij}$ | [$cm^2/s$] $\times 10^5$ | [$cm^2/s$] $\times 10^{-5}$ | Error (%) | [$cm^2/s$] $\times 10^{-5}$ | Error (%) |
| $D_{11}$ | 0.968 | 1.099 | 13.5 | 1.006 | 3.9 |
| $D_{12}$ | 0.266 | 0.366 | 37.5 | 0.211 | 20.7 |
| $D_{21}$ | 0.225 | 0.187 | 16.9 | 0.085 | 62 |
| $D_{22}$ | 1.031 | 1.007 | 2.3 | 0.955 | 7.4 |